

2006-07-01

## The Synthesis of Zinc Oxide by Direct and Indirect Methods

Grainne Duffy  
*Technological University Dublin*

Follow this and additional works at: <https://arrow.tudublin.ie/scienmas>

 Part of the [Medicinal-Pharmaceutical Chemistry Commons](#)

---

### Recommended Citation

Duffy, G. (2006). *The synthesis of zinc oxide by direct and indirect methods*. Masters dissertation. Technological University Dublin. doi:10.21427/D71S5B

This Theses, Masters is brought to you for free and open access by the Science at ARROW@TU Dublin. It has been accepted for inclusion in Masters by an authorized administrator of ARROW@TU Dublin. For more information, please contact [arrow.admin@tudublin.ie](mailto:arrow.admin@tudublin.ie), [aisling.coyne@tudublin.ie](mailto:aisling.coyne@tudublin.ie), [vera.kilshaw@tudublin.ie](mailto:vera.kilshaw@tudublin.ie).

The synthesis of zinc oxide by direct and indirect  
methods

Gráinne Duffy, BA(Mod)

Thesis submitted in partial fulfilment for the award of  
MPhil

Dublin Institute of Technology

Under the supervision of

Prof. Michael S. Wong (Rice University)

Dr. Suresh C. Pillai,

& Dr. Declan E. McCormack

School of Chemical and Pharmaceutical Sciences

July 2006

## Abstract

The synthesis of zinc oxide through three routes was investigated; carboxylic acid chelation, polymer assisted synthesis in an alcoholic medium and slow thermolysis of precursor. In the case of carboxylic acid chelation, it was determined that the rate at which the precursor is formed has a significant effect on the quality of zinc oxide particles produced. Investigation of the effect of concentration, pH and species of chelating agent used on the purity and structure of product was undertaken. Examination of the composition and morphology of materials produced revealed the presence of single-crystalline spheres, the packing density and aggregation morphology of which was dependent on the chelating agent used. Polymer stabilised particles were synthesized in alcoholic solutions at room temperature and their stability to the addition of water was examined. Conditions were found under which particles of diameter  $< 10\text{nm}$ , synthesized at room temperature, were stable after the addition of small amounts of water. The slow thermolysis of zinc acetate precursor in organic solutions yielded quantum-confined zinc oxide particles and it was found that these particles *did not* grow as synthesis time was increased. Particles of diameter  $\cong 20\text{nm}$ , capped with both amine and carboxyl groups, were produced and the role of water in the growth of particles above the quantum regime was examined.


## **Declaration**

I certify that this thesis which I now submit for examination for the award of MPhil, is entirely my own work and has not been taken from the work of others save and to the extent that such work has been cited and acknowledged within the text of my work.

This thesis was prepared according to the regulations for postgraduate study by research of the Dublin Institute of Technology and has not been submitted in whole or in part for an award in any other Institute or University.

The work reported on in this thesis conforms to the principles and requirements of the Institute's guidelines for ethics in research.

The Institute has permission to keep, to lend or to copy this thesis in whole or in part, on condition that any such use of the material of the thesis be duly acknowledged.

Signature  Date 29/9/06  
Candidate

## **Acknowledgements**

I'd like to thank the FÁS Science Challenge and BioLink USA-Ireland for providing partial funding for my studies in Rice; Mr. John Cahill, Dr. Denis Headon and Dr. Pauline Ward for their infrastructural support.

I'd like to thank Will Knowles for obtaining TEM images at Rice and Martha Hidalgo for SEM images in DIT.

I'd like to thank the DIT Research Support Unit and Meath County Council for funding my studies.

I'd like to thank my supervisors for their intellectual input into this work.

I'd like to thank all the people that I've met in over the past two years that have helped and supported me.

I'd like to thank my family and friends for their constant support.



*For Oliver*

## **Abbreviations and symbols used in the text**

Bulk bandgap value, ( $E_g$ )

Deionised water, (*DIW*)

Differential scanning calorimetry, (*DSC*)

Diffraction angle, ( $\theta$ )

Electron volts, (*eV*)

Fluorescence spectroscopy, (*PL*)

Full width at half of maximum intensity, (*FWHM*)

Hexagonal close packed, (*hcp*)

Hexadecylamine, (*HDA*)

Measured band-edge value, ( $E^*$ )

Oleic acid, (*OA*)

Poly(vinyl pyrrolidone), (*PVP*)

Powder diffraction file, (*PDF*)

Scanning electron microscopy, (*SEM*)

Transmission electron microscopy, (*TEM*)

Ultraviolet light, (*UV*)

Ultraviolet-visible absorption spectroscopy, (*UV/vis*)

Wavelength, ( $\lambda$ )

**X-ray diffraction, X-ray diffractometry, (*XRD*)**



## Table of contents

Abstract .....	ii
Declaration .....	iii
Acknowledgements .....	iv
Abbreviations and symbols used in the text.....	vi
Table of contents .....	1
List of figures and tables .....	3
1 INTRODUCTION.....	9
1.1 Zinc oxide.....	9
1.2 Synthesis.....	10
1.3 Optical properties of zinc oxide .....	13
1.4 Structural determination via X-Ray diffractometry .....	15
1.5 Research objectives .....	16
1.6 Novelty of the current work .....	17
2 EXPERIMENTAL TECHNIQUES .....	19
2.1 Materials .....	19
2.2 Characterisation Methods.....	19
2.3 Synthesis Methods.....	22
3 POWDERS PREPARED THROUGH CARBOXYLIC ACID CHELATION .....	24
3.1 Use of oxalic acid as a chelating agent .....	24
3.2 Use of isophthalic acid as a chelating agent.....	24
3.3 Results - oxalic acid as a chelating agent .....	25
3.4 Results - isophthalic acid as a chelating agent .....	43
3.5 Conclusions .....	50



4	PARTICLES PREPARED THROUGH POLYMER-ASSISTED ALKALINE HYDROLYSIS.....	51
4.1	Results .....	51
4.2	Conclusions .....	60
5	ORGANIC-CAPPED ZINC OXIDE .....	61
5.1	Results .....	61
5.2	Conclusion.....	78
6	DISCUSSION .....	80
6.1	Powders prepared by carboxylic acid chelation .....	80
6.2	Polymer-assisted synthesis .....	82
6.3	Organic capped particles .....	82
7	Future work .....	84
7.1	Organic-capped particles .....	84
7.2	Polymer-assisted synthesis .....	84
7.3	Carboxylic acid chelation .....	85
8	Conclusion.....	86
9	References .....	87
10	APPENDIX .....	93
10.1	Powders prepared through the use of oxalic acid.....	93
10.2	Powders prepared through the use of isophthalic acid .....	97
10.3	Non-hydrolytic synthesis.....	100
10.4	Polymer-assisted synthesis .....	105
	Presentations and publications .....	106

## List of figures and tables

Table 1 Parameters used to estimate particle size from band edge calculations.....	21
Table 2 Dissociation constants of materials used, in dilute aqueous solutions at 25°C..	25
Figure 1 XRD patterns for powders synthesized rapidly and calcined at various temperatures. ....	26
Figure 2 XRD patterns for powders synthesized in a reaction longer than the gelation time and calcined at various temperatures. ....	27
Table 3 Resolvable XRD peaks for precursor powders calcined to 300°C .....	28
Figure 3 DSC of precursor powders.....	29
Table 4 Resolvable XRD peaks for precursor powders calcined to 350°C .....	30
Figure 4 Schematic of precursor proposed to have formed under rapid combination of reagents.....	32
Figure 5 Schematic of structure proposed to have formed under slow combination of reagents.....	32
Figure 6 FTIR spectra of powders prepared through rapid combination of reagents: 350°C, 375°C and 475°C .....	34
Figure 7 FTIR spectra of powders formed through slow combination of reagents: 350°C, 375°C and 475°C .....	34
Figure 8 FTIR spectra of powders calcined to 400°C.....	35
Figure 9 Size distribution of particles calcined to 350°C, 375°C and 475°C .....	36
Figure 10 XRD patterns for powders synthesized in a 1:1 and 1:2 ratio through diffusion of reagents only .....	37
Table 5 Resolvable XRD peaks 1:1 and 1:2 precursor powders calcined to 300°C .....	39
Figure 11 TEM image of precursor material calcined to 500°C, 40000X .....	40

Figure 12 XRD patterns of 1:2 precursor powders synthesized with 15mmol (black) and 87mmol (red) acetic acid, calcined to 500°C .....	41
Table 6 Resolvable XRD peaks for powders synthesized in an excess of acetic acid ....	42
Table 7 Particle sizes estimated from the Scherrer equation.....	42
Figure 13 TEM images at 200000x of powders made from solutions containing 1mmol zinc acetate and (l) 15mmol acetic acid, (r) 87mmol acetic acid, calcined to 500°C .....	43
Figure 14 XRD patterns for powders made from an isophthalic acid precursor, calcined to 500°C.....	44
Figure 15 XRD patterns for powders made from an isophthalic acid precursor, calcined to 800°C.....	44
Table 8 Scherrer equation estimation of crystallite size for particles synthesized using an isophthalate precursor and calcined to 500°C and 800°C .....	45
Figure 16 FTIR spectra of powders synthesized through isophthalic acid chelation and calcined to 500°C .....	46
Figure 17 FTIR spectra of powders synthesized through isophthalic acid chelation and calcined to 800°C .....	47
Figure 18 SEM images of 1:1 (l) and 1:2 (r) powders calcined to 500°C, 5000X magnification.....	48
Figure 19 TEM images of powders synthesized in 1:1 (l) and 1:2 (r) ratios of zinc ion to acid concentration and calcined to 800°C, 20000X .....	48
Figure 20 TEM image of powders synthesized in a 1:100 ratio with isophthalic acid and sintered to 800°C, 40000X.....	49
Figure 21 UV/vis spectra of samples prepared through conventional method .....	52
Figure 22 UV/vis spectra of samples synthesized at room temperature .....	52
Figure 23 UV/vis absorption spectra for samples containing various quantities of PVP53	



Table 9 Optical properties of samples made with different quantities of PVP .....	53
Figure 24 Fluorescence spectra for samples synthesized containing various PVP concentrations.....	54
Figure 25 UV/vis spectra of zinc oxide solutions after varying amounts of water were added .....	55
Figure 26 Fluorescence spectra of solutions synthesized with small amounts of water added .....	55
Figure 27 UV/vis absorption spectra for solutions synthesized with different amounts of PVP.....	56
Table 10 Optical properties of samples containing different quantities of PVP .....	56
Figure 28 Absorption spectra of solutions shown in Figure 27 after the addition of water .....	56
Figure 29 Fluorescence spectra of solutions after the addition of water.....	57
Figure 30 UV/vis absorption spectra of solutions after different amounts of water is added to each.....	58
Figure 31 UV/vis absorption spectra obtained after the addition of water of different acidities.....	58
Figure 32 UV/vis absorption spectra of solutions containing varying quantities of base and 0.5mls water .....	59
Figure 33 UV/vis absorption spectra of zinc oxide particles synthesized at different temperatures .....	62
Figure 34 XRD patterns of samples synthesized at different temperatures .....	63
Table 11 Sizes of particles calculated from XRD data shown in Fig. 33 .....	64
Figure 35 TEM image of particles synthesized at 175°C.....	64
Figure 36 XRD patterns of samples synthesized using zinc chloride as a precursor.....	65

Figure 37 UV/vis absorption spectra of samples synthesized at 200°C, containing various combinations of OA .....	66
Figure 38 XRD patterns of material shown in Figure 37 .....	67
Table 12 XRD peaks resolved for samples synthesized containing 1.34mmol oleic acid at 200°C.....	68
Table 13 Particle size estimations using Scherrer equation of particles synthesized at 200°C.....	69
Figure 39 Diffraction patterns of samples synthesized at 175°C using various concentrations of OA .....	70
Table 14 Particle size estimates using the Scherrer equation.....	70
Figure 40 Absorbance spectra for solutions synthesized at 175°C containing various amounts of OA, after 2 hours .....	71
Figure 41 Absorption evolution over time for samples synthesized at 175°C in a [Zn <sup>2+</sup> ]:[OA] ratio of 1:2 .....	72
Table 15 Particle sizes calculated from the absorption spectra of solutions.....	73
Figure 42 TEM image of particles synthesized at 175°C with 4.2mls OA, histogram of the sizes of these particles .....	73
Figure 43 Absorption spectra for samples synthesized at 175°C containing 4.2mls OA and subsequently washed .....	74
Figure 44 XRD patterns of samples synthesized at 175°C with 4.2mls OA and washed .....	75
Table 16 Particle size estimates for samples synthesized at 175°C with 4.2mls OA .....	75
Figure 45 Fluorescence spectra of samples synthesized at 175°C with a [Zn <sup>2+</sup> ]:[OA] ratio of 1:3 .....	76

Figure 46 XRD patterns of samples before and after the introduction of water to the reaction.....	77
Figure 47 Fluorescence spectra of samples taken before and after the introduction of water to the reaction vessel .....	78
Table A 1 XRD peaks resolvable for precursor particles calcined to 300°C .....	93
Table A2 Resolvable XRD peaks for precursor powders calcined to 375°C.....	93
Table A3 Resolvable XRD peaks for precursor powders calcined to 400°C.....	94
Table A4 Resolvable XRD peaks for precursor powders calcined to 425°C.....	94
Table A5 Resolvable XRD peaks for precursor powders calcined to 450°C.....	95
Table A6 Resolvable peaks for precursor powders calcined to 500°C .....	95
Figure A 1 TEM Size distributions of particles calcined to 350°C, as a fraction of total .....	96
Figure A 2 TEM size distributions for powders calcined to 375°C, as a fraction of total .....	97
Table A7 Resolvable peaks and intensities for XRD patterns for powders calcined to 500°C.....	97
Table A8 Resolvable peaks for XRD pattern for powders calcined to 800°C .....	99
Figure A 3 Identification of peaks for sample synthesized containing 0.38ml oleic acid at 200°C.....	100
Table A9 XRD peaks resolved for sample synthesized containing no oleic acid at 200°C .....	100
Table A10 XRD peaks resolved for sample synthesized containing 0.25ml OA at 200°C .....	101
Table A11 XRD peaks resolved for samples synthesized containing 0.5ml oleic acid at 200°C.....	103



Figure A 4 Time evolution of samples synthesized at 175°C in a [Zn <sup>2+</sup> ]:[OA] ratio of 1:3 .....	104
Figure A 5 Time evolution of samples synthesized at 175°C in a [Zn <sup>2+</sup> ]:[OA] ratio of 2:5 .....	105
Figure A 6 Effect of water on particle size .....	105

# 1 INTRODUCTION

## 1.1 Zinc oxide

Zinc oxide is a wide, direct bandgap semiconductor which has been used in areas such as catalysis,<sup>1,2</sup> gas sensing,<sup>3</sup> lasing,<sup>4</sup> in surface acoustic wave filters,<sup>5</sup> as a piezoelectric actuator<sup>6</sup> and as a transparent conducting oxide layer for solar cell applications.<sup>7,8</sup> Its possible ferromagnetic<sup>9</sup> applications arise from the hole-mediated ferromagnetism shown for magnetic impurities tetrahedrally coordinated in III-V and II-VI semiconductors<sup>10</sup> and are of interest because of their use in the emerging area of spintronics. The non-stoichiometric nature of zinc oxide, its propensity for the formation of zinc interstitials and oxygen vacancies<sup>11</sup> is the source of its green fluorescence and electrical conductivity. Luminescence of zinc oxide generated by excitonic behaviour<sup>12</sup> and tuneable through the variation of particle size, is found in the UV region and has generated interest in its possible applications in UV emitting devices.<sup>13,14</sup>

### 1.1.1 Growth habit of zinc oxide

The predominant stable phase in which binary zinc oxide forms is the wurtzite (hcp) structure,<sup>15</sup> although zinc blende has also been reported.<sup>16</sup> Wurtzite zinc oxide exhibits a hexagonal crystal structure with polar (001) faces. Each element is tetragonally coordinated to four atoms of the opposing species. The symmetry exhibited by crystals with a wurtzite structure is that of the  $p6_3mc$  space group, so that the  $\{10\bar{1}0\}$  planes are equivalent – the electric field on any of these faces is identical. However, because of the tetragonal nature of the zinc oxide bonding, there exists an asymmetry in the third,  $c$ -axis, direction.<sup>17,18</sup> Thus, the electric fields of the (001) and (00 $\bar{1}$ ) faces are *not*

identical. This asymmetry is thought to be the source of the oriented *c*-axis growth frequently found for ZnO<sup>19,20</sup> and oriented *a*-axis growth has been rarely reported.<sup>21,22</sup>

The nucleation and growth of monodisperse colloidal particles has been related to the supersaturation concentration by LaMer and co-workers.<sup>23</sup> Separation of nucleation and growth regimes through the introduction of precursors to a high temperature solvent has been successfully used in the synthesis of monodisperse nanometre particles.<sup>24,25</sup> The growth mechanism for small particles has been suggested by Ostwald<sup>26</sup> and described by Lifshitz and Slyozov<sup>27</sup> and by Wagner.<sup>28</sup> This growth mechanism has been associated with alcoholic zinc oxide sols.<sup>29</sup> The effect of particle encounters are examined here as a kinetic approximation that contributes to the growth of small grains that would otherwise be sacrificed to ripening, valid even in solutions with a low level of supersaturation. The growth is a function of the time derivative of the concentration gradient, so the electrical properties of the solvent affect the surface stability of the product through the diffusion coefficient. The stability has been enhanced through surface passivation by polymers<sup>30</sup> and surfactant ligands,<sup>31</sup> although the effect of steric isolation of particles from each other to prevent aggregation cannot be neglected.<sup>32</sup>

## 1.2 Synthesis

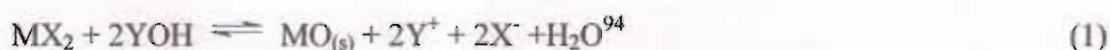
While numerous methods of synthesis of zinc oxide films and structures have been investigated including solid state reactions,<sup>33,34,35</sup> laser ablation,<sup>36,37</sup> molecular beam epitaxial growth,<sup>13,38</sup> chemical vapour deposition,<sup>39</sup> spray pyrolysis,<sup>40,41,42</sup> high- and low-frequency sputtering,<sup>5,43,44</sup> single molecular precursor methods,<sup>31,45,46</sup> chemical bath deposition,<sup>47,48</sup> electroless chemical deposition,<sup>49</sup> electrophoretic deposition,<sup>50,51</sup> electrochemical deposition,<sup>52,53</sup> seeded growth,<sup>54,55</sup> solvothermal synthesis,<sup>17,56-67</sup> micro emulsions,<sup>68,69,70</sup> base hydrolysis<sup>134,71-83</sup> and double-jet precipitation,<sup>84</sup> the sol-gel route



is favourable because of its low cost and the non-destructive nature of the processing conditions involved. The number of useful synthesis methods belies the ease with which zinc oxide can be made and controlling the size and shape presents a challenge. Surface stabilisation has been investigated using the solution counterions,<sup>134,74,81-82</sup> the addition of surfactants,<sup>20,61,76,80,84,85</sup> formation in a host matrix<sup>43,83,86</sup> and polymer modifiers.<sup>58,67,78,79,87-91</sup> Sol-gel methods, especially those involving polymeric precursors,<sup>92</sup> have also been investigated.<sup>93</sup>

### 1.2.1 Synthesis in an aqueous system

The base hydrolysis reaction producing zinc oxide can be expressed as



where the solid oxide nucleates and eventually precipitates from solution. The solubility and hydrolysis product of zinc oxide is established<sup>95</sup> in aqueous media; existing data<sup>96</sup> indicates that the least soluble equilibrium product of the reaction



in the median pH range, at 25°C, is zinc oxide. However, the growth and precipitation of this material is uncontrolled and uniform morphology is not easily obtained. The synthesis route used in mild temperature solution processing relies upon the dehydration of (soluble) zincates formed in a basic solution<sup>65,97</sup> and the preferential growth of zinc oxide.<sup>60</sup> The energy of formation values of zinc oxide in alcohols are much smaller than those in water,<sup>98</sup> since it has been reported<sup>99,100</sup> that the addition of small quantities of water catalyses the reaction, it is unclear whether this is due to the quantity of water present or the dielectric polarisability of the medium.<sup>101</sup> Either case admits the possibility of producing stable zinc oxide sols.<sup>100</sup>

### 1.2.2 Polymeric capping agents

Both hydrothermal and solution techniques for zinc oxide synthesis have been modified to include polymer composites. Poly(vinylpyrrolidone) has been most commonly investigated,<sup>79,102-105</sup> for low temperature processing, although poly(hydroxyethyl methacrylate),<sup>106</sup> poly(ethylene glycol) methyl ether,<sup>107</sup> poly(vinylalcohol)<sup>108</sup> and diblock copolymers have also been used.<sup>109,110</sup> Poly(vinylpyrrolidone) is the most widely known of the poly(vinylamide)s, with the special property that both the nitrogen atoms and carbonyl groups allow dissolution in water at a wide range of temperatures and pHs.<sup>111</sup> PVP-stabilised zinc oxide is included through the usual base hydrolysis methods, particles are considered to be stable to aggregation over a longer period of time than particles without a polymer capping layer,<sup>79</sup> even for those in the quantum confined size range. The passivation of the surface by these methods has been associated with quenching of the visible luminescence of quantum structures.<sup>105</sup> The source of the broad visible emission peak for zinc oxide is uncertain, however, it is generally attributed to the recombination of free electrons with interstitial zinc ions on the particle surface.<sup>112</sup> A reduction in the intensity of the visible light emitted may therefore indicate the more crystalline nature of the zinc oxide particles.<sup>81</sup>

### 1.2.3 Non-hydrolytic synthesis

Steric isolation of particles has also been investigated for the synthesis of zinc oxide particles through stabilisation with organic ligands, usually long-chained alkylamines or carboxylic acids, in a coordinating or non-coordinating solvent.<sup>31,68,85,113,114,115</sup> Both hot-injection and slow thermolysis have been investigated; the former relies upon the rapid injection of precursor to generate a nucleation event and subsequent drop in temperature to hinder crystal growth,<sup>32</sup> the latter on the stepwise thermal decomposition of a precursor for monodisperse growth.<sup>116</sup> In this way, monodisperse spheres and hexagonal



structures have been produced, indicative of synthesis through nucleation only and also of ripening at the reaction temperature.

#### 1.2.4 Polyol synthesis

The polymeric precursor method of synthesis<sup>117</sup> involves the formation of a precursor gel network and subsequent calcination to form the metal oxide particles. Polydentate carboxylic acids, such as citric<sup>118</sup> acid are used to chelate the zinc ions and the inclusion of polyols which act as bridging molecules to these precursor elements allows the formation of a gel. Thermal decomposition of the dried gel above 300°C then results in the formation of the product material; grain growth through sintering may occur and the particles produced are usually quite large, however, a low size distribution of the initial precursor particles is inherent in the gel formation, this can be reflected in a monodispersity of the particles produced.<sup>119</sup> Substantially lower synthesis temperatures and homogeneity of mixing is often obtained.<sup>120</sup> A common modification excludes the polyol and utilises the weaker hydrogen bonding present to form an amorphous gel.<sup>121</sup>

### 1.3 *Optical properties of zinc oxide*

#### 1.3.1 Size dependent absorption

Finitely small crystals of zinc oxide can be made such that their spatial dimensions are less than the radius of an exciton in the bulk material.<sup>122</sup> These quantum confined structures exhibit definite, tuneable absorption and fluorescence as a property of their size,<sup>12</sup> for zinc oxide, the Bohr radius is calculated to be  $\cong 3\text{nm}$  and quantum confined effects detected for particles of diameter  $\leq 8\text{nm}$ .<sup>77</sup> Confinement effects result from the change in energy of the discrete states, an artefact of the Coulomb interaction of the slowly moving exciton.<sup>123</sup> The energy of this state can be related to the size of the exciton via the effective mass approximation by



$$E^* \cong E_g + \frac{\hbar^2 \pi^2}{2R^2} \left[ \frac{1}{m_e} + \frac{1}{m_h} \right] - \frac{1.8e^2}{\epsilon R} + \text{smaller terms} \quad (4)$$

where  $E_g$  is the bulk bandgap energy,  $\hbar$  is Plancks' constant,  $m_e$  and  $m_h$  ( $= m_e m_0, m_h m_0$ ) are the effective masses of electron and hole respectively,  $e$  is the charge on an electron,  $\epsilon$  ( $= \epsilon \epsilon_0$ ) is the dielectric constant of the material and  $R$  is the exciton radius. An equivalent description has also been obtained from *ab initio* methods,<sup>124</sup> however in the work presented below, size determination was made in all cases using the former equation (4), since it is the most widely used. The absorption coefficient of an incident photon,  $\alpha$ , is related via the imaginary component of the real electric dipole moment to the bandgap of a direct bandgap semiconductor,  $E^*$ , by<sup>125</sup>

$$(\alpha h\nu)^2 = A^2 (h\nu - E^*) \quad (5)$$

where  $A$  is a constant known as the edge width parameter.<sup>42</sup> From a plot of  $(\alpha h\nu)^2$  against  $h\nu$ , a value of the optical bandgap and the associated particle radius, can therefore be extracted.  $E^*$  has also been determined by equating with the wavelength at which the absorption is half of its value at the excitonic peak<sup>82</sup> The particle size distribution is related to inhomogeneous line broadening,<sup>126</sup> by

$$n(R) \propto -\frac{dA/dR}{\pi R^3} \quad (6)$$

where  $n(R)$  is the number of particles of radius  $R$ . This means that a narrower particle size distribution will be reflected in a steeper absorption edge and a sharper absorption peak at the band-edge.

### 1.3.2 Fluorescence

Both near band-edge and deep level emission have been reported for zinc oxide.<sup>127</sup> The former has been identified as a possible UV laser source.<sup>128</sup> The confinement of an exciton inside a structure smaller than its natural radius has been shown to result in

spectral emission redshifted with respect to the absorbance,<sup>129</sup> i.e. a Stokes' shift is found, along with an increase in fluorescence due to the density of states at the bottom of the valence band increasing. Nanocrystalline zinc oxide synthesized in an alcoholic or aqueous environment has been shown to exhibit tuneable luminescence,<sup>112</sup> whereas material synthesized through non-hydrolytic routes show very little excitonic luminescence.<sup>130,115</sup> Excitonic, or near band edge, emission have been detected for free excitons, at 3.38eV ( $\cong$  370nm) for bulk zinc oxide, defect bound excitons at 3.36eV and 3.32eV and their phonon replicas at 3.28eV (387nm) and 3.21eV (386nm).<sup>127,131,132</sup> Zinc oxide exhibits green ( $\lambda \cong$  540nm, 2.29eV) fluorescence under irradiation by UV light, in this case recombination of electrons with interstitial zinc ions or oxygen vacancies on the surface has been shown<sup>133,134,135</sup> to be the mechanism by which this light is emitted. The necessity for charge transfer events related to a defect is also a characteristic of the phosphorescence of doped metal chalcogenide semiconductors.<sup>136,137</sup> Quenching of the visible zinc oxide fluorescence has been reported through surface passivation<sup>138,139</sup> and particles synthesized with no hydroxyl termination have been shown to have no surface related luminescence.<sup>131</sup> The nature of surface ligation has been shown to have an effect on the UV luminescence also<sup>139</sup> and this may explain the various UV peak intensities reported.<sup>81,62,75</sup>

#### ***1.4 Structural determination via X-Ray diffractometry***

XRD utilises the principle of Bragg reflection<sup>140</sup> to determine the location and, by extension, the arrangement of and distance between atoms in a crystal lattice. For very small domain sizes, the finite number of crystal planes means that this scattering is not ideal and a relationship between the broadening of diffracted peaks and average domain size is due to Scherrer;<sup>141</sup> for domains assumed spherical, this is



$$d = \frac{0.9\lambda}{\sqrt{B^2 - B_{ins}^2} \cos\theta_B} \quad (7)$$

where  $d$  is the diameter of the domain,  $\lambda$  is the wavelength of the incident radiation,  $\theta_B$  is the angle at which it is diffracted,  $B$  the FWHM of the peak, a measure of the peak broadening due to the small size of the domain and  $B_{ins}$  is broadening due to instrument artefacts such as the coherency of the incident beam. It should be noted that this value, because it depends upon the measurement of the FWHM of the diffraction peak, represents an average, with larger domains having a greater weight. In the case of non-spherical particles with a directional anisotropy, estimation of domain sizes along different axes will yield different results. Thus in the results presented below, Scherrer estimation of the size from the three most prominent peaks is presented where possible. TEM sizing has been used to verify that the domain size and particle size are equivalent, so domain size estimation using the Scherrer equation has been used to represent crystallite size.

### 1.5 Research objectives

The substitution of lattice cations in a II-VI or III-V semiconductor such as zinc oxide with certain transition metal ions has been found to result in ferromagnetism of the material,<sup>142</sup> in some cases above room temperature.<sup>143</sup> While discrete nanocrystals produced containing 1-5% transition metal dopants show superparamagnetic behaviour because of their size, aggregates and films composed of these nanoparticles may exhibit a greater degree of monodispersity in domain size and effective control over the anisotropy may be achieved. Thus, a solution phase synthesis route may afford the requisite conditions for production of materials with optimal properties. To this end, three routes for the synthesis of zinc oxide have been investigated, with the eventual aim of introducing transition metal dopants to these systems. Due to the coherency of

carriers required for ferromagnetic ordering, the formation of an aggregate of particles is necessary; hence the initial size of particles is not crucial to the controlled production of materials. The monodispersity of domain sizes and homogeneous distribution of dopants in the lattice *are* however important parameters.

## ***1.6 Novelty of the current work***

### **1.6.1 Carboxylic acid chelation**

Stable synthesis of a precursor gel was attempted here, in order to allow pointwise incorporation of dopants into the crystal lattice. This was investigated by varying a number of the synthesis conditions. Zinc oxide doped with transition metal ions through this method has been recently published,<sup>144</sup> but it used ethylene glycol to assist gelation and thus differs slightly from the route investigated here. The effect of the reaction conditions on the product morphology for this route has been briefly investigated,<sup>145</sup> but this study does not include the variation of chelating agent. The use of isophthalic acid for chelation of zinc ions has been previously reported.<sup>146</sup> However as far as is known, the morphology of zinc oxide powders formed from an isophthalate precursor has not yet been reported.

### **1.6.2 Polymer assisted synthesis**

The stabilisation of zinc oxide particles using poly(vinyl pyrrolidone) has been used as a modification of established routes. While the ratio of polymer to zinc ion has been previously studied,<sup>30</sup> the variation of total concentration of zinc ion in solution has not been investigated. It is believed that the positive effect of a polymer capping agent on the stability of zinc oxide nanoparticles in the presence of water has not been reported.

### 1.6.3 Organic capped zinc oxide

The thermal decomposition of precursors to form zinc oxide particles of variable size > 10nm has been reported, as has the decomposition of fixed size, quantum confined particles, by selection of appropriate capping ligands. The synthesis of quantum confined zinc oxide particles with a size dependent on the concentration of capping ligands through the slow decomposition of precursor has not been reported and was attempted here. While the variation of particle size through the inclusion of alcohols has been shown, the effect of water on an oil-phase system is presented



## 2 EXPERIMENTAL TECHNIQUES

### 2.1 Materials

Zinc acetate dihydrate,  $\text{Zn}(\text{CH}_3\text{COO})_2 \cdot 2\text{H}_2\text{O}$ , ACS,  $\geq 98\%$ , Sigma-Aldrich; Oxalic acid dihydrate,  $(\text{COOH})_2 \cdot 2\text{H}_2\text{O}$ , ACS,  $\geq 99\%$ , Sigma-Aldrich; Ethanol,  $\text{C}_2\text{H}_5\text{OH}$ , Spectroscopic grade,  $\geq 99.5\%$ , Sigma; Isophthalic acid,  $\text{C}_6\text{H}_4\text{-1,3-(COOH)}_2$ , 98%, Fluka; Acetic acid,  $\text{CH}_3\text{COOH}$ , ACS,  $\geq 99.7\%$ , Sigma-Aldrich; Isopropanol,  $\text{CH}_3\text{COHCH}_3$ , ACS,  $\geq 99.5\%$ , Sigma-Aldrich; Cyclohexanol,  $\text{C}_6\text{H}_{11}\text{OH}$ ,  $\geq 95\%$ , M&B; Poly(vinyl pyrrolidone), PVP,  $(\text{C}_6\text{H}_9\text{NO})_n$ ,  $M_w \sim 29,000$ , Aldrich; Sodium Hydroxide,  $\text{NaOH}$ , ACS,  $\geq 98\%$ , Sigma-Aldrich; Hydrochloric acid,  $\text{HCl}$ , 1N, 35.0%-37.0% ACS, Fisher; deionised water,  $\text{H}_2\text{O}$ ,  $18\text{M}\Omega\text{cm}$ , Barnstead NANOpure filter; 1-Hexadecylamine, HDA,  $\text{C}_{16}\text{H}_{35}\text{N}$ , technical grade, 90%, Aldrich; Oleic Acid, OA,  $\text{C}_{18}\text{H}_{34}\text{O}_2$ , technical grade, 90%, Aldrich; Methanol,  $\text{CH}_3\text{OH}$ , GR grade, 99%, Aldrich; Chloroform,  $\text{CHCl}_3$ , ACS, 99.8%, Aldrich; were used as received, except in the cases noted below.

### 2.2 Characterisation Methods

#### 2.2.1 X-Ray Diffraction Studies (XRD)

XRD patterns of powders were obtained by dropcasting an opaque layer of powder on a clean glass slide which was allowed to dry under ambient conditions. Patterns were recorded for  $2\theta$  values between  $10^\circ$  and  $80^\circ$  on a Siemens D500 X-Ray diffractometer operating at 40kV and 30mA and a Rigaku MSC D/Max X-ray diffractometer operating at 40kV and 40mA, both using  $\text{Cu K}_\alpha$  radiation,  $\lambda = 0.154 \text{ nm}$ . All diffraction patterns were acquired at room temperature. Estimation of the average particle size was performed using the Scherrer formula,<sup>147</sup>



$$d = \frac{0.9\lambda}{\sqrt{B^2 - B_{ins}^2 \cos^2 \theta_B}} \quad (8)$$

Where  $d$  is the crystallite size,  $\lambda$  is the wavelength of incident radiation,  $B$  is the full width at half height of the peak,  $B_{ins}$  is the full width at half height of a reference peak, an artefact of instrument broadening and  $\theta_B$  is the angle at which the radiation is diffracted.

### 2.2.2 Fourier Transform Infrared Spectroscopy (FTIR)

Transmission mode FTIR spectra were obtained between  $4000\text{cm}^{-1}$  and  $400\text{cm}^{-1}$  using a Perkin-Elmer Spectrum GX infrared spectrometer. Potassium Bromide, KBr, IR grade, Aldrich was used as a 10:1 diluent, the mixtures were finely ground and pressed under 15 tonnes to obtain a homogeneous disc.

### 2.2.3 Transmission Electron Microscopy (TEM)

Samples were deposited as dry powders on Formvar coated grids, or dropcast as solutions on carbon coated grids. Images were taken on a Jeol J100CX microscope under an accelerating voltage of 100kV, or a Jeol 2010 microscope under an accelerating voltage of 200kV.

### 2.2.4 Ultraviolet-visible absorbance spectroscopy (UV/vis)

UV/vis spectra for liquid samples were obtained between 500nm and 200nm on a Shimadzu UV-2401PC UV/vis spectrophotometer, with a resolution of 0.2nm. Quartz cuvettes, 1cm path length, containing 2.8mls of the solvent and 0.4mls of the sample solution were used. In each case, a pure sample of the solvent was used as a reference. Where band-edge estimations of particle size were made, the effective mass model<sup>123</sup> (4) was used, with parameters obtained from the literature.<sup>148</sup>

**Table 1 Parameters used to estimate particle size from band edge calculations**

Planck's constant	$\hbar$	$1.05 \times 10^{-34}$	J.s
Charge on an electron	$e$	$1.60 \times 10^{-19}$	C
Free electron mass	$m_0$	$9.11 \times 10^{-31}$	kg
Electron effective mass	$m_e$	0.26	
Hole effective mass	$m_h$	0.59	
Permittivity of free space	$\epsilon_0$	$8.85 \times 10^{-12}$	F m <sup>-1</sup>
Dielectric permittivity of zinc oxide	$\epsilon$	8.5	
Bulk band gap	$E_g$	3.2	eV

#### 2.2.5 Fluorescence spectroscopy (PL)

Photoluminescence emission spectra were obtained for liquid samples excited at 300nm, between 325nm and 580nm and for those excited at 325nm between 350nm and 625nm, using a Jobin Yvon/Horiba Fluoromax-3 spectrofluorometer. Four-windowed quartz cuvettes, with a 1cm side, were used and emission spectra were recorded at an angle of 90° to the excitation direction. Samples were prepared by diluting 100µls of the sample solution in 3.2mls of solvent.

#### 2.2.6 Differential Scanning calorimetry (DSC)

DSC was performed using a Rheometric QC DSC with a ramp rate of 5°C per minute under flowing nitrogen, from room temperature to 500°C. In each case, the sample was heated twice in order to ensure that the phase changes and decomposition reactions were identified.

#### 2.2.7 Scanning Electron Microscopy (SEM)

Powders were ground in isopropanol and the resulting slurry was deposited on a clean glass slide, which was then allowed to dry under ambient conditions. This was then coated with a layer of amorphous carbon. SEM images were recorded on a Jeol 8600 microprobe operated at an accelerating voltage of 15kV and 7.5kV.

## 2.3 Synthesis Methods

### 2.3.1 Powders prepared through carboxylic acid precursors

Stock solutions containing 1mmol (0.219g) zinc acetate dihydrate in 10mls ethanol, or an equal ratio, were prepared by stirring at 50°C for 30 minutes. Solutions of the carboxylic acid, at the concentration indicated in each experiment, were also prepared, by stirring at room temperature for 30 minutes. The total volume of solutions was kept constant and the ratio of zinc ions to carboxyl groups varied by changing the concentration of acid, if required. These solutions were combined and stirred at room temperature for 30 minutes. Products were dried at 100°C in an oven, ground and calcined at the required temperature in a muffle furnace with a ramp rate of 10°C per minute.

### 2.3.2 Nanoparticles prepared through polymer-assisted alkaline hydrolysis

Stock solutions were prepared containing 0.3mmol (68.57mg) zinc acetate dihydrate in 50mls isopropanol and 1mmol (40mg) sodium hydroxide in 50mls isopropanol, by vigorously stirring at room temperature. Solutions of the required concentration of PVP were similarly obtained. 4mls of the zinc acetate stock was vortex-mixed with 1ml of the polymer solution for 30 seconds. 2.5mls of the sodium hydroxide solution was added at room temperature and the solution was further vortex mixed. In the case where the amount of any reagent was varied, isopropanol was added to ensure that the total volume of sample remained constant.

### 2.3.3 Organic-capped zinc oxide

Zinc acetate dihydrate was calcined at 110°C for 4 hours to remove water of hydration. To the required concentration of this, 2mmol (5g) hexadecylamine and 5mmol (4.2ml)



oleic acid were stirred at room temperature under argon flow in a round bottomed flask for 30mins. This mixture was then heated to 100°C and maintained at that temperature for 1 hour, to allow complete dissolution of the reagents. This was then allowed to cool to room temperature and heated to the desired final temperature. All processes were carried out under flowing argon. After the determined period of time, the flask was allowed to cool, when it had reached 100-130°C, its contents were added to 50mls of methanol, allowed to settle and centrifuged at 3000 rev/min for 15mins. In the case where aliquots were taken, 1ml of the solution was withdrawn through a septum and added to 10mls of methanol. In some cases, the supernatant fluid was decanted and the white precipitate redispersed in isopropanol in an ultrasonic bath. This solution was centrifuged, the supernatant decanted and the powder dispersed in chloroform or toluene.

### 3 POWDERS PREPARED THROUGH CARBOXYLIC ACID CHELATION

Nanoparticulate zinc oxide was prepared through the high-temperature decomposition of an organic precursor material. The precursor powders were prepared through the gelation of carboxylic acids at mild temperatures, drying and subsequent calcination. Two bidentate carboxylic acids were investigated: oxalic acid and isophthalic acid.

#### 3.1 *Use of oxalic acid as a chelating agent*

Powders were synthesized in a  $[\text{Zn}^{2+}]:[(\text{COOH})_2]$  ratio of 1:2, calcined to temperatures in the range 100°C to 500°C and their composition and morphology investigated. Gelation occurs within minutes for this system, with associated increase in viscosity and possible reduction in reaction completeness. Because of this, comparison was thus made between powders synthesized over a period of time longer than the gelation time and those synthesized over time comparable to that of gelation. Additionally, gel powders were produced under no stirring in ratios  $[\text{Zn}^{2+}]:[(\text{COOH})_2]$  of 1:1 and 1:2. A  $[\text{Zn}^{2+}]:[(\text{COOH})_2]$  ratio of 1:100 was investigated with a total zinc concentration of one tenth that of the previous solutions; the supernatant fluid was decanted, dried at 100°C, calcined at 500°C and examined using TEM. Powders were also synthesized in the original ratio of zinc ions to oxalic acid, in an excess of acetic acid, in order to understand the role of acetic acid in this reaction.

#### 3.2 *Use of isophthalic acid as a chelating agent*

Oxalic acid and isophthalic acid are both bidentate carboxylic acids, of relatively low molecular weight, soluble in ethanol at the concentrations used here. Isophthalic acid shares with oxalic acid dissociation constants that are lower than that of acetic acid, the

analog of which forms the zinc counterion. These are shown in Table 2. The values refer to aqueous solutions. The less polar medium used here means that only the reagents' relative values can be examined. As can be seen from Table 2, the first deprotonation of each carboxylic acid molecule is a much more favourable event than the loss of the second proton, it is therefore possible that in an excess of the acid, each zinc ion becomes coordinatively bound to *two* of the bidentate ligands.

**Table 2** Dissociation constants of materials used, in dilute aqueous solutions at 25°C<sup>149</sup>

Material	Dissociation Constant	
	pK <sub>a1</sub>	pK <sub>a2</sub>
Oxalic Acid, (COOH) <sub>2</sub>	1.25	3.81
Acetic Acid, CH <sub>3</sub> COOH	4.76	
Isophthalic Acid, C <sub>6</sub> H <sub>4</sub> -1,3-(COOH) <sub>2</sub>	3.70	4.60

Since the solubility of isophthalic acid is much lower, the dissociation probability of zinc ions will also be higher for the precursor formed. The possible variation in surface stabilisation and change in particle size associated with this precursor and the change in gelation rate provide the motivation for investigating this chelating agent. Precursor powders were synthesized with [Zn<sup>2+</sup>]:[C<sub>6</sub>H<sub>4</sub>-1,3-(COOH)<sub>2</sub>] ratios of 1:1, 1:2 and 1:5 and calcined at 500°C and 800°C. XRD, TEM, SEM and FTIR analysis were used to characterise the resulting powders. The effect of solvent was investigated by synthesizing 1:10 powders in isopropanol and cyclohexanol and performing TEM analysis on powders calcined to 500°C.

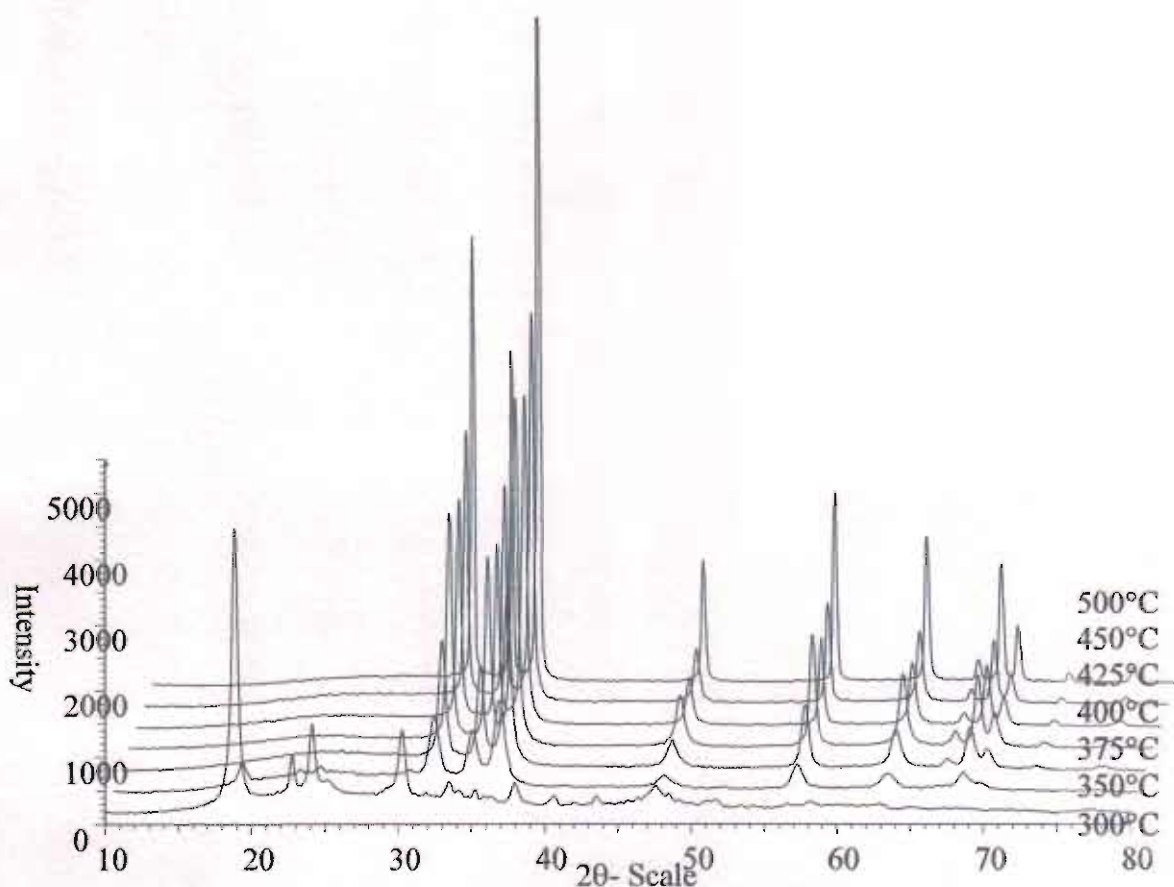
### 3.3 Results - oxalic acid as a chelating agent

#### 3.3.1 Effect of reaction time on temperature evolution of powders

The evolution of powders produced in short and long reaction times and calcined at 300°C, 350°C, 375°C, 400°C, 425°C, 450°C, 475°C, 500°C are shown in Figure 1 and

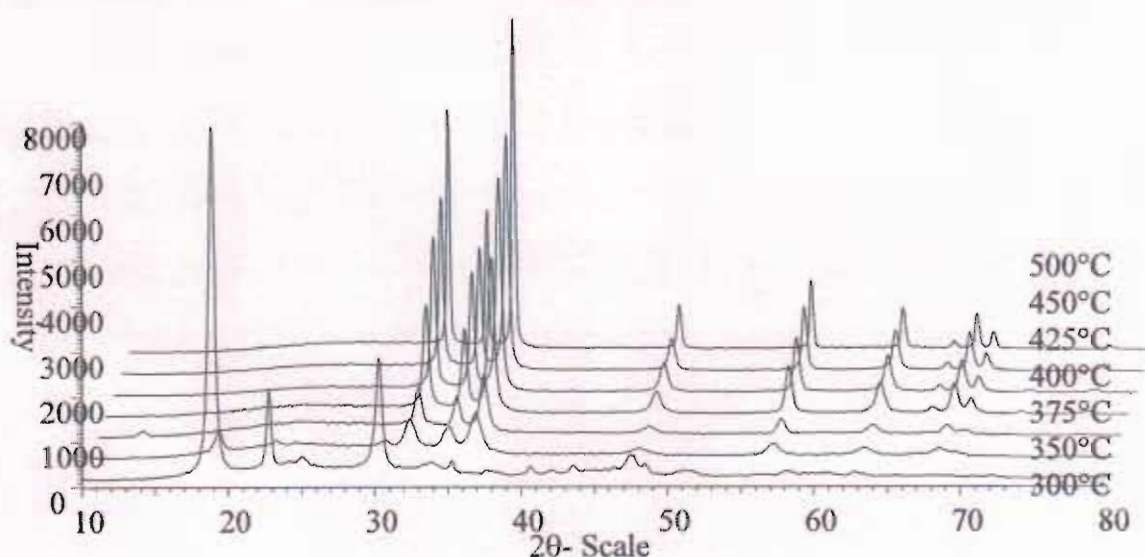


Figure 2. The gelation of the precursor was determined by observation of sample turbidity and the rate of addition of chelating agent adjusted so that this material was viscous and turbid before all of the reagents were combined.



**Figure 1 XRD patterns for powders synthesized rapidly and calcined at various temperatures.**

Both synthesis methods show a qualitative increase in crystallinity of the product and similar peak intensity for each calcination temperature can be seen. The intensity of each peak detected depends, in addition to the crystallinity of the material being examined, on the amount of powder present and the number of X-rays emitted by the source. While attempts were made to reduce the variation of both these factors, their influence cannot be neglected and inhibit quantitative comparison of diffractograms.



**Figure 2** XRD patterns for powders synthesized in a reaction longer than the gelation time and calcined at various temperatures.

The angles at which peaks were found for powders calcined to 300°C, their relative intensities and reference peaks that can be associated with each are shown in Table 3. It was immediately obvious that more peaks were resolved in the case of the powders synthesized in a short reaction time, since they were of low (<10% of maximum) intensity, this could reflect a more crystalline product, or simply more of it. In both cases peaks were detected that could be assigned to zinc oxalate hydrate<sup>150</sup> ( $C_2O_4Zn \cdot 2H_2O$ ), anhydrous zinc oxalate<sup>151</sup> ( $C_2O_4Zn$ ) and to zincite<sup>15</sup> ( $ZnO$ ). Peaks were also present that could be assigned to the monoclinic and orthorhombic phases of anhydrous oxalic acid, in particular the strong peaks of monoclinic oxalic acid<sup>152</sup> coincided with peaks found in the powders synthesized through rapid addition of reagents, possibly due to the excess of chelating agent used. However, these peaks varied in position by up to a degree from the card values and could be associated with zinc oxalate with similar accuracy. The maximum intensity peaks of zinc acetate, in its



anhydrous or hydrated forms, were not detected; this was as expected since the salt was completely dissolved before mixing.

**Table 3 Resolvable XRD peaks for precursor powders calcined to 300°C**

Slow addition, 2 $\theta$	Intensity, %	Rapid addition, 2 $\theta$	Intensity, %	Assignment
		15.217	5.2	Unidentified peak
18.854	100.0	18.854	100.0	C <sub>2</sub> O <sub>4</sub> Zn.2H <sub>2</sub> O (-202)
22.745	27.0	22.737	22.8	C <sub>2</sub> O <sub>4</sub> Zn.2H <sub>2</sub> O (002)
		24.097	33.1	C <sub>2</sub> H <sub>2</sub> O <sub>4</sub> (011)
25.058	8.3	25.152	14.6	C <sub>2</sub> O <sub>4</sub> Zn.2H <sub>2</sub> O (-112)
30.294	36.1	30.258	31.1	C <sub>2</sub> O <sub>4</sub> Zn.2H <sub>2</sub> O (-402)
31.687	5.6	31.907	10.2	ZnO (100)
33.875	6.6	33.473	13.9	C <sub>2</sub> O <sub>4</sub> Zn.2H <sub>2</sub> O (-113)
		34.151	10.9	C <sub>2</sub> H <sub>2</sub> O <sub>4</sub> (021)
35.263	7.0	35.250	11.3	C <sub>2</sub> O <sub>4</sub> Zn.2H <sub>2</sub> O (021)
		36.348	8.8	C <sub>2</sub> H <sub>2</sub> O <sub>4</sub> (-211)
37.647	4.4			Unidentified peak
		37.949	13.5	C <sub>2</sub> O <sub>4</sub> Zn (210)
40.632	5.3	40.636	9.0	C <sub>2</sub> O <sub>4</sub> Zn.2H <sub>2</sub> O (022)
43.622	5.6	43.524	8.8	C <sub>2</sub> O <sub>4</sub> Zn.2H <sub>2</sub> O (-223)
		45.687	7.4	C <sub>2</sub> O <sub>4</sub> Zn.2H <sub>2</sub> O (-422)
46.378	5.0	46.423	8.5	Unidentified peak
47.517	8.4	47.598	12.5	Unidentified peak
48.507	6.1	48.475	9.9	C <sub>2</sub> O <sub>4</sub> Zn.2H <sub>2</sub> O (023)
		49.205	7.7	Unidentified peak
51.746	4.1	51.600	7.7	C <sub>2</sub> O <sub>4</sub> Zn.2H <sub>2</sub> O (130)
		52.508	5.7	Unidentified peak
53.622	2.8	53.348	5.8	Unidentified peak
		54.287	5.9	C <sub>2</sub> O <sub>4</sub> Zn.2H <sub>2</sub> O (131)
		56.608	6.4	Unidentified peak
58.246	4.0	58.162	7.1	Unidentified peak
62.820	3.8	62.968	6.7	C <sub>2</sub> O <sub>4</sub> Zn.2H <sub>2</sub> O (-804)
63.349	3.5	63.296	6.1	C <sub>2</sub> O <sub>4</sub> Zn.2H <sub>2</sub> O (-621)

A number of low intensity peaks were detected that cannot be associated with any of the possible material present. These could be spurious peaks resulting from the low signal to noise ratio of the diffraction patterns. As previously stated, the dissociation constants of the oxalic acid and the concentrations of reagents used may have led to the chelation of each zinc ion with two, singly deprotonated, oxalic acid ligands. No reference was found for a crystalline phase of this nature in the standard library.

The diffraction patterns for both samples calcined to 350°C exhibited a relatively low signal to noise ratio, this may have been because of the decomposition of the precursor, leading to amorphous material after heating at this temperature. DSC was performed to identify the temperature at which this decomposition occurred and these measurements are shown in Figure 3. Both samples showed that heat was absorbed between 350°C and 400°C. This may indicate the formation of a crystalline product, possibly through decomposition of chelating ligands. The low intensity of XRD patterns for samples heated to below this temperature may reflect the temperature at which the formation reaction occurred.

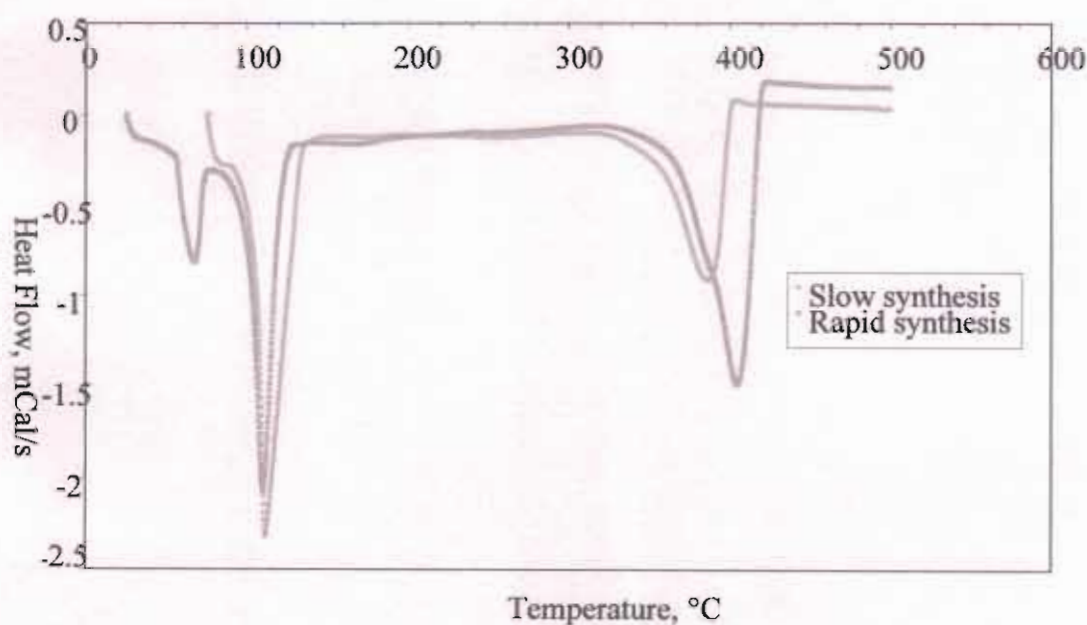


**Figure 3 DSC of precursor powders**

XRD peaks resolved for both sets of powders calcined to 350°C are shown in Table 4. Here, the low crystallinity and small quantity of material characterised may have led to a decreased signal to noise ratio and the detection of low intensity, spurious peaks. In both the samples calcined to 300°C and 350°C, combination of reagents before the



gelation proceeds led to the observation of both hydrated zinc oxalate and the diffraction pattern associated with anhydrous zinc oxalate or with anhydrous oxalic acid. Only crystalline zinc oxalate hydrate was identified for the samples synthesized in the reaction occurring over timescales equivalent to that of the gelation of the precursor.

The resolvable peaks for XRD patterns of samples calcined to 375°C, 400°C, 425°C, 450°C and 500°C are tabulated in Tables A2 – A6 in the Appendix. In all cases, powders synthesized through rapid addition of reagents showed only peaks that could be associated with zinc oxide, whereas the slow addition of reagents, which led to only hydrated zinc oxalate being detected initially, showed additional low intensity diffraction peaks. Since these peaks could not be associated with any existing patterns and are not present in consecutive diffraction patterns, it was probable that they reflected the poorer resolution of these powders.

**Table 4 Resolvable XRD peaks for precursor powders calcined to 350°C**

Slow addition, 2 $\theta$ value	Intensity, %	Rapid addition, 2 $\theta$ value	Intensity, %	Assignment
13.100	15.8			Unidentified peak
18.783	66.4	18.807	38.9	C <sub>2</sub> O <sub>4</sub> Zn.2H <sub>2</sub> O (-202)
22.739	47.5	22.727	31.8	C <sub>2</sub> O <sub>4</sub> Zn.2H <sub>2</sub> O (-202)
		23.380	30.2	Unidentified peak
		24.155	34.6	C <sub>2</sub> H <sub>2</sub> O <sub>4</sub> (011)
26.595	39.7			Unidentified peak
30.266	46.9			C <sub>2</sub> O <sub>4</sub> Zn.2H <sub>2</sub> O (-402)
31.899	88.6	31.952	83.7	ZnO (100)
34.541	73.9	34.546	70.6	ZnO (002)
36.000	77.1			Unidentified peak
36.353	100.0	36.384	100.0	ZnO (101)
37.560	28.9			Unidentified peak
47.531	30.1	47.622	25.8	ZnO (102)
56.833	39.2	56.751	36.6	ZnO (110)
61.732	20.9			Unidentified peak
62.984	31.2	62.898	26.4	ZnO (103)
67.743	26.2	63.096	26.6	Unidentified peak
68.076	30.7	68.147	28.8	ZnO (112)
69.185	23.0	75.429	10.4	ZnO (201)

Diffraction peaks related to anhydrous zinc oxalate were not seen for powders calcined at 375°C or above, however, those assigned to zinc oxalate hydrate were present in the XRDs of the precursor powders synthesized through slow addition of reagents when calcined to 375°C. This may reflect the greater proportion of hydrated zinc oxide present in this sample. DSC shows that the decomposition of precursors continued to higher temperatures for the sample containing both hydrated zinc oxalate and the second material detected than for that with only hydrated zinc oxalate. The XRD patterns may indicate that amorphous material is present at this temperature, or the more complete conversion to zinc oxide of the precursor powder formed by rapid addition of reagents.

### 3.3.2 The nature of the oxalate precursors

In the above experiments, both synthesis routes involved identical quantities of reagents, a stirring step after their combination and subsequent drying and calcination steps, in order to eliminate the potential for variation in product properties due to processing. The only difference in synthesis methods was the monotonic increase in viscosity and related reduction in diffusivity caused by the gelation of the reaction products under the slow addition of oxalic acid. Thus, for the powders synthesized through slow addition, it was possible for the system to attain local equilibrium, *i.e.*, for oxalic acid molecules that have been doubly deprotonated to chelate. Both hydrated zinc oxalate and what could be anhydrous zinc oxalate were present in the precursor prepared through rapid addition, but only the hydrated form was present in those prepared by slow addition. In order to explain the differences in precursors formed and product crystallinity between these reactions, the following hypothesis is proposed. It is believed that, in the case of precursors synthesized through rapid combination of



reagents, the pseudo-instantaneous reaction allows the chelation of each zinc ion to two (the stoichiometric ratio) oxalic acid molecules, thus:



**Figure 4 Schematic of precursor proposed to have formed under rapid combination of reagents**

For precursors synthesized through slow combination of reagents, the concentration of oxalic acid increases with time, however, the viscosity also increases with time. It is suggested that in this case initially, each oxalate molecule is coordinatively bound to two zinc ions, as below. The rapid gelation of this material prevents the solution reaching the equilibrium proposed in Figure 4 for all species and a greater amount of unreacted oxalic acid may also be present. In short, the uncommonly rapid gelation in this process overwhelms the potential of the excess to dissociate and act to stabilise the system.

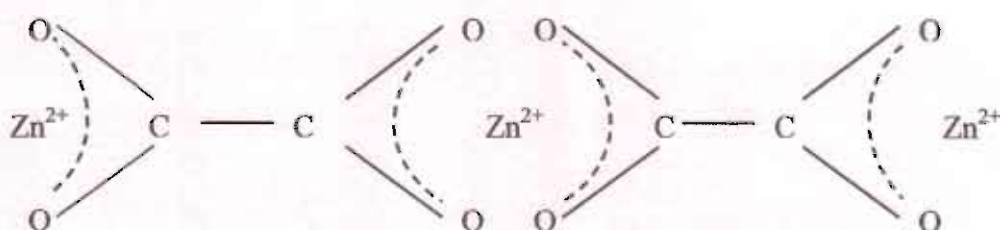


**Figure 5 Schematic of structure proposed to have formed under slow combination of reagents**

From the XRD data presented, it is clear that two phases are detected for the precursor powders synthesized through *rapid* combination of reagents, but not for those synthesized through *slow* combination of reagents. This does not fully support the



hypothesis outlined on p31. However, it must be borne in mind that rapid combination of reagents only imitates an instantaneous reaction and the precursor proposed in Figure 5 may also be formed, to a much lesser extent. The PDF for the structure shown in Figure 4 was not found, so it was not possible to relate the unidentified peaks found in the precursor to this material. Also, an amorphous precursor will not be detected by this method, for this reason, FTIR spectroscopy was performed on several of the precursor and product powders.

### 3.3.3 Surface properties of the particles

FTIR spectroscopy was performed on powders calcined at 350°C, 375°C and 475°C and the spectra are presented in Figure 6 and Figure 7. Figure 8 shows transmission spectra for powders synthesized through both methods and calcined to 400°C. Both spectra show that the symmetric carboxylic peaks at  $1365\text{cm}^{-1}$  and  $1320\text{cm}^{-1}$ , present in precursor powders when calcined to 350°C, were absent in those calcined at higher temperatures. A prominent peak related to the asymmetric  $\text{COO}^-$  bond at  $1620\text{cm}^{-1}$  was present in all powders synthesized through slow addition of reagents, this may have been due to stabilisation of the surfaces of the product particles by the counterion, or may have been indicative of unreacted reagent. Since a peak, thought to be the absorbance of atmospheric water, was present at approximately  $3400\text{cm}^{-1}$  in all powders, it is unlikely that the changing intensity of the peak at  $1625\text{cm}^{-1}$  could have been related to water. The shape of this peak for the powders calcined to 350°C is also of interest.

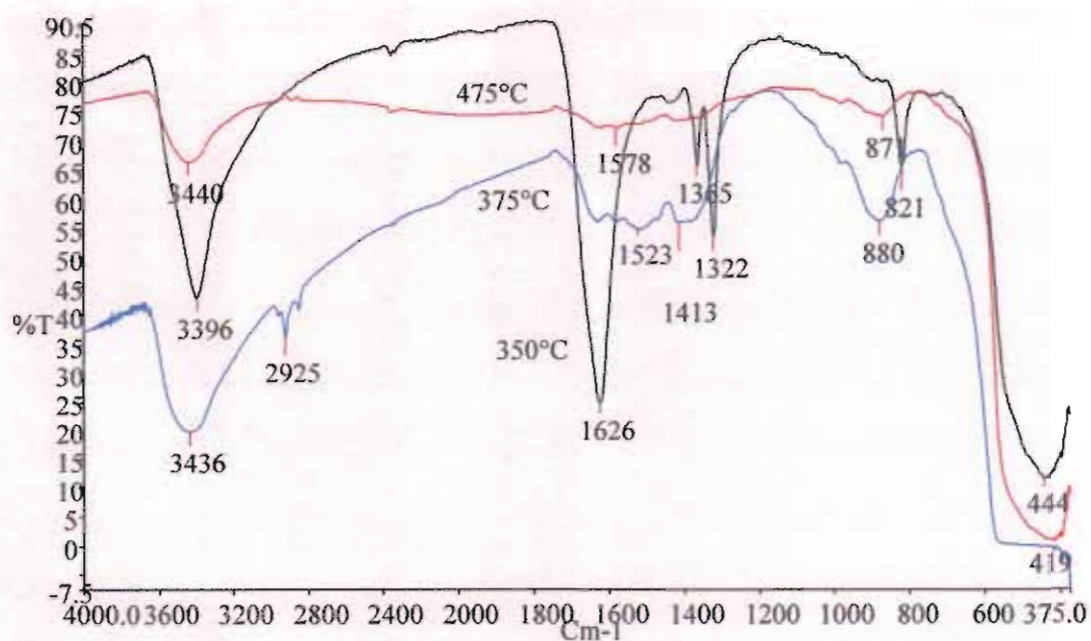


**Figure 6 FTIR spectra of powders prepared through rapid combination of reagents: 350°C, 375°C and 475°C**

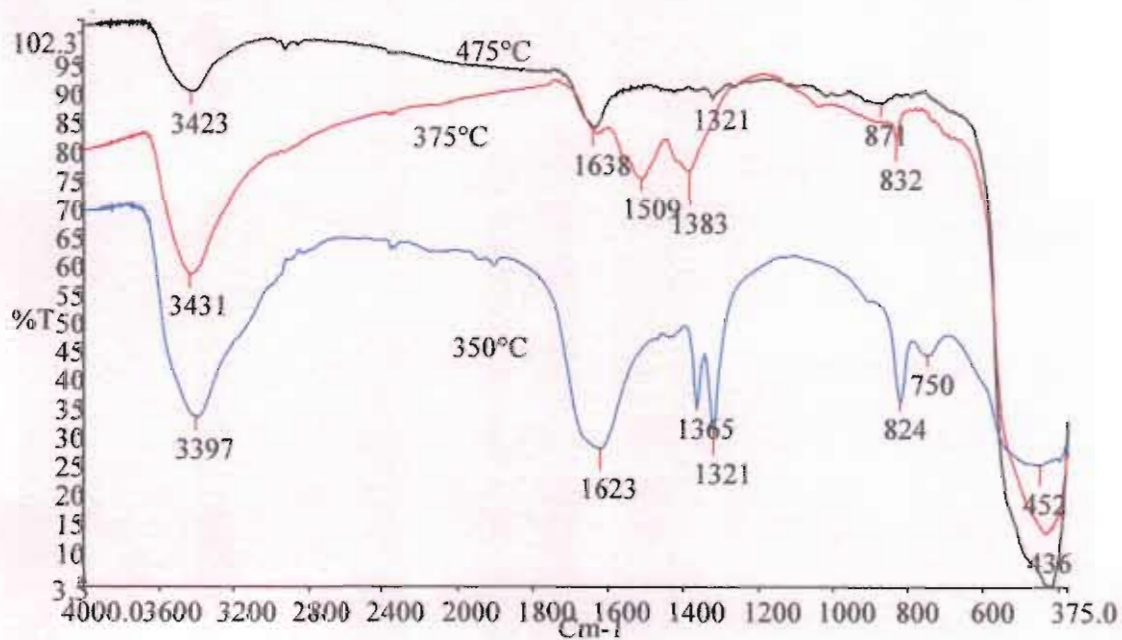


**Figure 7 FTIR spectra of powders formed through slow combination of reagents: 350°C, 375°C and 475°C**

From the hypothesis outlined in section 3.3.2, it is believed that rapid combination of reagents leads to a more homogeneous precursor than their combination over an extended time period, which it is proposed, contained carboxyl groups coordinatively bound to either hydrogen or zinc ions. The absorbance band at  $1622\text{cm}^{-1}$  was asymmetrically broadened, but exhibited a sharp apex, indicating that one resonance dominated here. For the precursor powders synthesized through slow addition of reagents, it was found that the equivalent peak was much flatter, in agreement with the hypothesis that a transient state had been preserved and oxalate molecules bound to two zinc ions *and* oxalic acid molecules were present, as well as oxalate molecules chelating zinc ions in the stoichiometric ratio of the experiment. This spectrum also contained an absorbance at  $750\text{cm}^{-1}$ , not present in the equivalent spectrum shown in Figure 6. Figure 8 shows that carboxyl groups remained for the powders synthesized through slow addition of precursor, but a lesser absorption was apparent for particles synthesized by rapidly combining powders.

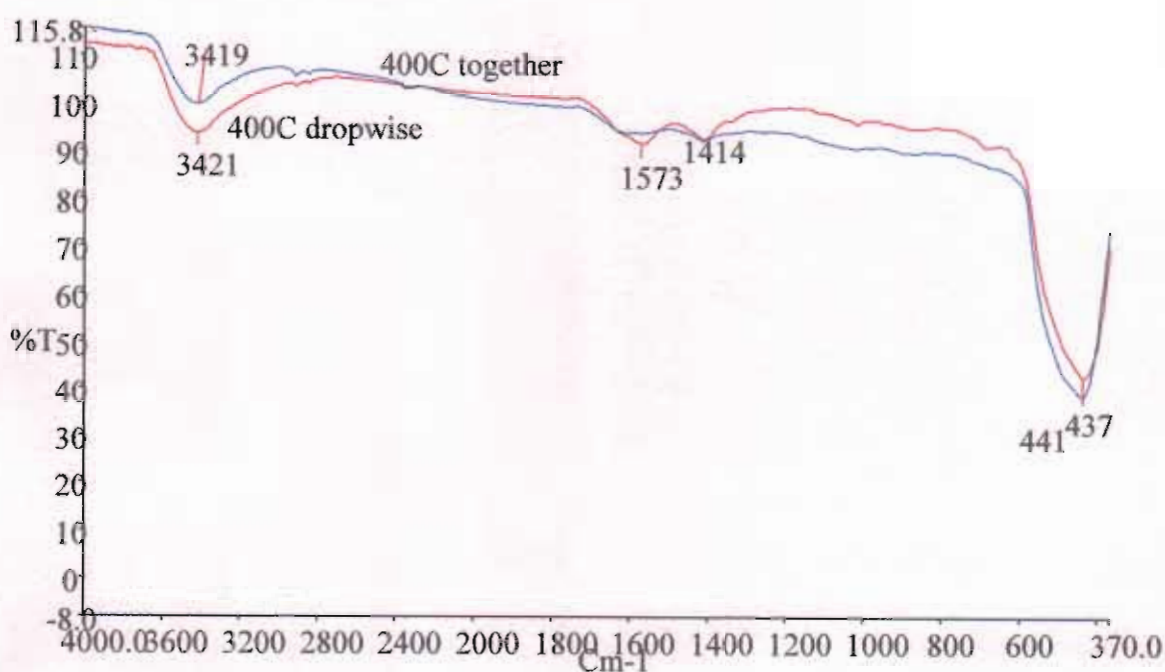


**Figure 8** FTIR spectra of powders calcined to  $400^{\circ}\text{C}$



TEM images of the precursor powders were obtained at magnifications of 50,000x and 150,000x. Particles were counted and size distributions obtained over approximately 50 particles. The distribution of the precursor powders synthesized through the slow addition of reagents, normalised for the total number of particles in each image, is presented in Figure 9. The broader size distribution evident for powders calcined to higher temperatures was probably a result of particle aggregation, while the particles calcined to 350°C, which showed incomplete decomposition of precursor, had sizes in the 10-25 nm range and a narrow distribution. Size distributions of particles produced through both methods and calcined to 350°C and 375°C are shown in Figure A 1 and Figure A 2 of the Appendix. It can be seen that there was no substantial variation in particle size between synthesis methods.

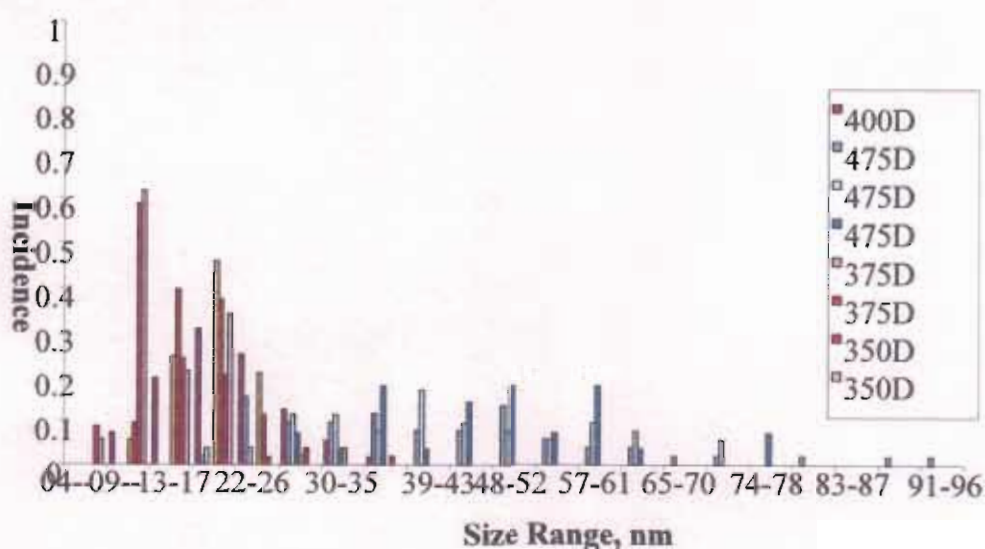


**Figure 9 Size distribution of particles calcined to 350°C, 375°C and 475°C**

From the data presented above, it is apparent that the rate at which an experiment was conducted had a significant effect on the precursor produced; it is counter-intuitive that a more homogeneous precursor was formed through the rapid combination of reagents.

An explanation has been presented for this in terms of the short gelation time in the case of this precursor. FTIR and XRD studies further showed that the more homogeneous precursor, upon calcination up to 500°C, produced a product of approximately the same size, but with fewer surface groups and affecting more intense diffraction peaks, than in the case of slow combination of reagents. This precursor is thought to consist of a network of zinc ions each coordinatively bound to two oxalate molecules, as opposed to a network of zinc ions bound to each of the carboxyl groups of oxalate molecules.

### 3.3.4 Variation of carboxylic acid concentration

XRD patterns for precursor powders synthesized through the rapid addition of oxalic acid in  $[\text{Zn}^{2+}]:[(\text{COOH})_2]$  ratios of 1:1 and 1:2, *without* stirring of the gelating product, are shown in Figure 10.

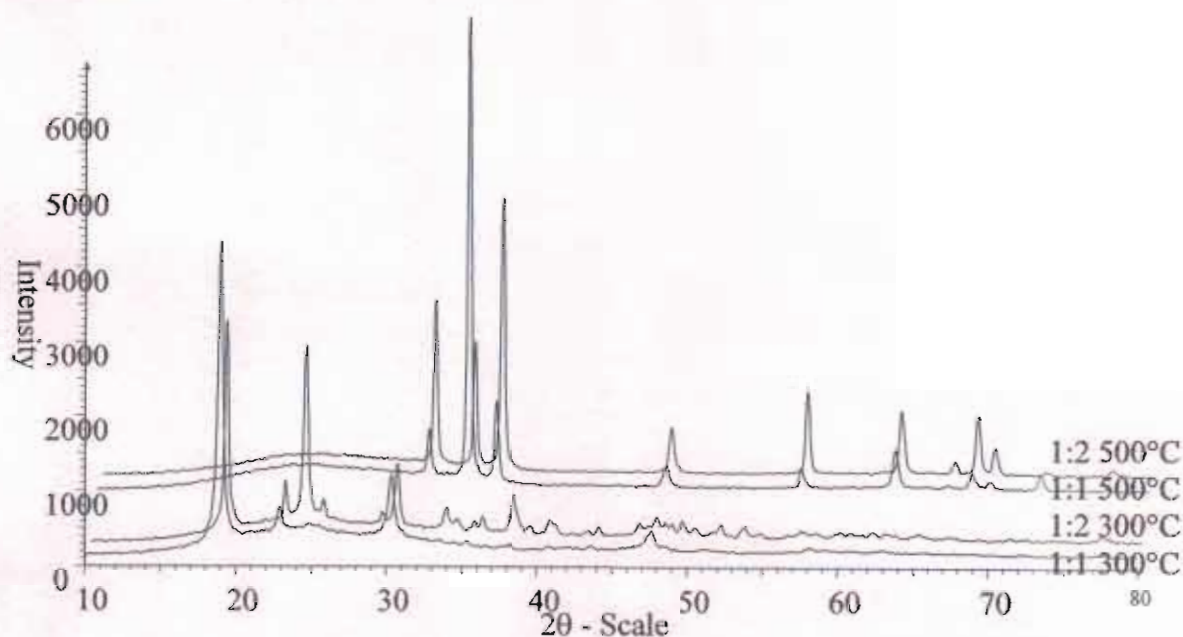


**Figure 10 XRD patterns for powders synthesized in a 1:1 and 1:2 ratio through diffusion of reagents only**

From this, it is clear that two phases were present in the powders containing a 1:2 ratio of reagents, only one of which was present in the 1:1 precursor powders. Both samples,



when calcined to 500°C, showed only peaks characteristic of zinc oxide. The most intense peak in the diffraction pattern for the 1:1 sample was the (002) peak, indicating that the material made through this method was oriented or had aggregated in the *c*-axis direction. Orientation may have been an artefact of the method of preparation. Glass slides of the precursor powders, which were then calcined, were prepared in this case. The 1:1 precursor can be viewed as the limiting case of slow combination of reagents and the converse is true for the 1:2 sample here, *i.e.* the system endeavours to mimic an infinitely long and short reaction time with respect to gelation. A 1:1 ratio of reagents is also a system with greater likelihood of attaining an equilibrium such as that shown in Figure 5 more quickly. The fact that two phases appeared in the 1:2 sample here may again reflect the finite time required for addition of oxalic acid in this case. The resolvable peaks for both powders when calcined to 300°C are provided in Table 5 (a table for equivalent precursors synthesized through slow and rapid combination of reagents is shown in the appendix, Table A1). The peaks present in both spectra were indexed to hydrated zinc oxalate, those found in the 1:2 sample only have been associated with anhydrous oxalic acid and anhydrous zinc oxalate, this agrees with the previous study. However, both matches exhibited discrepancies in the intensities of peaks, the zinc oxalate hydrate pattern listed strong peaks for which there is no evidence, at  $2\theta = 24.7^\circ$  and  $33.7^\circ$ , similarly the anhydrous zinc oxalate pattern listed many weak peaks, most but not all of which could be matched to within  $2\theta = 0.3^\circ$  to those detected. These peaks all coincided within a degree with the strong peaks of anhydrous oxalic acid and have been assigned to this phase in Table 5. However, both materials, as well as some other, unidentified phase, are possible. Additionally, both diffraction patterns exhibited low intensity peaks that could not be assigned to either pattern; however, these may have been related to impurities or the substrate background.



Previous examination of the effect of synthesis method on the crystallinity of the zinc oxide product showed more intense peaks for the powders synthesized through *rapid addition* of oxalic acid, indicating that the material present in only the 1:2 powders decomposed at slightly higher temperatures, but with a more crystalline yield. The height of the (101) peak in samples calcined to 500°C was used to gauge their crystallinity in this case; this correlated with previous findings, regardless of orientation of the sintered particles.

**Table 5 Resolvable XRD peaks 1:1 and 1:2 precursor powders calcined to 300°C**

1:2 300°C 2θ	Intensity, %	1:1 300°C 2θ	Intensity, %	Assignment
18.962	100.0	18.945	100.0	C <sub>2</sub> O <sub>4</sub> Zn.2H <sub>2</sub> O (-202)
22.883	29.8	22.877	17.9	C <sub>2</sub> O <sub>4</sub> Zn.2H <sub>2</sub> O (002)
24.264	88.8			C <sub>2</sub> H <sub>2</sub> O <sub>4</sub> (011)
25.422	21.9			C <sub>2</sub> H <sub>2</sub> O <sub>4</sub> (-111)
29.391	16.5			C <sub>2</sub> H <sub>2</sub> O <sub>4</sub> (020)
30.334	37.4	30.342	27.4	C <sub>2</sub> O <sub>4</sub> Zn.2H <sub>2</sub> O (-402)
33.606	18.4			C <sub>2</sub> H <sub>2</sub> O <sub>4</sub> (-102)
34.277	13.7			Unidentified peak
35.451	12.5	35.342	7.6	C <sub>2</sub> O <sub>4</sub> Zn.2H <sub>2</sub> O (021)
35.991	14.6			C <sub>2</sub> H <sub>2</sub> O <sub>4</sub> (-211)
38.086	23.9	38.149	6.7	Slide background
39.153	10.4			C <sub>2</sub> H <sub>2</sub> O <sub>4</sub> (-202)
40.531	13.0	40.782	6.1	C <sub>2</sub> O <sub>4</sub> Zn.2H <sub>2</sub> O (022)
42.989	8.4			C <sub>2</sub> O <sub>4</sub> Zn (21-2)
43.740	10.4	43.688	6.3	C <sub>2</sub> O <sub>4</sub> Zn.2H <sub>2</sub> O (221)
46.449	11.6			C <sub>2</sub> O <sub>4</sub> Zn (121)
47.566	14.4	47.614	10.6	C <sub>2</sub> O <sub>4</sub> Zn.2H <sub>2</sub> O (-421)
		48.700	6.1	C <sub>2</sub> O <sub>4</sub> Zn.2H <sub>2</sub> O (023)
49.358	12.8			C <sub>2</sub> O <sub>4</sub> Zn (220)
50.132	9.9			C <sub>2</sub> O <sub>4</sub> Zn (112)
51.913	11.2			C <sub>2</sub> O <sub>4</sub> Zn (022)
53.458	10.5			C <sub>2</sub> O <sub>4</sub> Zn (31-2)
54.492	7.6			Unidentified peak
57.342	8.5			C <sub>2</sub> O <sub>4</sub> Zn (031)
58.255	7.9	58.349	5.6	Unidentified peak
59.793	8.3			C <sub>2</sub> O <sub>4</sub> Zn (32-1)
61.995	8.1			C <sub>2</sub> O <sub>4</sub> Zn (301)
62.955	7.7			Unidentified peak
65.059	7.7			C <sub>2</sub> O <sub>4</sub> Zn (40-2)
77.355	6.6			C <sub>2</sub> O <sub>4</sub> Zn (14-1)

Because of the better crystallinity resulting from the phase found only in the 1:2 precursor powders, higher ratios of oxalic acid to zinc ions were investigated. For particles synthesized in a 1:100 excess of oxalic acid, a reduction in zinc ion concentration by one order of magnitude was necessary to ensure complete dissolution of reagents. Because of the possibility that precursor particles would be stabilised in the liquid state by the chelating molecules, the supernatant fluid was calcined and analysed in this case.

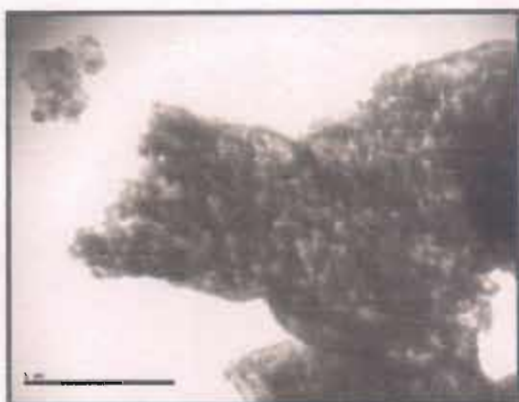


**Figure 11 TEM image of precursor material calcined to 500°C, 40000X**

A TEM image of the powders calcined to 500°C, at magnification of 40,000x, is presented in Figure 11. Here, it is possible to identify from the columnar superstructure, the oriented aggregation of the sintered particles. The presence of a large collection of such columns may have been indicative of a more extensive precursor gel than for lower ratios of zinc ion to chelating ligand.

Variation of the ratio of zinc ion to oxalate molecule led to the conclusion that higher ratios resulted in a more crystalline product. In order to ensure that the increased number of protons was not a factor, experiments were undertaken using different amounts of acetic acid. Powders were synthesized in a ratio of zinc acetate to acetic acid



of 1:15 and 1:87, *i.e.* by replacing 15mmol (0.86ml) and 87mmol (5ml) acetic acid for equal volumes of the solvent in the standard preparation. Acetic acid, being unidentate, will not have the chelating effect of similar quantities of oxalic acid, but may enhance stabilisation of the surface or reduce dissociation of the second proton from each oxalic acid molecule.

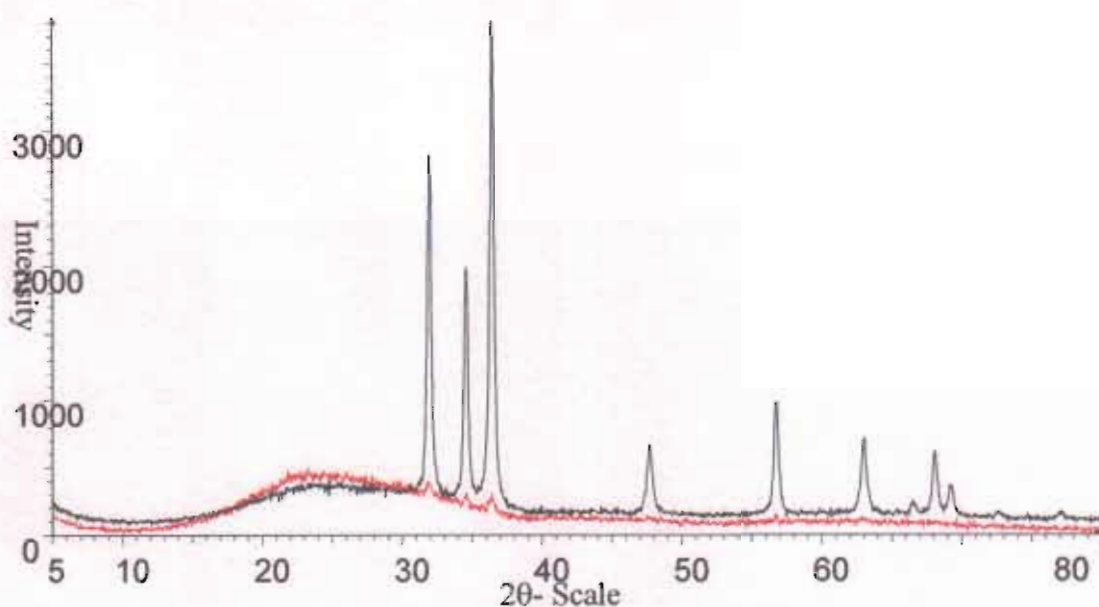


**Figure 12 XRD patterns of 1:2 precursor powders synthesized with 15mmol (black) and 87mmol (red) acetic acid, calcined to 500°C**

Precursor powders thus formed were calcined to 500°C and examined by XRD and TEM. XRD patterns of both are shown in Figure 12. The resolvable peaks for these patterns and their relative intensities are shown in Table 6. Both patterns could be indexed to polycrystalline zinc oxide, as expected for particles calcined to 500°C. The powders synthesized under an excess of acetic acid showed substantially lower peak intensity, combined with a greater amorphous background peak than those made in a smaller excess of acid, when the concentration of bidentate oxalic acid was varied, this situation was reversed. The Scherrer equation was applied to estimate the sizes of the crystallites present and results are given in Table 7. It can be seen that the zinc oxide



particles synthesized under a 1:87 excess of acetic acid were slightly larger than those from a 1:15 ratio of acetic acid. The substantially lower crystallinity of these powders may have resulted from the excess of acetic acid, such that chelation with oxalic acid ligands did not occur.

**Table 6 Resolvable XRD peaks for powders synthesized in an excess of acetic acid**

<b>1:15 Zinc acetate: acetic acid</b>	<b>Angle,</b>	<b>d value,</b>	<b>Intensity,</b>	<b>Intensity,%</b>	<b>Assignment</b>
	<b>2θ°</b>	<b>Angstrom</b>	<b>Count</b>		
	31.933	2.80029	2721	73.7	ZnO (100)
	34.581	2.59171	1986	53.8	ZnO (002)
	36.417	2.46513	3693	100	ZnO (101)
	47.714	1.90455	661	17.9	ZnO (102)
	56.782	1.62002	994	26.9	ZnO (110)
	60.627	1.52617	190	5.2	Unidentified peak
	63.042	1.47339	721	19.5	ZnO (103)
	65.375	1.42633	192	5.2	Unidentified peak
	66.528	1.40439	247	6.7	ZnO (200)
	68.116	1.37545	626	17	ZnO (112)
	69.267	1.35539	374	10.1	ZnO (201)
	72.676	1.29998	181	4.9	ZnO (004)
	77.083	1.23628	178	4.8	ZnO (202)
<b>1:87 zinc acetate: acetic acid</b>	<b>Angle,</b>	<b>d value,</b>	<b>Intensity,</b>	<b>Intensity,%</b>	
	<b>2θ°</b>	<b>Angstrom</b>	<b>Count</b>		
	31.884	2.80448	472	100	ZnO (100)
	34.556	2.5935	382	81	ZnO (002)
	36.369	2.46832	362	76.7	ZnO (101)
	56.75	1.62088	218	46.1	ZnO (110)

**Table 7 Particle sizes estimated from the Scherrer equation**

	<b>Angle,</b>		<b>FWHM,</b>	<b>FWHM,</b>	<b>Size,</b>	<b>Error,</b>
	<b>2θ°</b>	<b>Cos θ</b>	<b>2θ°</b>	<b>Radians</b>	<b>nm</b>	<b>nm</b>
<b>1:15</b>	31.9	0.96	0.30	0.0026	56	25
	34.6	0.95	0.30	0.0026	56	25
	36.4	0.95	0.34	0.003	49	17
<b>1:87</b>	31.9	0.96	0.29	0.0025	58	28

The Scherrer equation provides an estimation of the sizes of crystallites, as opposed to particles, present; as such the results shown in Table 7 indicated that the discrete zinc

oxide regions synthesized under two different excesses of acetic acid were similarly sized. From this, it can be deduced that the precursor surface stabilisation under both conditions was equivalent. TEM images were taken at 200,000x magnification to determine the size and morphology of the product powders and these are shown in Figure 13.



**Figure 13** TEM images at 200000x of powders made from solutions containing 1mmol zinc acetate and (l) 15mmol acetic acid, (r) 87mmol acetic acid, calcined to 500°C

The slightly larger size of the particles calcined in a large excess of acetic acid is shown in the image presented here.

### **3.4 Results - isophthalic acid as a chelating agent**

#### **3.4.1 Particles synthesized in ethanol**

XRD patterns were recorded for powders synthesized with isophthalic acid as chelating agent and calcined to 500°C and to 800°C. All XRD patterns obtained identified the product powders as polycrystalline zinc oxide. Domain sizing was performed using the Scherrer equation on the main intensity peaks. The diffraction patterns for samples calcined to 500°C and 800°C are presented Figure 14 and Figure 15, the resolved peaks are tabulated in the Tables A7 and A8. Particle sintering and associated peak sharpening is expected at such high calcination temperatures and was found here. The crystallite

sizes estimated by the Scherrer equation are listed in Table 8. The anticipated increase in size at the higher calcination temperature is shown in the sizes calculated here. Both powders calcined to 500°C showed similar crystallite sizes, as did the samples calcined to 800°C.

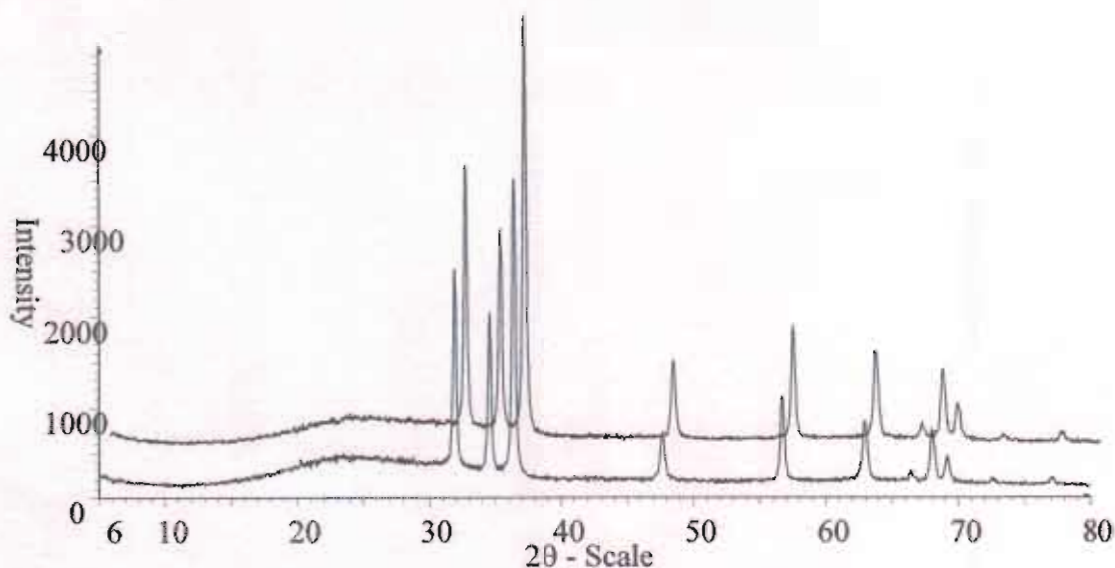


**Figure 14 XRD patterns for powders made from an isophthalic acid precursor, calcined to 500°C**

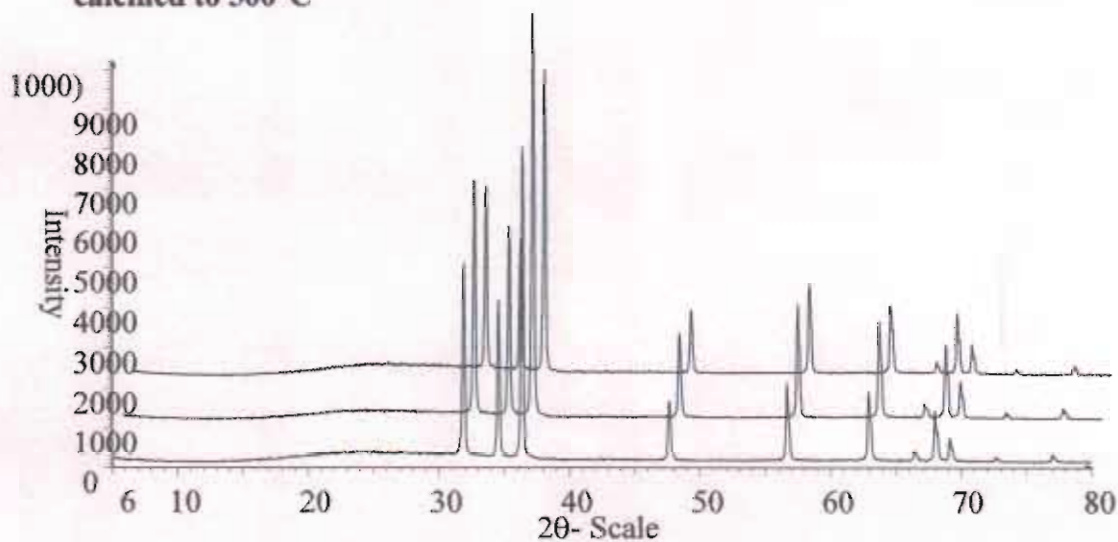


**Figure 15 XRD patterns for powders made from an isophthalic acid precursor, calcined to 800°C**

The variation in particle size along different axes was ~5nm for the low calcination temperature, but up to ~50nm for the higher calcination temperature material. While this



may have indicated oriented growth, it is also likely that the sharpness of the peak reduced the accuracy of measurement of the FWHM. The polydispersity of the particles after being sintered at this temperature would also affect a cumulative distribution such as an XRD pattern and render an average estimation like the Scherrer equation uncertain. It should be noted here that the domain sizes measured here were approximately 10nm smaller than those synthesized through oxalic acid chelation (Table 6). This could be a result of more efficient surface stabilisation using this material.

**Table 8 Scherrer equation estimation of crystallite size for particles synthesized using an isophthalate precursor and calcined to 500°C and 800°C**

	Cos $\theta$ , radians	FWHM, radians	Size, nm	Error, nm
<b>1:1 500</b>	0.96	0.0024	60	33
	0.95	0.0024	61	34
	0.95	0.0027	54	24
<b>1:2 500</b>	0.96	0.0024	60	33
	0.95	0.0024	61	34
	0.95	0.0026	56	27
<b>1:1 800</b>	0.96	0.0017	85	508
	0.95	0.0018	81	196
	0.95	0.0018	81	454
<b>1:2 800</b>	0.96	0.0018	80	184
	0.95	0.0017	86	600
	0.95	0.0018	81	454
<b>1:5 800</b>	0.96	0.0017	85	508
	0.95	0.001	86	600
	0.95	0.0018	81	454

In order to ascertain whether the chelating agent had been fully decomposed by calcination, FTIR spectra of these samples were obtained and are shown in Figure 16 and Figure 17. The absorbance bands at  $1620\text{cm}^{-1}$  and  $870\text{cm}^{-1}$  that, for the material chelated with oxalic acid and calcined up to  $500^\circ\text{C}$ , were associated with unreacted reagents or the surface stabilisation by the counterion, were present here in powders

synthesized in a 1:2 ratio of zinc ion to chelating agent, but not in a 1:1 ratio. The zinc oxide absorbance peak was much sharper for the 1:1 powder than for the 1:2 material; this may have indicated a more effective chelation for this ratio.

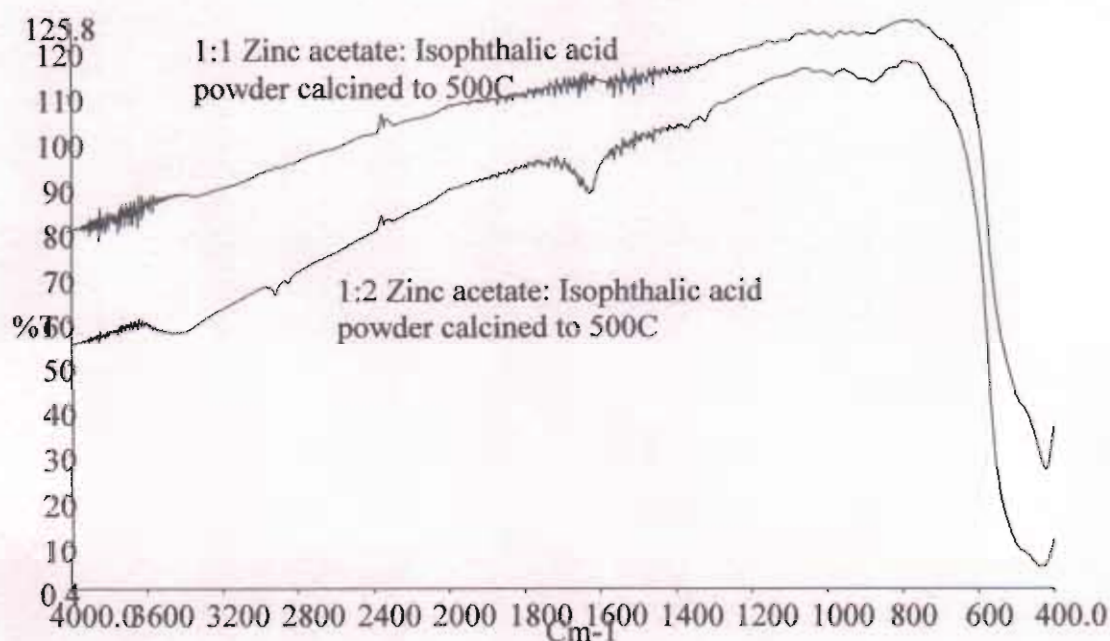


**Figure 16 FTIR spectra of powders synthesized through isophthalic acid chelation and calcined to 500°C**

For powders calcined to 800°C, both 1:1 and 1:2 ratios of zinc ion to acid show minimal absorbance above 600cm<sup>-1</sup> and definite peaks were visible around 875cm<sup>-1</sup>. This indicated the presence of carboxylic groups even after calcination at this temperature, which may have been due to inefficient decomposition of precursor. The incomplete calcination of precursor had been previously noted in DSC studies of these materials, where a black material was found after heating under nitrogen flow to 500°C. For equivalent samples synthesized with oxalic acid as chelating agent, no black products were found. Very weak peaks could be resolved here for the 1:2 particles. Also, the 1:1 sample formed zinc oxide with no impurities present after calcination at 800°C. The



absence of an absorbance peak at  $1622\text{cm}^{-1}$  for these spectra suggests that the peak at this frequency in the 1:2 sample calcined to  $500^\circ\text{C}$  was related to the precursor material.

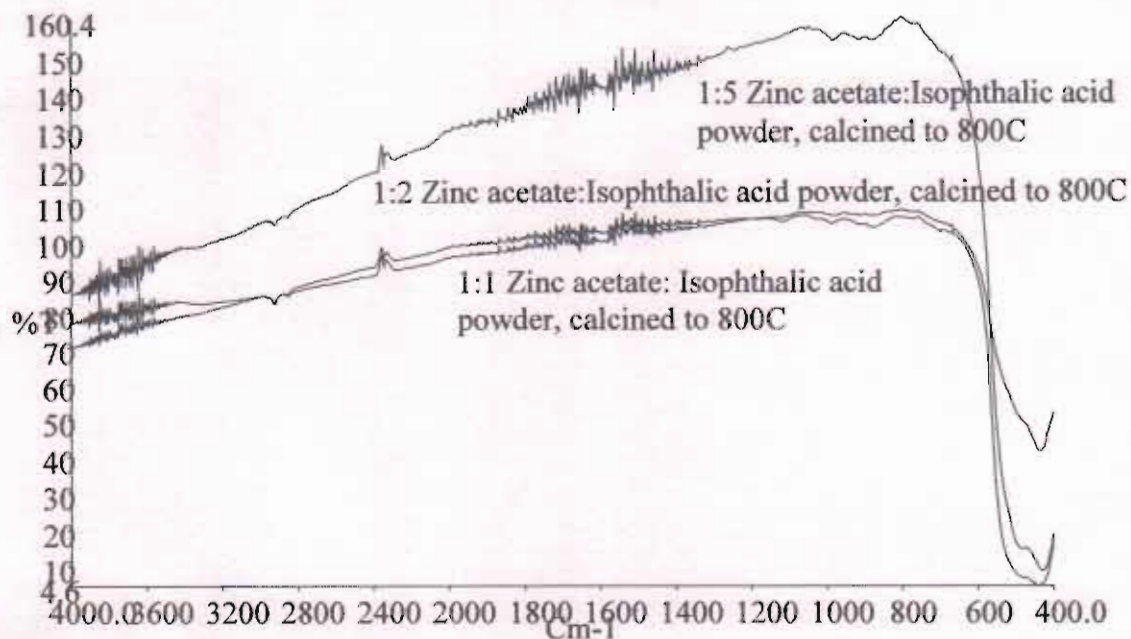


**Figure 17 FTIR spectra of powders synthesized through isophthalic acid chelation and calcined to  $800^\circ\text{C}$**

SEM images of the powders calcined to  $500^\circ\text{C}$  were obtained at a magnification of 5,000X and are shown in Figure 18. Both powders showed flake-like superstructure between tens and hundreds of microns in size and ten microns or less in thickness, with a porous interior. The image on the left has uniform contrast on both its surface and interior, while in the case of the 1:2 powder; one surface seemed brighter and smoother than the other. Since FTIR indicates that this sample contained some residual carboxylic impurities, it is possible that this was present on the more insulating surfaces. It should be noted that the accelerating voltage used to obtain these images differed in the images shown in Figure 18; this is because charge was seen to accumulate on the surfaces of the samples synthesized in a 1:2 ratio, even though both sets of powders had been coated with identical layers of amorphous carbon. This may indicate that a larger amount of



residual surface impurities were present in this sample. The sample preparation on this case involved the grinding of product powders, thus it is possible that the fractures visible here were post annealing artefacts.

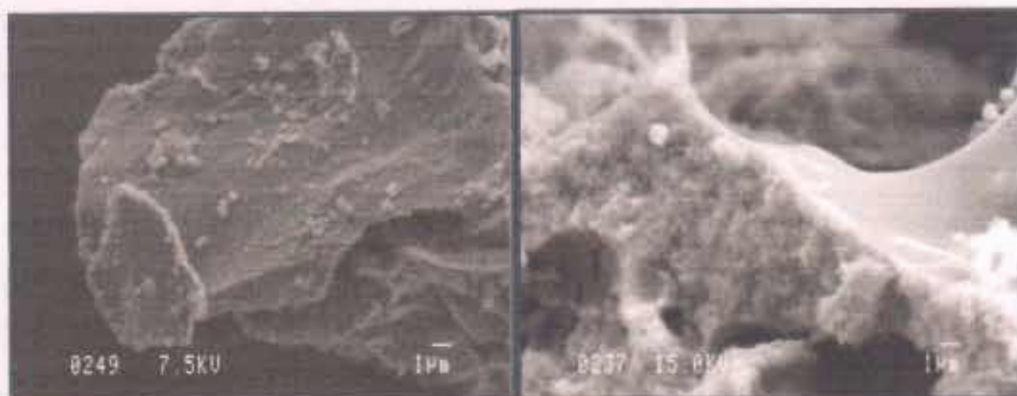


**Figure 18 SEM images of 1:1 (l) and 1:2 (r) powders calcined to 500°C, 5000X magnification**

Transmission electron microscopy was performed on the powders calcined at 500°C and 800°C. Images obtained at 20,000 times magnification for the particles calcined to 800°C are shown in Figure 19.

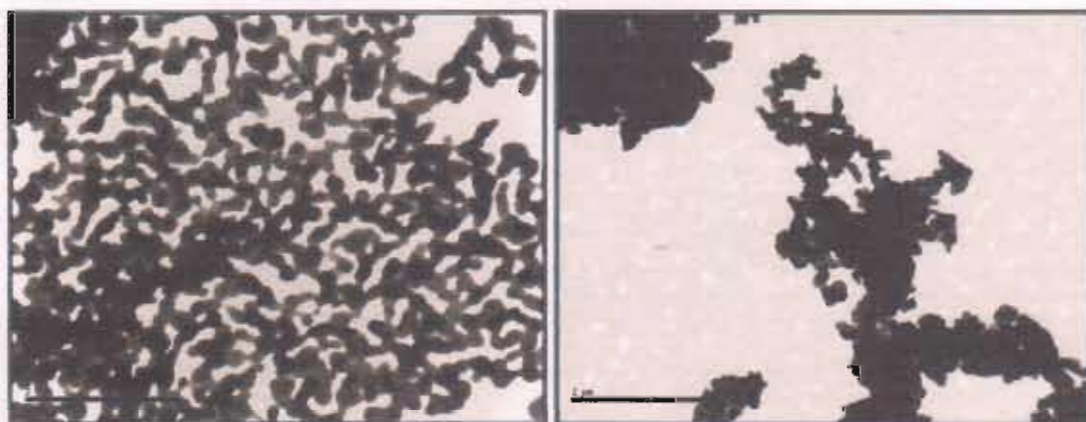


**Figure 19 TEM images of powders synthesized in 1:1 (l) and 1:2 (r) ratios of zinc ion to acid concentration and calcined to 800°C, 20000X**

The images presented here show particles  $\leq 200\text{nm}$  in diameter. This correlates with the Scherrer estimation and indicates that the particles shown were single crystalline. The polydispersity of particles was also evident here and again was probably due to the high

calcination temperature. The porous nature of the particle superstructure is obvious here and permeates the TEM analysis. The powders calcined at 500°C revealed polydispersity with a greater frequency of smaller particles. This was mirrored in the synthesis of zinc oxide through chelation with oxalic acid. The powders calcined at 500°C reveal polydispersity with a greater frequency of smaller particles; this was also found in the synthesis of zinc oxide through chelation with oxalic acid. These powders were also synthesized in a 1:100 ratio of zinc ion to chelating ligand, an image is shown in Figure 20. The arrangement of these products, as can be seen, was entirely different to that of those synthesized through oxalic acid chelation.



**Figure 20 TEM image of powders synthesized in a 1:100 ratio with isophthalic acid and sintered to 800°C, 40000X**

#### 3.4.2 Influence of solvent on morphology

Unlike oxalic acid, which is water soluble, the structure of isophthalic acid leads to it having a low solubility in polar solutions. Atmospheric water and water of hydration introduced by the zinc acetate salt may thus have had an effect on the structure of the product powders. In order to investigate this, powders were synthesized in two solvents less polar than ethanol, namely isopropanol and cyclohexanol. A ratio of zinc ion to acid concentration of 1:10 was chosen to ensure chelation of each zinc ion. It was found that the cage-like superstructure of particles was maintained even when calcined to 500°C.

Particles remained 50nm in diameter or less and grain boundaries were not observed within discrete particles. This indicates that the unique morphology found here was a consequence of the chelating agent, as opposed to the solvent, used.

### **3.5 Conclusions**

In the experiments shown in this chapter it has been found that reagents combined rapidly led to a product powder with a greater crystallinity and equivalent size to those synthesized by an adiabatic route. An explanation has been presented for this in terms of the homogeneity of precursor material and it has been ascertained that this held true only for bidentate ligands. The relative concentration and species of chelating agent has been varied and these parameters have been shown to affect the crystallinity and morphology, respectively, of the zinc oxide nanoparticles produced.



## 4 PARTICLES PREPARED THROUGH POLYMER-ASSISTED ALKALINE HYDROLYSIS

Zinc oxide synthesis through hydrolysis with sodium hydroxide was investigated. Poly(vinylpyrrolidone) (PVP) was used to enable steric isolation of the product in solution, which was characterised by UV/vis and fluorescence spectrometry. The effect of water on the stability of particles was investigated.

Solutions were made by an established method,<sup>94</sup> namely dilution of the heated zinc acetate solution to 8% of its initial concentration with additional solvent and addition of sodium hydroxide below room temperature. Comparative study was made of this method and room temperature synthesis for samples containing 0g, 0.01g and 1g PVP, respectively. In the latter two cases this corresponds to ratios of  $[Zn^{2+}]:[PVP]$  of 1:14.4 and ~1:1440. UV/vis spectrometry was used to establish the presence and estimate the size of zinc oxide produced. The effect of different amounts of polymer included was further investigated for the optimised process and various amounts of water were introduced to the system. The role of pH in dilute solutions was examined.

### 4.1 Results

The absorption spectra for samples synthesized through the conventional route and at room temperature are shown in Figure 21 and Figure 22. Both sets of samples were prepared through identical methods; the obvious difference in absorption can be thus associated with the difference in polymer concentration between the solutions. Both spectra showed that no zinc oxide was formed when 1g of PVP was used and that an absorption shoulder corresponding to the bulk band gap energy was present in solutions

synthesized with 0g and with 0.01g PVP. The solution synthesized at room temperature containing no polymer additive exhibited scattering at wavelengths above 400nm. This turbidity was reduced for solutions containing increased amounts of PVP, possibly reflecting a reduced rate of aggregation or growth for these particles.

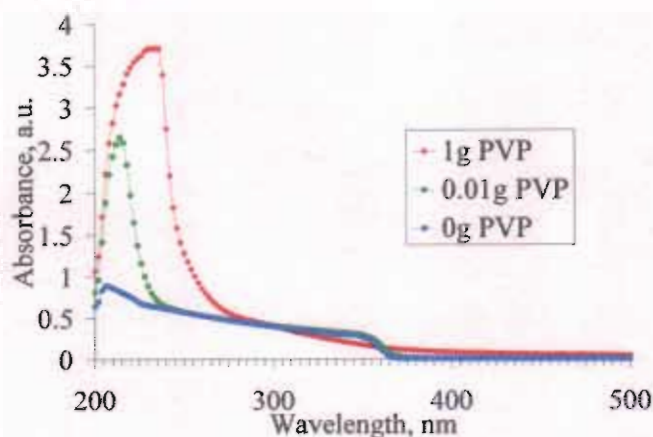


**Figure 21 UV/vis spectra of samples prepared through conventional method**

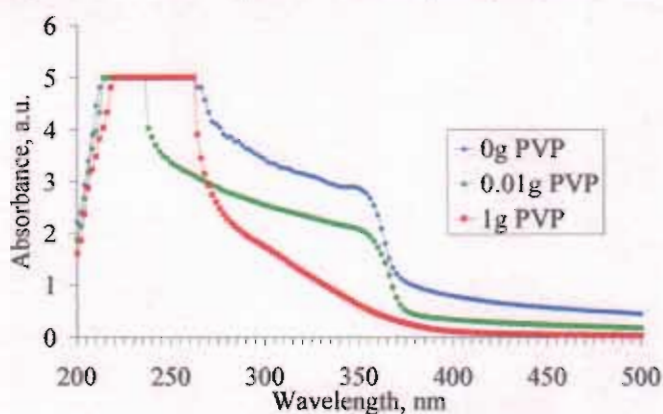


**Figure 22 UV/vis spectra of samples synthesized at room temperature**

The room temperature synthesis method was further investigated, using 0g, 0.01g, 0.05g, 0.1g, 0.5g and 1g PVP and the UV/vis spectra of these samples, taken after aging at room temperature for one day, are shown in Figure 23. In this case, only the sample containing no polymer capping agent exhibited turbidity.

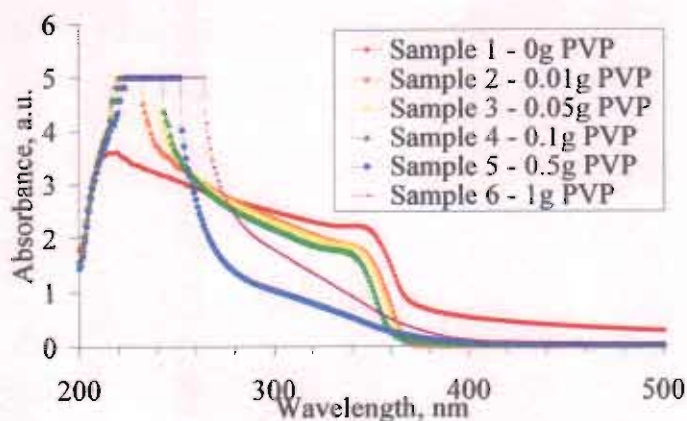


**Figure 23 UV/vis absorption spectra for samples containing various quantities of PVP**

The bandgap energies and calculated radii of these particles are shown in Table 9. These show that the addition of 0.01g - 0.1g PVP per sample resulted in a solution containing crystallites of diameter slightly larger than that necessary for quantum confined effects to become apparent. For amounts of polymer below this, bulk zinc oxide was found. In the case of larger concentrations no zinc oxide absorbance is detected.

**Table 9 Optical properties of samples made with different quantities of PVP**

Amount PVP, g/ml	Amount of PVP, mmol	Ratio $[Zn^{2+}]:[PVP]$	Bandgap Energy $E^*$	Radius, m	Diameter, nm	Error, nm
1	34.5	1:1437	2.94	-	-	-
0.5	17.2	1:718	2.97	-	-	-
0.1	3.4	1:144	3.35	3.0E-09	6.0	0.6
0.05	1.7	1:71.8	3.33	3.2E-09	6.4	0.7
0.01	0.3	1:14.4	3.33	3.2E-09	6.4	0.7
0	0	0	3.14	-	-	-

Photoluminescence measurements on these samples were undertaken for these samples at an excitation wavelength of 325nm. Their emission spectra are shown in Figure 24.



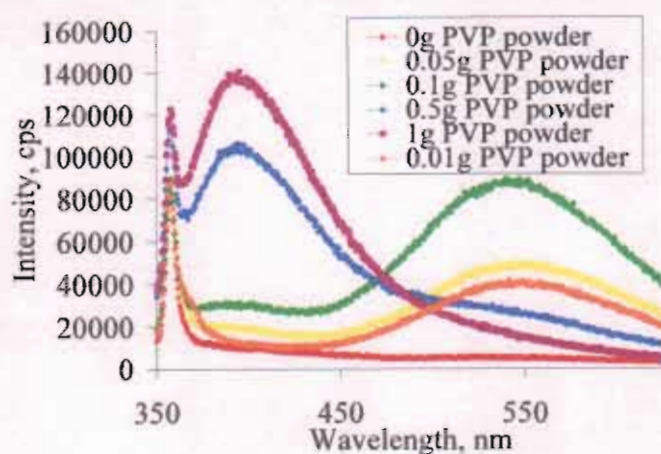


**Figure 24 Fluorescence spectra for samples synthesized containing various PVP concentrations**

As can be seen above, the zinc oxide luminescence peak at visible wavelengths was present for intermediate amounts of PVP, but was increasingly quenched with larger ratios of  $[PVP]:[Zn^{2+}]$ . For the sample containing 0.01g PVP, which showed bulk absorption properties, a shoulder to the solvent Raman peak, at 370nm, was present. Samples containing larger amounts of PVP exhibited broad peaks with maxima at 395nm. This included the samples for which no absorption edge was detected.

#### 4.1.1 Addition of water to the system

Solutions were made containing 0.1g PVP per sample and small amounts of deionised water were added to each. Absorption spectra of each were recorded and are presented in Figure 25. The bandgap energies of these solutions, calculated from the absorbance shoulder, were all below 3.4eV and decreased with increasing amounts of water added to the system. The turbidity and lower intensity of excitonic shoulder, found for the sample with 0.5ml DIW added, correlated with probable particle growth under the addition of water. Bulk zinc oxide was also found in the photoluminescence spectra of this solution, shown in Figure 26.

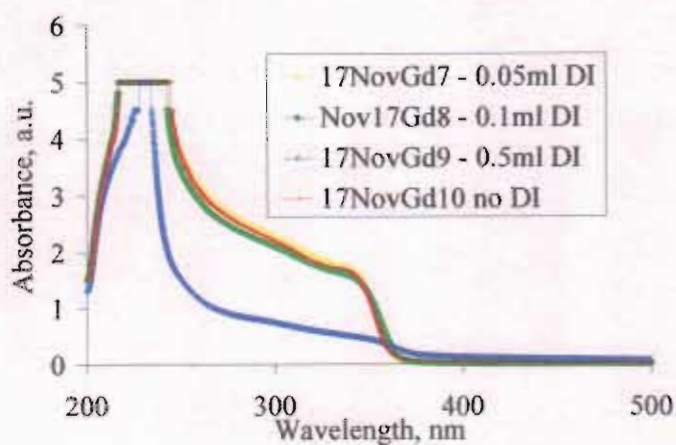


**Figure 25 UV/vis spectra of zinc oxide solutions after varying amounts of water were added**

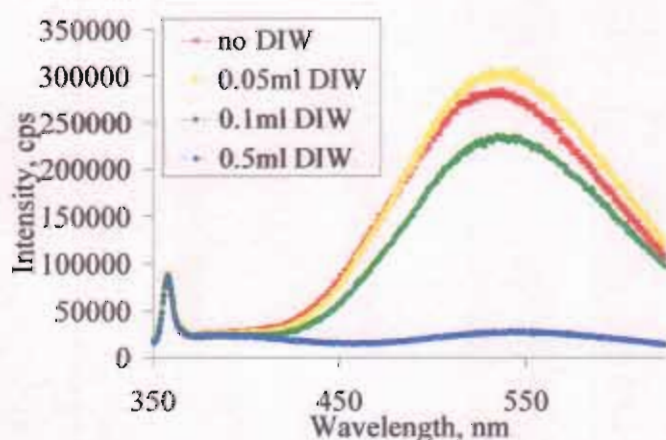


**Figure 26 Fluorescence spectra of solutions synthesized with small amounts of water added**

Solutions were made containing between 0.1g and 0.5g PVP and 0.5mls of DIW was added to each. Absorption spectra were recorded before the addition of water and absorption and photoluminescence spectra after subsequent aging for one day. UV/vis spectra are shown for the fresh solutions in Figure 27. Of these samples, only the solution containing the maximal quantity of PVP showed an absorbance edge corresponding to the bulk value. This may be because of a smaller yield in this case.

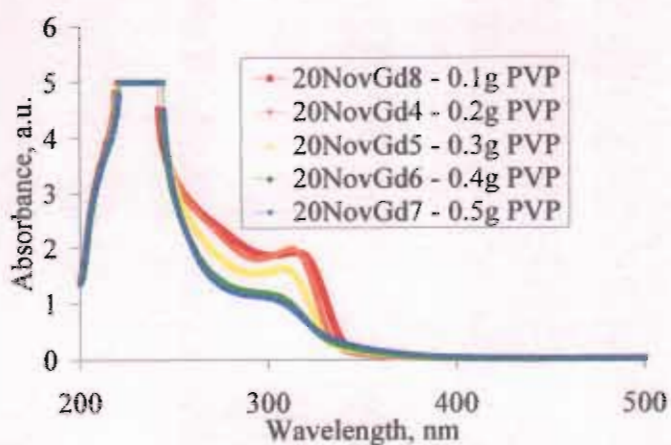


**Figure 27 UV/vis absorption spectra for solutions synthesized with different amounts of PVP**

The estimated sizes of the particles synthesized are in Table 10.

**Table 10 Optical properties of samples containing different quantities of PVP**

Amount PVP, g/ml	Amount of PVP, mmol	Ratio $[Zn^{2+}]:[PVP]$	Bandgap Energy $E^*$	Radius, m	Diameter, nm	Error, nm
0.1	3.45	1:144	3.54	2.2E-09	4.4	0.2
0.2	6.89	1:287	3.6	2.0E-09	4.1	0.2
0.3	10.34	1:431	3.6	2.0E-09	4.1	0.2
0.4	13.79	1:575	3.45	2.5E-09	4.9	0.3
0.5	17.24	1:718	3.33	3.2E-09	6.4	0.7

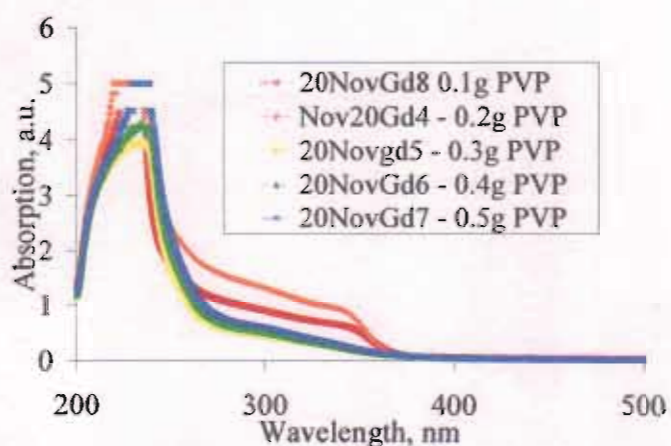


**Figure 28 Absorption spectra of solutions shown in Figure 27 after the addition of water**



The absorption spectra obtained after the addition of water and subsequent aging at room temperature for one day are shown in Figure 28. It is immediately apparent that the addition of water resulted in the growth of particles. For samples containing 0.2g PVP, which showed the most blue-shifted absorption edge initially, the largest bandgap energy and most intense band-edge absorption was present after the addition of water. Solutions containing larger quantities of PVP showed no discernible absorption edge after the addition of water. The bulk properties of the suspended particles were confirmed by fluorescence spectra, shown in Figure 29.

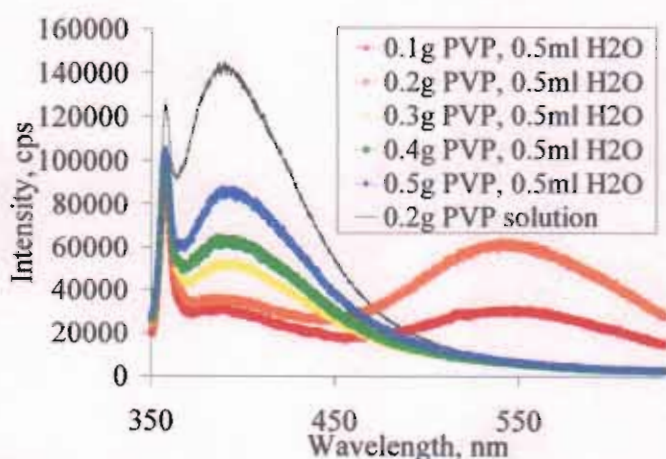


**Figure 29 Fluorescence spectra of solutions after the addition of water**

Also shown here is the emission spectrum of a PVP solution. The broad UV peak occurring with increasing intensity as the amount of PVP present in each solution was increased could thus be related to the luminescence of the polymeric material.<sup>153</sup> The absence of excitonic emission peaks from any spectrum observed correlated with the bulk bandgap absorption spectra measured.

#### 4.1.2 Influence of water on the system

Solutions were prepared containing 0.2g of PVP per sample and up to 3ml deionised water was added to each. The absorption spectra of these are presented in Figure 30.

From these it can be seen that while the addition of 0.5mls of water allowed the formation of bulk zinc oxide (Figure 28), larger amounts did not show any bulk absorbance.

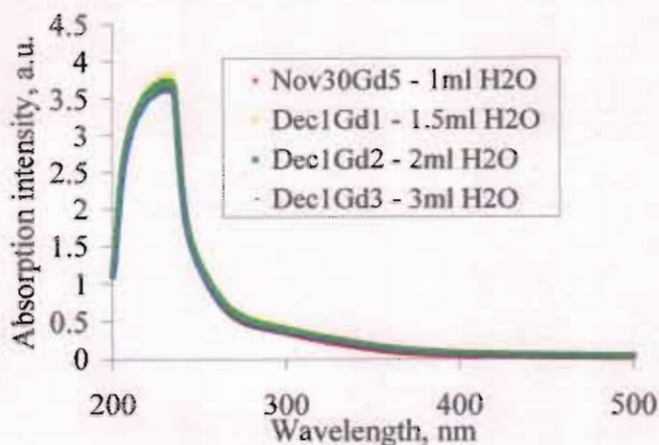


**Figure 30 UV/vis absorption spectra of solutions after different amounts of water is added to each**

The effect of pH was studied by adding 0.5mls of a HCl-DIW solution to samples prepared using 0.01g PVP per sample. Their absorption spectra are shown in Figure 31.

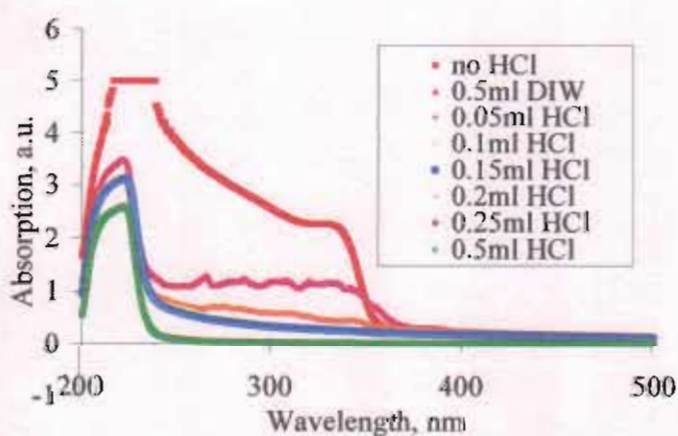


**Figure 31 UV/vis absorption spectra obtained after the addition of water of different acidities**

It is clear from these that the addition of small amounts of acid reduced the intensity of the bulk absorption edge. Samples were also synthesized using smaller relative

concentrations of base. Their absorption spectra after the addition of water and aging at room temperature for two days are shown in Figure 32.

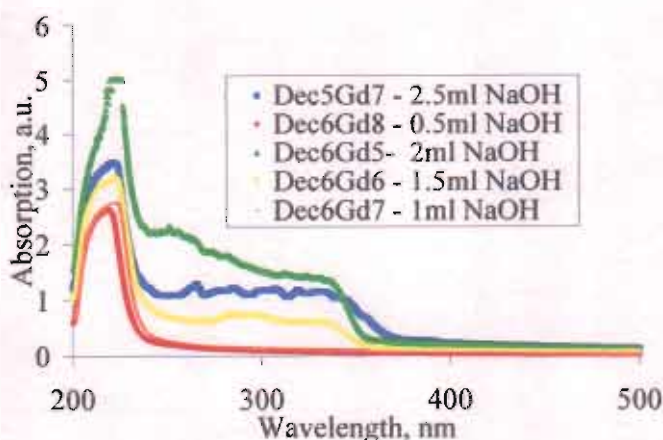


**Figure 32 UV/vis absorption spectra of solutions containing varying quantities of base and 0.5mls water**

These show that upon the addition of small quantities of water, samples containing 2mls sodium hydroxide exhibited a band-edge absorption corresponding to the bulk value, whereas for other amounts, the product solutions had a greater degree of turbidity. Further evidence of this was seen by the instability of the solutions. In all cases, precipitation had occurred after approximately one week. The spectra obtained after the addition of water showed that at polymer ratios which in the absence of water showed quantum confined absorption characteristics, subsequent addition of water to these systems resulted in their instability. It is possible that this is due to the increased solubility of PVP in the resulting overall medium. That is, it is possible that the number of PVP ligands attached to each zinc oxide particle after the addition of water was smaller than for particles in the as-synthesized solution.



## 4.2 Conclusions

It has been shown that the addition of a polymeric stabilising agent can aid the stability of zinc oxide particles of diameter  $\leq 10\text{nm}$  at room temperature. The benefit of this stabilising agent was such that particles could be made in solutions of a higher concentration than is generally reported. Under certain conditions, zinc oxide solutions containing up to 6% DIW remained stable and retained their small size for several hours. The properties of solutions after the addition of larger amounts of water, of varying levels of pH, were investigated and it is thought that growth through aggregation or ripening led to their subsequent precipitation.

## 5 ORGANIC-CAPPED ZINC OXIDE

Nanoparticulate zinc oxide, capped with an organic ligand, was synthesized in a coordinating solvent. The slow decomposition of precursor was investigated as a method to synthesize monodisperse zinc oxide quantum confined particles.

The synthesis of zinc oxide through slow thermolysis of precursor entailed the degassing under flowing argon of reaction mixture at 110°C, then heating to the reaction temperature and maintaining at this temperature for up to three hours. Aliquots were taken at intervals and samples were purified by precipitation with methanol, isopropanol and resuspension in chloroform or toluene. Particles were synthesized with a final aging temperature of 100°C, 140°C, 150°C, 160°C, 175°C and 200°C for one hour, in a 1:1 ratio of zinc ion to oleic acid. Particles were synthesized at 160°C and at 200°C in ratios of zinc precursor to oleic acid, (OA), of 1:1, 1:2 and 1:4. Both zinc acetate and zinc chloride as zinc precursors and the relative concentration of zinc ion to hexadecylamine, (HDA) were also explored. An aging step, at 100°C and at 140°C for one hour, was included subsequent to the formation reaction for samples synthesized at 160°C and its effects investigated. The effect of a reductant, ethylene glycol, on the particles produced, was also investigated. The formation of particles over time was studied and the influence of water on particle formation was examined. XRD, TEM, UV/vis and fluorescence spectroscopy were used to characterise the particles produced.

### 5.1 Results

#### 5.1.1 Dependence on synthesis temperature

UV/vis spectra of particulate solutions synthesized at different temperatures are shown in Figure 33. It was immediately apparent that the solution synthesized at 200°C was

much more turbid than any of the solutions heated at lower temperatures. This could have been simply because larger particles were produced, which are more easily precipitated by an excess of methanol, or because of a larger yield of product at this temperature.

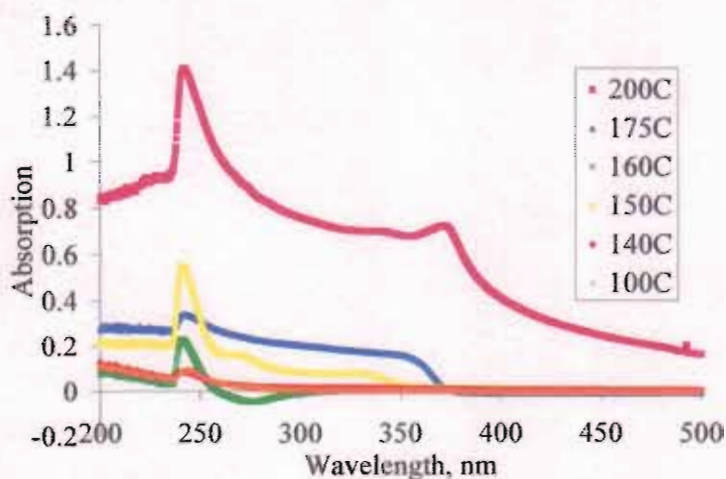


**Figure 33 UV/vis absorption spectra of zinc oxide particles synthesized at different temperatures**

The peaks present around 250nm in all were also present in UV/vis spectra of the precursor heated to 90°C and of the ligand solution and were probably related to the absorbances of chloroform and of hexadecylamine. The XRD pattern of the ligand material, after heating to 200°C, could be indexed to neither hexadecylamine nor oleic acid, which is liquid at room temperature; however, it could be matched to stearic acid, <sup>154</sup> C<sub>18</sub>H<sub>36</sub>O<sub>2</sub>, or in some cases zinc stearate. The transformation of oleic acid to stearic acid at high temperatures may have contributed to the sample turbidity found here. Samples synthesized at a reaction temperature of 200°C and 175°C both showed an absorbance in the region of 360nm, corresponding to that of bulk zinc oxide. The absorbance spectrum of the solution synthesized at 160°C also showed a shoulder, but it was several times less intense than the former spectra. For lower reaction temperatures,



no shoulder was found. While this absorbance was a discernible peak in the case of the 200°C sample, it was present as a shoulder in the lower temperature sample; this may indicate the presence of particles with sizes in the quantum regime.

XRD patterns of the same material are presented in Figure 34. The different quantities of the stearic acid produced here were reflected in the different intensities of those peaks. The 200°C and 100°C samples were withdrawn as aliquots of a much smaller volume than the remaining samples; nevertheless, well-defined zinc oxide peaks were present for the sample synthesized at 200°C. The sample synthesized at 175°C also showed a wurtzite ZnO diffraction pattern, whereas the remaining solutions exhibited peaks that can be associated with anhydrous zinc acetate.<sup>155</sup>

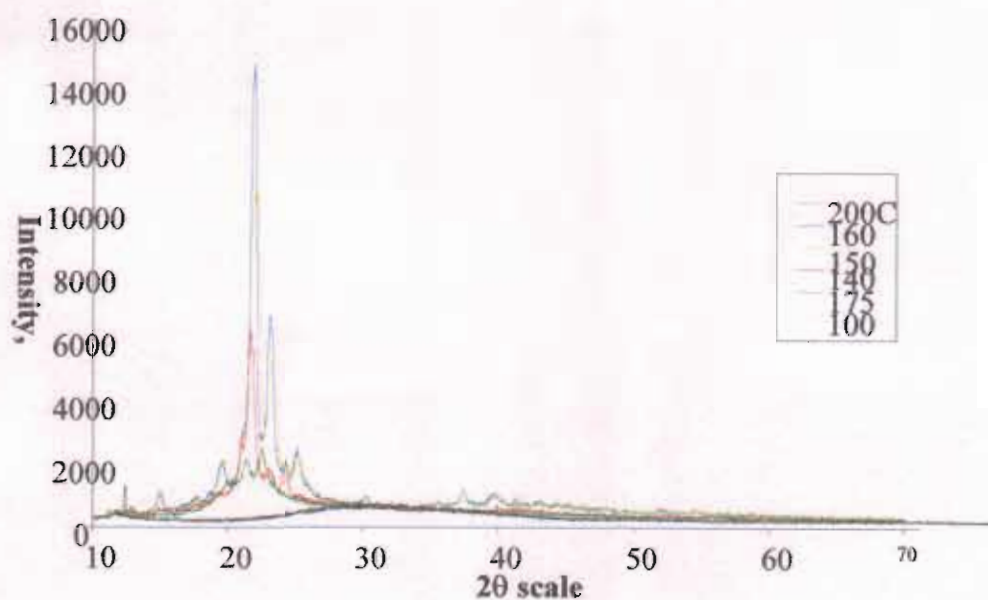


**Figure 34 XRD patterns of samples synthesized at different temperatures**

It is clear from both absorbance and diffractometry measurements that the formation of zinc oxide occurred at temperatures above 160°C and that crystalline phases of the precursor material were present for synthesis temperatures of 160°C and below. The peaks related to stearic acid increased in intensity with higher synthesis temperatures,

indicating the continued decomposition of oleic acid at higher temperatures. The particle sizes calculated from the (100), (002) and (101) peaks, are listed in Table 11. No zinc oxide peaks were resolvable for the sample synthesized at 160°C. This could have been because of the diffraction of large amounts of zinc stearate,<sup>156</sup> which showed coincident peaks at  $2\theta = 32.6^\circ$ ,  $35^\circ$  and  $37.9^\circ$ . The low intensity of zinc oxide peaks may also have resulted in discrepancies in particle size estimations shown in Table 11. The (002) peak being the least intense, obviously exhibited a lower signal-to-noise value and consequently showed greater peak broadening.

**Table 11** Sizes of particles calculated from XRD data shown in Figure 33

200°C	2 $\theta$	Cos $\theta$ , rad	FWHM, deg	Size, nm	Error, nm
(100)	31.7	0.96	0.1	99	139
(002)	34.3	0.96	0.22	48	38
(101)	36.2	0.95	0.18	72	107
175°C					
(100)	31.8	0.96	0.61	14	2
(002)	34.4	0.96	0.41	21	5
(101)	36.2	0.95	0.73	12	1

Since zinc oxide particles were detected at a formation temperature of 175°C, it is possible that non-uniform aggregation caused the growth of oddly shaped particles at a reaction temperature of 200°C.

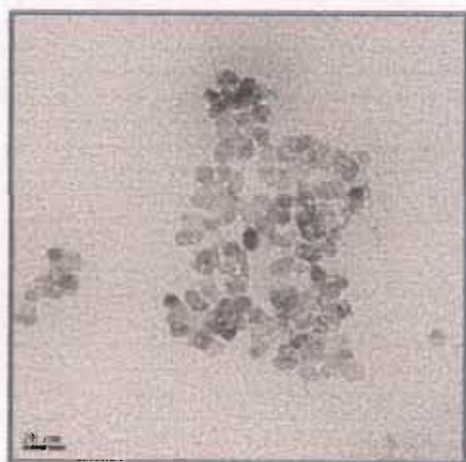


**Figure 35** TEM image of particles synthesized at 175°C

TEM images of the particles were obtained in order to ensure that the XRD size estimation reflected particle, as opposed to domain, size, one of which is shown in Figure 35. Because of the small size and low cross-section of the material involved, as well as the presence of substantial amounts of stearic acid homogeneously coating each sample, these particles were not readily resolved. However, they did confirm that the particles were single crystalline.

### 5.1.2 The effect of zinc counterion on material produced

Samples were synthesized substituting zinc chloride for zinc acetate and heating to 100°C, 200°C and 280°C, in the presence and absence of oleic acid. XRD patterns of the solutions prepared at 200°C and 280°C are shown in Figure 36.

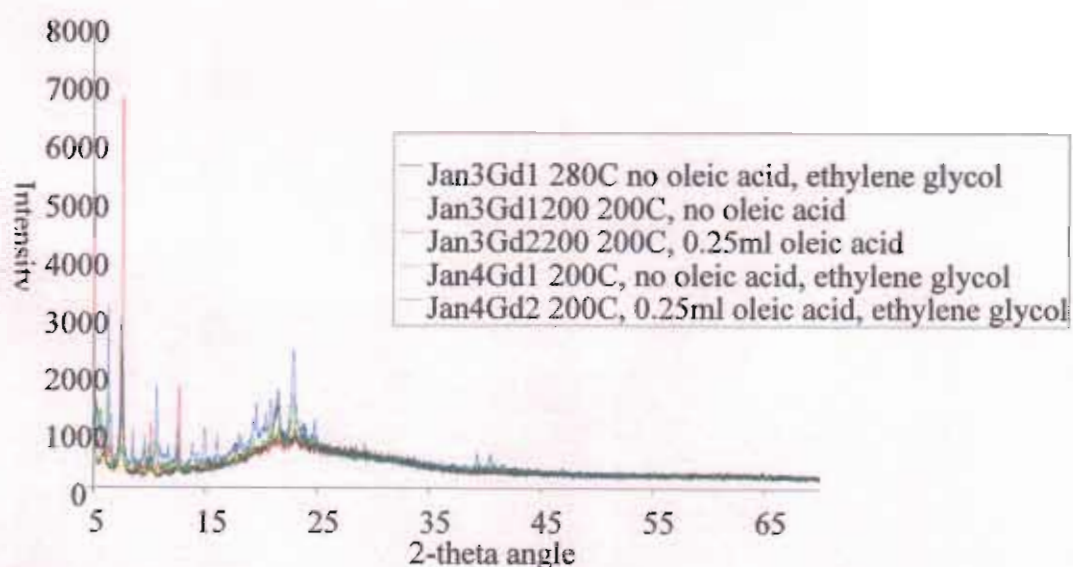


**Figure 36 XRD patterns of samples synthesized using zinc chloride as a precursor**

In all cases, 5g hexadecylamine and 1mmol (0.136g) zinc chloride were combined and 0.89mmol (0.25ml) oleic acid and 0.3ml ethylene glycol were added in the cases indicated, *i.e.* identical conditions to those used to synthesize the particles shown in Figure 34. From these diffractograms, it was evident that zinc oxide was not present,



even after synthesis at 200°C, whereas it was formed in the case where zinc acetate was used. For this reason, all subsequent experiments were performed using zinc acetate as zinc precursor.

### 5.1.3 Variation of concentration of oleic acid to zinc ion

Samples were synthesized at 200°C as described in section 5.1.1, but containing increased amounts of oleic acid. Absorption spectra of these are presented in Figure 37. The spectra of all samples shown in Figure 37 exhibited bulk band edges and scatter above 400nm, indicating that the particles formed had sizes above the quantum confined range. The band-edge of the sample synthesized with 0.5mls oleic acid was calculated to be 3.17eV. This discrepancy from reported bulk values may have been associated with turbidity.

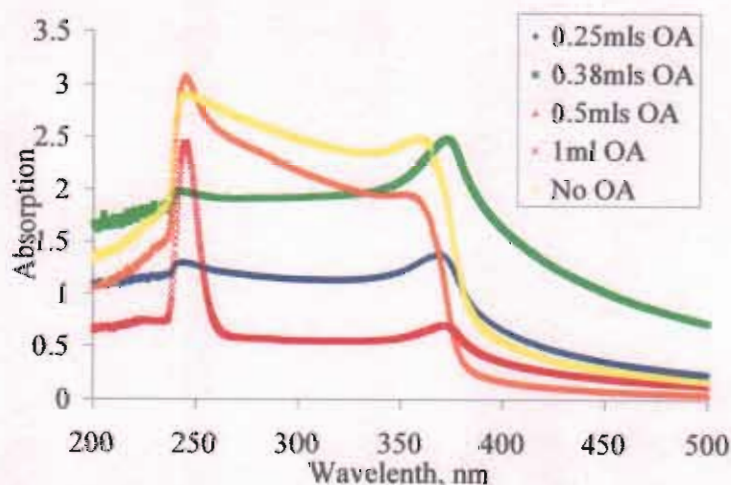


**Figure 37 UV/vis absorption spectra of samples synthesized at 200°C, containing various combinations of OA**

The XRD patterns of the dried powder samples are shown in Figure 34. Included in this also is the diffraction pattern of the material produced through reacting the solvent and surfactant under identical conditions. From comparison of these diffraction patterns,

many of the intense peaks found in the samples synthesized can be identified as relating to an organic material.

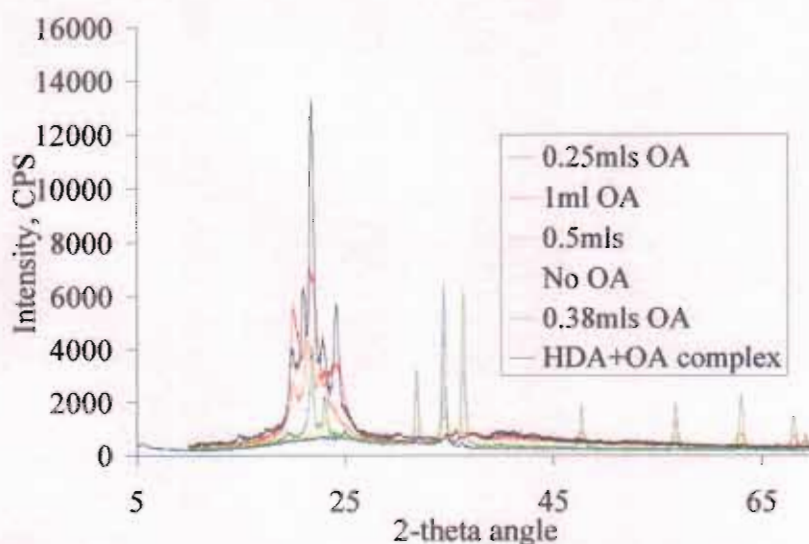


**Figure 38 XRD patterns of material shown in Figure 37**

The peaks resolved for the sample containing 0.38mls OA are shown in Table 12. Equivalent information for the remaining ratios of oleic acid to zinc precursor are appended in Tables A9, A10 and A11. The variation of relative intensities of peaks was thought to be due in part to orientation of the particles as they are deposited on a glass slide, in addition to possible non-uniform growth at this temperature. While the diffraction patterns showed peaks characteristic of zinc oxide, also identifiable are the peaks characteristic of anhydrous zinc acetate and stearic acid, along with some minor peaks that remained unidentifiable. Scherrer equation estimates of the major zinc oxide peaks are shown in Table 13. From the data given, it is apparent that while the variation of relative concentration of oleic acid with respect to that of zinc precursor had an effect on the sizes of particles formed, as this relative concentration was increased, a reduction in the total amount of zinc oxide formed in the reaction also resulted.



**Table 12 XRD peaks resolved for samples synthesized containing 1.34mmol oleic acid at 200°C**

2-Theta	d(A)	Height	I%(h)	Phase ID	( h k l )	2-Theta	Delta
11.093	7.9695	79	4.8	C18H36O2	( 5 0 0 )	11.11	0.017
11.577	7.6374	141	8.6	C4H6O4Zn		11.79	0.213
18.554	4.7781	256	15.5	C18H36O2	(-2 1 0)	18.446	-0.109
18.779	4.7214	315	19.1	C18H36O2	(-1 0 2)	18.947	0.167
19.089	4.6455	359	21.8	C18H36O2	(-3 1 0)	19.116	0.027
19.418	4.5676	440	26.7	C4H6O4Zn		19.493	0.076
19.999	4.436	1265	76.8	C18H36O2	(-4 1 0)	20.022	0.023
20.426	4.3442	130	7.9	C18H36O2	( 1 1 1 )	20.485	0.058
21.477	4.134	1276	77.5	C18H36O2	( 3 1 1 )	21.631	0.153
21.919	4.0517	938	57	C18H36O2	(-4 1 1)	21.841	-0.078
22.439	3.959	357	21.7	C18H36O2	( 4 1 1 )	22.49	0.052
22.548	3.9401	542	32.9				
23.157	3.8378	684	41.5				
23.998	3.7052	533	32.4	C18H36O2	(-6 1 1)	23.888	-0.11
24.061	3.6956	412	25	C4H6O4Zn		24.164	0.103
24.743	3.5953	260	15.8	C18H36O2	( 6 1 1 )	24.78	0.037
25.141	3.5393	262	15.9	C18H36O2	(-7 1 1)	25.157	0.016
25.176	3.5344	292	17.7				
25.375	3.5071	289	17.5	C18H36O2	(-8 1 0)	25.339	-0.036
31.067	2.8763	49	3	C4H6O4Zn		30.807	-0.26
31.86	2.8065	1264	76.7	ZnO	(100)	31.769	-0.091
34.501	2.5975	595	36.1	ZnO	(101)	34.421	-0.08
36.3	2.4727	1647	100	ZnO	(002)	36.252	-0.048
40.145	2.2444	84	5.1	C18H36O2	(-14 1 2)	40.04	-0.105
47.079	1.9287	138	8.4				
47.502	1.9125	284	17.2	ZnO	( 1 0 2 )	47.538	0.036
47.681	1.9057	339	20.6				
47.958	1.8954	231	14	C4H6O4Zn		47.834	-0.124
56.116	1.6376	159	9.7				
56.642	1.6237	721	43.8	ZnO	( 1 1 0 )	56.602	-0.04
62.011	1.4953	73	4.4	C4H6O4Zn		62.258	0.247
62.643	1.4818	220	13.4				
62.941	1.4755	387	23.5	ZnO	( 1 0 3 )	62.862	-0.078
63.279	1.4684	229	13.9				
67.861	1.38	279	16.9	C4H6O4Zn		67.859	-0.001
68.097	1.3758	345	20.9	ZnO	( 1 1 2 )	67.961	-0.136
69.16	1.3572	172	10.4	ZnO	( 2 0 1 )	69.098	-0.061



The material formed showed bulk optical properties at all ratios of surfactants to precursor and had a calculated crystallite size of greater than 10nm.

**Table Particle size estimations using Scherrer equation of particles synthesized at 200°C**

	Peak	2 $\theta$	Cos $\theta$	FWHM, degrees	Size, nm	Error, nm
<b>No OA</b>	(100)	31.7	0.96	0.25	39	22
	(002)	34.4	0.96	0.54	16	3
	(101)	36.2	0.95	0.40	22	6
<b>0.25ml OA 0.89mmol</b>	(100)	31.7	0.96	0.10	99	139
	(002)	34.3	0.96	0.22	48	38
	(101)	36.2	0.95	0.18	72	107
<b>0.38ml OA 1.34mmol</b>	(100)	31.8	0.96	0.23	45	31
	(002)	34.5	0.96	0.30	31	13
	(101)	36.3	0.95	0.25	39	22
<b>0.5ml OA 1.79mmol</b>	(100)	31.9	0.96	0.40	22	6
	(002)	34.5	0.96	0.73	12	1
	(101)	36.3	0.95	0.50	17	3
<b>1ml OA 3.57mmol</b>	(100)	31.9	0.96	0.38	23	7
	(002)	34.6	0.95	0.40	22	6
	(101)	37.1	0.95	1.7	5	0.2

#### 5.1.4 Variation of concentration of hexadecylamine to zinc ion

As shown in section 5.1.3, this reaction formed a ternary system in which all components had a role. For this reason, the variation of the relative concentrations of zinc precursor and coordinating solvent was investigated. Samples were synthesized at 175°C from 5g (~20.7mmol) HDA, 5mmol (0.917g) dehydrated zinc acetate and oleic acid in various amounts. Molar ratios of  $[Zn^{2+}]:[OA]$  of 1:1, 1:2, 2:5, 1:3, 2:7 and 1:4 were attempted, where a 1:1 ratio indicates 0.917g zinc acetate and 1.4mls oleic acid. Aliquots of the solutions were taken at intervals up to two hours after achieving the reaction temperature.

Diffraction patterns for aliquots taken after two hours at 175°C are shown in Figure 39. The reduction of the peaks intensity with increasing amounts of oleic acid was accompanied by peak broadening and for ratios of  $[Zn^{2+}]:[OA]$  above 1:3 no peaks characteristic of zinc oxide were detected after 2 hours synthesis time.

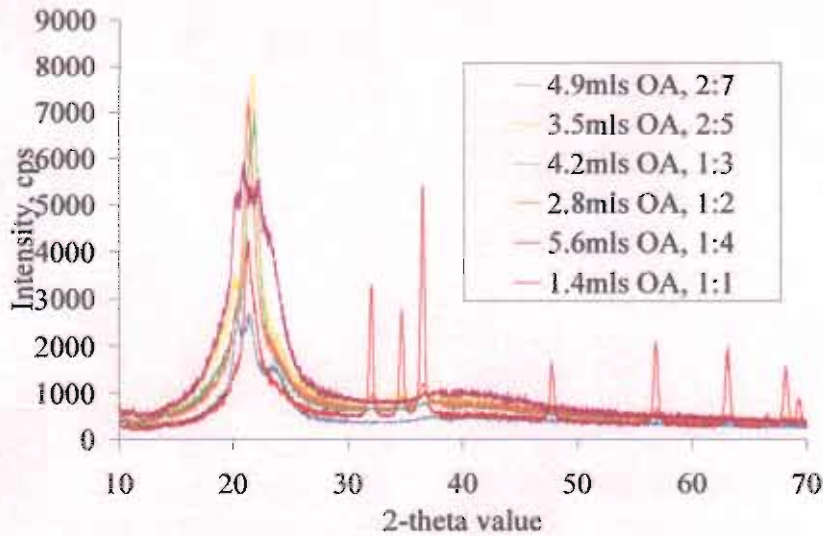


**Figure 39** Diffraction patterns of samples synthesized at 175°C using various concentrations of OA

Scherrer equation estimates of these particles are shown in Table 14.

**Table 14** Particle size estimates using the Scherrer equation

	Peak	2θ angle	Cos θ	FWHM	Size, nm	Error, nm
<b>1.4ml OA</b>	(100)	31.9	0.96	0.30	31	13
<b>1:1 ratio</b>	(002)	34.6	0.95	0.36	25	8
	(101)	36.4	0.95	0.30	31	13
<b>2.8ml OA</b>	(100)	31.9	0.96	0.53	16	3
<b>1:2 ratio</b>	(002)	34.6	0.95	0.61	14	2
	(101)	36.5	0.95	0.67	13	2
<b>4.2ml OA, 1:3</b>	(100)	32.1	0.96	1.27	7	0.4
<b>3.5ml OA</b>	(100)	32	0.96	0.36	25	7
	(002)	34.3	0.96	0.68	12	2
	(101)	36.3	0.95	1.47	6	0.3

For particles synthesized using a ratio of  $[\text{Zn}^{2+}]:[\text{OA}]$  of 1:3, Scherrer equation estimation of the particle size was 6.6nm, however, the small quantity of product and presence of coincident zinc stearate peaks hindered reliable estimation using all three peaks, as was also the case for the diffraction pattern of the sample synthesized in a  $[\text{Zn}^{2+}]:[\text{OA}]$  ratio of 2:5. In order to ascertain the presence and size of the particles, absorbance spectra of the solutions were obtained and are presented in Figure 40.

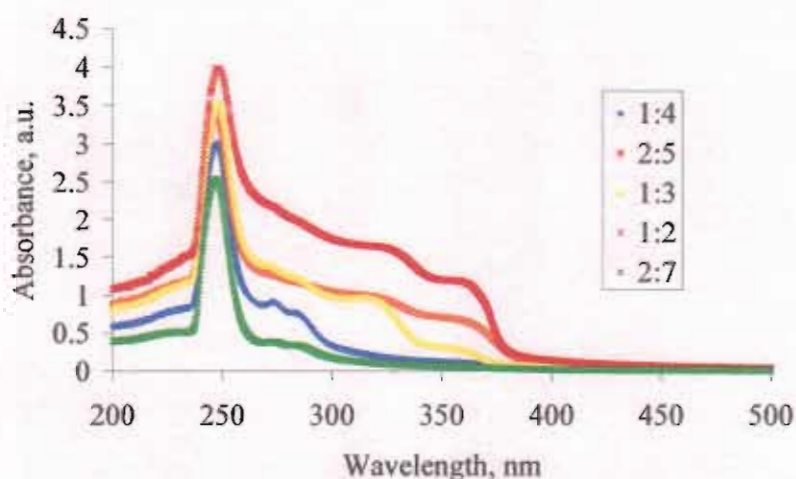


**Figure 40 Absorbance spectra for solutions synthesized at 175°C containing various amounts of OA, after 2 hours**

The presence of an absorbance edge the intensity of which decreased as the amount of oleic acid was increased and which corresponds to a band edge of 3.2eV, up to a  $[\text{Zn}^{2+}]:[\text{OA}]$  ratio of 1:3, agreed with the X-ray results of > 8nm particles in these samples. These samples also exhibited an absorbance with a band edge energy  $\sim 0.2\text{eV}$  above the former. However, samples synthesized with larger ratios of oleic acid did not show this absorbance. Absorbance peaks at approximately 270nm and 280nm were present with increasing intensity as the amount of oleic acid in the system increased but this was not true for the lower energy peaks.



The behaviour of the system over time was investigated; aliquots were taken from reactions containing  $[Zn^{2+}]:[OA]$  ratios of 1:2, 2:5 and 1:3 while at a reaction temperature of 175°C. Absorbance spectra of the samples synthesized in a 1:2 ratio are shown in Figure 41. Those for other amounts are appended in Figures A4 and A5.

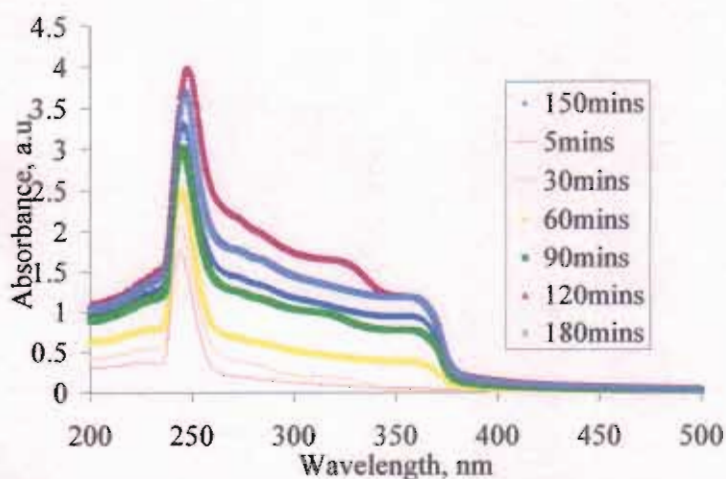


**Figure 41 Absorption evolution over time for samples synthesized at 175°C in a  $[Zn^{2+}]:[OA]$  ratio of 1:2**

The particle sizes calculated from the absorption edges of these spectra are contained in Table 15. It can be seen that, for lower ratios of zinc ion to oleic acid, the calculated band edge after a reaction time of two hours corresponded to the bulk value. This is in agreement with XRD results. For the sample containing 3.5mls oleic acid, the wavelength of the higher energy peak did not vary with increase of synthesis time, until the point when bulk zinc oxide became apparent. After two hours' reaction time for the sample containing 4.2mls oleic acid, the particle size was estimated to be 5.2nm. However, the presence of a small absorbance at 3.2eV may have affected the calculation of particle size in this case. In order to ensure that the particle sizing was accurate, TEM of the samples synthesized with 4.2mls oleic acid was undertaken and is shown in Figure 42. Size analysis of this image showed particles of  $6nm \pm 1.4nm$  in diameter,

however, the low absorbance cross-section of zinc oxide and the presence of a homogeneous stearic acid matrix surrounding the particles hindered accurate measurement.

**Table 15 Particle sizes calculated from the absorption spectra of solutions**

[Zn <sup>2+</sup> ]:[OA] Ratio	Synthesis Time	Band edge, eV	Radius, m	Diameter, nm	Error, nm
<b>2:5</b> <b>3.5mls OA</b>	15mins	3.56	2.1E-09	4.3	0.2
	30mins	3.58	2.1E-09	4.2	0.2
	60mins	3.56	2.1E-09	4.3	0.2
	90mins	3.09	-	-	-
	120mins	3.08	-	-	-
	150mins	3.09	-	-	-
<b>1:2</b> <b>2.8mls OA</b>	15mins	2.3	-	-	-
	30mins	3.44	2.5E-09	5.0	0.3
	60mins	3.2	7.5E-09	15.0	14.7
	90mins	3.21	6.2E-09	12.4	7.2
	120mins	3.2	7.5E-09	15.0	14.7
	150mins	3.21	6.2E-09	12.4	7.2
<b>1:3</b> <b>4.2mls OA</b>	180mins	3.21	6.2E-09	12.4	7.2
	30mins	7.28	0.7E-10	1.4	0.03
	60mins	3.55	2.2E-09	4.3	0.2
	90mins	3.58	2.1E-09	4.2	0.2
	120mins	3.39	2.8E-09	5.5	0.4
	150mins	3.2	7.5E-09	15.0	14.7
	180mins	3.22	5.5E-09	11.0	4.6

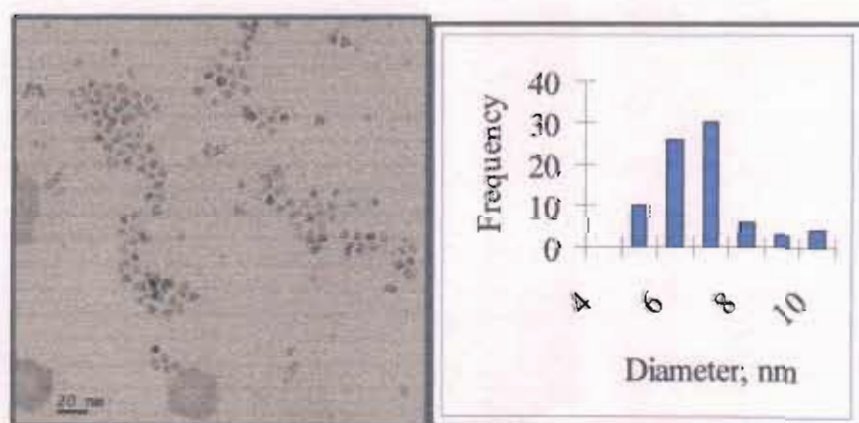


**Figure 42 TEM image of particles synthesized at 175°C with 4.2mls OA, histogram of the sizes of these particles**

### 5.1.5 Removal of stearic acid

As has been previously noted, both stearic acid and zinc stearate were detected in the samples above. An attempt was made to separate these by-products from the organic-capped zinc oxide, by washing in isopropanol. After each washing step, the supernatant was checked under UV light for the presence of ZnO. Absorbance spectra of the washed samples, redispersed in chloroform, are presented in Figure 43.

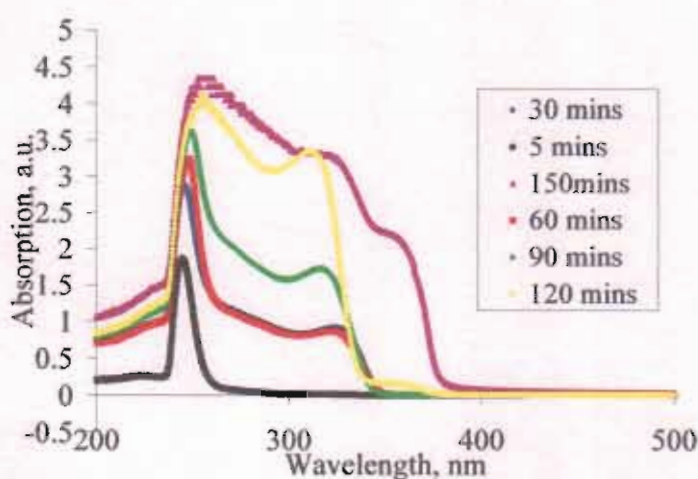


**Figure 43 Absorption spectra for samples synthesized at 175°C containing 4.2mls OA and subsequently washed**

Diffraction patterns of the same material are also shown in Figure 44. From these, it can be seen that while a single washing step reduced the intensity of the diffraction peaks that can be indexed to stearic acid or zinc stearate, the intensity of the absorption shoulders at 3.2 – 3.6eV were *not* similarly decreased. Particles sizes, calculated from both XRD and absorption measurements, are shown in Table 16. In the case of Scherrer equation estimates, the width of the (100) peak was used to assess the average particle size, since this was the most easily resolvable.



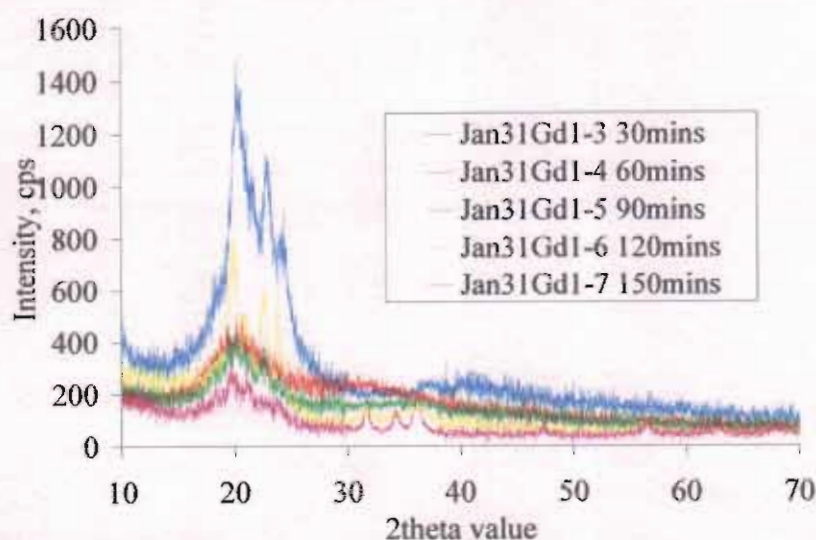


**Figure 44 XRD patterns of samples synthesized at 175°C with 4.2mls OA and washed**

Zinc oxide peaks were not resolvable for aliquots taken after 15mins, 30mins or 60mins' reaction time. This may be due to the amount of material present, or the lower limit of XRD particle size analysis.

**Table 16 Particle size estimates for samples synthesized at 175°C with 4.2mls OA**

UV/vis	Reaction Time	E*, eV	Radius, m	Diameter, nm	Error, nm
	15mins	3.56	2.1E-09	4.3	0.2
	30mins	3.54	2.2E-09	4.4	0.2
	60mins	3.54	2.2E-09	4.4	0.2
	90mins	3.57	2.1E-09	4.2	0.2
	120mins	3.62	2.0E-09	4.0	0.2
	150mins	3.24	4.7E-09	9.3	2.6
XRD	2θ value	Cosθ	FWHM	Diameter, nm	Error, nm
90mins	31.9	0.96	1.41	6	0.4
120mins	31.8	0.96	1.68	5	0.2
150mins	31.6	0.96	0.32	28	10

The low intensity and associated low signal to noise ratio of these peaks may also have accounted for the discrepancy in particle sizes. The fact that the size, estimated by the Scherrer equation, was lower for longer reaction times may support this. Particle size estimations from the absorption spectra also showed a slight reduction in diameter with

increasing synthesis time; again, this may have been due to an increase in the number of particles and associated peak sharpening.

Fluorescence spectra of these samples were recorded and are presented in Figure 45. Of the fluorescence spectra shown below, all samples exhibited surface-defect related luminescence in the visible region characteristic of zinc oxide, except for the aliquot taken after a synthesis time of 15mins, which also showed no band edge related absorption. The intensity of both the visible and UV luminescence peaks increased with reaction time until two hours had passed. The visible peak is in all cases approximately one order of magnitude more intense than that of the excitonic emission.

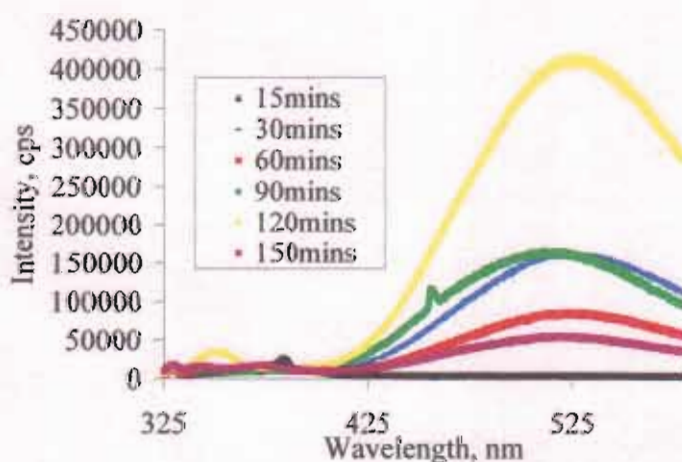


**Figure 45** Fluorescence spectra of samples synthesized at 175°C with a  $[Zn^{2+}]:[OA]$  ratio of 1:3

#### 5.1.6 Effect of the introduction of water to the system

As can be seen for the sample set described in section 5.1.5, the particles produced at 150 minutes had markedly different characteristics from the aliquots taken previously. This was reflected in the properties of the solution; turbidity of the solution was only

observed for samples which were subsequently found to have bulk properties. While an argon pad was passed over the reaction flask over the course of each reaction and all reagents were heated at 110°C for one hour in order to remove any water of hydration, the presence of minute quantities of water or oxygen in the system, that may have encouraged the growth of the particles, cannot be discounted. In order to understand this occurrence, the effect of water on the system was examined. The reaction was initiated in the usual manner and allowed to proceed for one hour, at which point approximately 50% of the solution was withdrawn. 1ml of DIW was added to the remaining material. The solution became turbid almost immediately and after ten minutes a 1ml aliquot was taken from the now turbid solution. XRD patterns of aliquots of equal volume of these samples, washed once in methanol and twice in isopropanol, are shown in Figure 46.

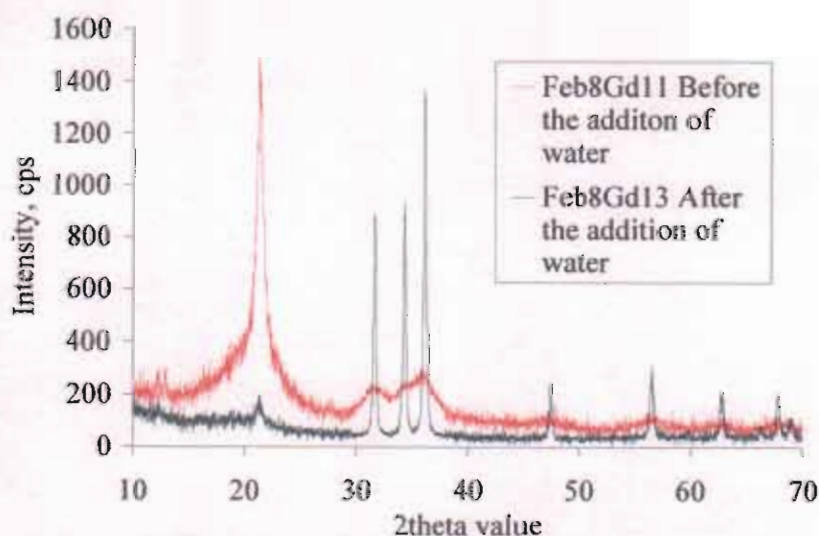


**Figure 46 XRD patterns of samples before and after the introduction of water to the reaction**

The sharp increase in intensity of the zinc oxide peaks was coincident with a decrease in intensity of the peak at  $2\theta = 21.6^\circ$ . One of the strong lines of stearic acid is at  $21.2^\circ$ . Concomitant with this was the enlargement of the particles, from a size calculated by



application of the Scherrer equation to the (100) peak of 3nm to one of approximately 45nm, found from evaluation of the three main peaks. Absorption spectra of these samples are shown in Figure A6 of the appendix. These show that while the aliquot taken before the addition of water exhibited blue-shifted band edge absorption, calculated to indicate a particle diameter of 4.4nm, the sample taken after the addition of water was turbid with bulk absorption characteristics. Fluorescence spectra of these samples are shown in Figure 47. In these, for the sample synthesized before the addition of water, a prominent visible fluorescence and a UV emission of FWHM of 12nm were present. For the sample obtained after the addition of water, a peak at 380nm (3.24eV), possibly corresponding to bound excitons in the bulk material<sup>127</sup> was present and the green luminescence was quenched.

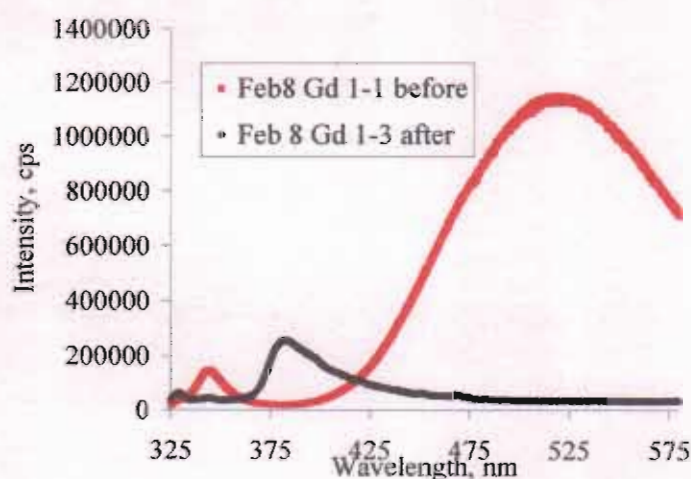


**Figure 47** Fluorescence spectra of samples taken before and after the introduction of water to the reaction vessel

## 5.2 Conclusion

The production of quantized particles by slow decomposition of precursor in the presence of carboxylic capping agents has been demonstrated. Particles of diameter < 20nm, capped with both alkylamines and carboxylic acids, have also been produced. The dependence of the size of the product particles on the amount of capping ligands

present has been demonstrated and the effect of the introduction of water on the number of these capping ligands and consequently on the size of particles produced has been investigated.

## 6 DISCUSSION

### 6.1 *Powders prepared by carboxylic acid chelation*

Investigation of the rate of addition of chelating agent showed that for precursor powders synthesized in the *same* ratios, several differences in the precursor material produced were found. Two crystalline phases, hydrated zinc oxalate together with what may have been anhydrous oxalic acid, anhydrous zinc oxalate, or some other material, were detected for samples prepared through rapid addition of reagents. However when calcined to high temperatures these samples did not show significant infra-red absorption in regions associated with organic material and only crystalline zinc oxide phases were detected by XRD. Of the five phases of oxalic acid listed by the International Centre for Diffraction Data, the phase assigned here was one of "intermediate" frequency. Additionally, while the hydrated form of zinc oxalate was found, the anhydrous phase of oxalic acid was detected at both 300°C and 350°C. In contrast, the precursor prepared by slow combination of reagents showed only hydrated zinc oxalate diffraction peaks at low temperature and the product powders exhibited absorption at 1600cm<sup>-1</sup>. Clearly, the rapid combination of reagents resulted in better crystallinity at lower temperatures of the product material. This may be understood by considering the viscosity of the precursor solution and relative concentrations of the reagents. The slow addition of reagents occurs in an environment with monotonically increasing viscosity, whereas, in the ideal case, rapid combination takes place at constant viscosity. In the case of slow addition, the ratio of zinc ions to oxalic acid molecules also increases slowly until a final value of 1:2 is reached. Thus, the reaction occurred at all intermediate values of the ionic ratio in this case, whereas for rapid combination of reagents only the final ratio is pertinent.



#### 6.1.1 Variation of ratios of reagents

For the variation of the relative concentrations of reagents, the precursor powders showed diffraction patterns similar to those found in the case described in section 6.1. The precursor powders synthesized in a 1:2 ratio of  $[\text{Zn}^{2+}]:[\text{C}_2\text{H}_2\text{O}_4]$  and allowed to mix by diffusion also showed more peaks than the precursor made with equimolar amounts of reagents. These peaks are identical to those assigned previously to anhydrous zinc oxalate or oxalic acid, but not those of the precursor zinc acetate. Thus, it has been shown that in this case the rapid combination of reagents more precisely mimicked the effects of an excess of chelating agent and led to higher crystallinity of product than their slow combination.

#### 6.1.2 Chelation with isophthalic acid

Isophthalic acid was investigated as an analogue to oxalic acid, sharing the property that the dissociation constants of both ligands are less than that of acetic acid. It was found that particles formed in a dendrite superstructure, with crystallite size of the order of 40nm at 500°C and particle growth occurring as the calcination temperature was increased. FTIR spectra reveal that organic material was present in the powders synthesized in a 1:2 ratio of zinc precursor to isophthalic acid even after calcination at 500°C. Equivalent oxalate powders showed that no organic absorption occurred for particles calcined to this temperature. The presence of the surface bound isophthalate ligands may have contributed to the physical separation of particles calcined at such a high temperature, at the expense of monodispersity of particles. Neither of the other isomers of isophthalic acid shares the property that the dissociation constants of both ligands are less than that of acetic acid; thus chelation using these may not be possible.

However, as shown, an excess of chelating agent such that the solution contained a 1:2 ratio of zinc ions to chelating agent may have led to a more crystalline product. Thus, investigation of both remaining isomers of isophthalic acid is warranted.

## 6.2 *Polymer-assisted synthesis*

While the literature methods for synthesizing polymer-stabilised zinc oxide call for heating, cooling and dilution steps, this work has shown that equivalent results can be achieved without adherence to this procedure. However, the quantity of PVP required for this was quite high, with a molar ratio of the polymer to zinc ions of three orders of magnitude. It was found that the addition of water to these particles resulted in their uncontrolled growth and precipitation from solution. Hence, it is possible that because of the high solubility of PVP in water, the polymer ligands did not interact solely with the particle surface. Thus, while it has been shown that zinc oxide may be synthesized at room temperature in alcohol, it is probable that equivalent water-based systems may require investigation of polymer properties.

## 6.3 *Organic capped particles*

Particles with diameter in the quantum-confined regime could be synthesized by the slow thermolysis of a zinc acetate solution in a combination of surfactants. The surfactants used were single-chained, in contrast to existing methods for the synthesis of zinc oxide quantum sized particles by the thermal decomposition of precursors. The particles produced did *not* ripen over time at the reaction temperature; this may have been due to the very effective passivation of the surface by the oleic acid. The production of larger pyramidal crystals through esterification of surfactant has been previously reported.<sup>157</sup> Nevertheless, the agreement of XRD, TEM, absorption and luminescence spectra on the existence and size of the zinc oxide particles has been

obtained. The uncontrolled growth of product particles in the presence of oxygen has also been previously noted through the introduction of alcohols and again was found here, with the use of water.



## 7 Future work

### 7.1 *Organic-capped particles*

The homogeneous incorporation of dopants into the crystal lattice is requisite for room temperature ferromagnetic ordering. This work substantiates that the thermal decomposition of precursors allows the preparation of small particles and the capping ligands used hinder particle growth over time. It has also been shown that uniform particles can be obtained through the decomposition of precursor in the presence of small amounts of water. It has been determined<sup>158</sup> that the incorporation of dopants to similar systems, in a core-shell structure, can be achieved through hot injection of reagents and the subsequent growth of particles. Possible future directions could then include:

- i. The doping of zinc oxide through this method, for quantum-confined particles capped with a carboxylic acid. The extent of incorporation into the zinc oxide lattice can easily be determined by XRD and optical absorption spectroscopy, in addition to electron microscopies.
- ii. The synthesis of slightly larger particles capped with both amine and carboxyl groups. Additionally, further studies can be performed on the optical properties of particles capped with both amine and carboxyl group. Ligand exchange of the smaller particles may be investigated, in order to contrast *their* optical properties.

### 7.2 *Polymer-assisted synthesis*

Investigation of polymer-assisted synthesis was originally motivated with the aim of aqueous phase synthesis of zinc oxide at room temperature. Results in this respect were unsatisfactory. This has been attributed to the exceptionally high solubility in water of

the polymer used. Thus, investigation of similar poly(amides) is proposed. Further investigation of the system under the addition of small amounts of water is also warranted; specifically the behaviour of particles in buffered solutions.

### **7.3 Carboxylic acid chelation**

In the case of precursor particles chelated with carboxylic acids, two avenues of enquiry are possible. The variation of ratios of zinc ion to chelating ligand may be extended to smaller values. While the positive effect on particle size in this case may be slight, the stability of the gel may be enhanced by the inclusion of such a large number of chelating ligands. This would allow greater control over particle doping. The investigation of isomers of isophthalic acid for their effect on particle purity and morphology and on the physical properties of the precursor is also required. The identification of the precursor attributed to either excess oxalic acid or anhydrous zinc oxalate in the text may be aided by thermal gravimetric analysis, TEM analysis of the crystallinity of the precursor powders or more accurate XRD studies.

## 8 Conclusion

The synthesis of zinc oxide particles has been explored through three routes, with a view to introducing transition metal dopants to the material. It was found that, for particles produced through a polymeric precursor method, the method of preparation of precursor had a significant effect on the product purity, *i.e.* the final state was not independent of synthesis parameters. The variation of chelating agent was associated with a change in the structure of aggregates of the particles produced. Investigation of zinc oxide synthesis through polymer assisted alkaline hydrolysis yielded the result that it was possible to produce particles of sizes  $< 10\text{nm}$ , stable for a number of days at room temperature, without the necessity to dilute solutions. Finally, examination of organic phase synthesis was undertaken and a reaction suitable for synthesis of 6nm particles, stable in the reaction medium, in which the particles produced *do not* grow as the reaction time increases, was developed.



## 9 References

---

- [1] H. G. El-Shobaky, M. Mokhtar, G. A. El-Shobaky *Applied Catalysis A* 180 (1999) 335
- [2] G. Glaspell, L. Fuoco, M. Samp El-Shall, *Journal of Physical Chemistry B* 109 (2005) 17350
- [3] B. Bott, T. A. Jones, B. Mann, *Sensors and Actuators* 5 (1984) 65
- [4] M. Huang, S. Mao, H. Feick, H. Yan, Y. Wu, H. Kind, E. Weber, R. Russo, P. Yang, *Science* 292 (2001) 1897.
- [5] Y. Yoshino, T. Makino, Y. Katayama, T. Hata, *Vacuum* 59 (2000) 538
- [6] H. Nanto, T. Minami, S. J. Takata, *Applied Physics* 60 (1986) 482
- [7] T. Minami, *MRS Bulletin* 25 (2000) 38
- [8] D. C. Look, *Materials Science and Engineering B* 80 (2001) 383
- [9] T. Dietl, H. Ohno, *Science* 287 (2000) 1019
- [10] H. Ohno, *Science* 281 (1998) 951
- [11] A. E. Jimenez-Gonzalez, J. A. Soto Urueta, R. Suarez-Parra, *Journal of Crystal Growth* 192 (1998) 430
- [12] L. E. Brus, *Journal of Chemical Physics*, 80 (1984) 4403
- [13] D. M. Bagnall, Y. F. Chen, Z. Zhu, T. Yao, S. Koyama, M. Y. Shen, T. Goto, *Applied Physics Letters* 70 (1997) 2230
- [14] D. Vanmaekelbergh, P. Liljeroth, *Chemical Society Reviews*, 34 (2005) 299
- [15] Powder Diffraction File 00-036-1451, ICDD, 2006
- [16] Powder Diffraction File 00-021-1486, ICDD, 2006
- [17] W.-J. Li, E.-W. Shi, W.-Z. Zhong, Z.-W. Yin, *Journal of Crystal Growth* 203 (1999) 186
- [18] C. Ronning, N. G. Shang, I. Gerhards, H. Hofsass, M. Seibt, *Journal of Applied Physics*, 98 (2005) 034307
- [19] C. Wang, E. Shen, E. Wang, L. Gao, Z. Kang, C. Tian, Y. Lan, C. Zhang, *Materials Letters* 59 (2005) 2867
- [20] U. Pal, P. Santiago, *Journal of Physical Chemistry B* 109 (2005) 15317
- [21] L.C. Nistora,, C. Ghica, D. Matei, G. Dinescu, M. Dinescu, G. Van Tendeloo, *Journal of Crystal Growth* 277 (2005) 26
- [22] D. Ledwith, S. C. Pillai, G. W. Watson, J. M. Kelly, *Chemical Communications*, (2004) 2294
- [23] V. K. LaMer, R. H. Dinegar, *Journal of the American Chemical Society*, 72 (1950) 4847
- [24] A. L. Rogach, D. V. Talapin, E. V. Shevchenko, A. Kornowski, M. Haase, H. Weller, *Advanced Functional Materials*, 12 (2002) 653
- [25] C. B. Murray, C. R. Kagan, M. G. Bawendi, *Annual Review of Materials Science*, 30 (2000) 545
- [26] W. Ostwald, *Analytische Chemie*, 3<sup>rd</sup> Ed., Engelmann, Leipzig, 1901, p. 23
- [27] I. M. Lifshitz, V. V. Slyozov, *J. Phys. Chem. Solids* 19 (1961) 35
- [28] C. Wagner, *Z. Elektrochem*, 65 (1961) 581
- [29] E.M. Wong, J. E. Bonevich, P. C. Searson, *Journal of Physical Chemistry B* 102 (1998) 7770

- [30] L. Guo, S. Yang, C. Yang, P. Yu, J. Wang, W. Ge, G. K. L. Wong, *Applied Physics Letters* 76 (2000) 2901
- [31] P. D. Cozzoli, A. Kornowski, H. Weller, *Journal of Physical Chemistry B* 109 (2005) 2638
- [32] C. B. Murray, D. J. Norris, M. G. Bawendi, *Journal of the American Society* 115 (1993) 8706
- [33] H. M. Yang, X. C. Zhang, A. D. Tang, W. Q. Ao, *Materials Science and Technology*, 20 (2004) 1493
- [34] S.-I. Park, G. Y. Ahn, I.-B. Shin, C. S. Kim, *Journal of Magnetism and Magnetic Materials* 282 (2004) 321
- [35] Z. L. Wang, *Materials Today*, (2004) 26
- [36] J. H. Kim, H. Kim, D. Kim, S. G. Yoon, W. K. Choo, *Solid State Communications* 131 (2004) 677
- [37] J. A. Sans, A. Segura, M. Mollar, B. Mari, *Thin Solid Films* 453 (2004) 251
- [38] J. Lim, K. Shin, H. Kim, C. Lee, *Thin Solid Films* 475 (2005) 256
- [39] S. Fay, U. Kroll, C. Bucher, E. Vallat-Sauvain, A. Shah, *Solar Energy Materials & Solar Cells* 86 (2005) 385
- [40] K. Okuyama, I. W. Lenggoro, *Chemical Engineering Science* 58 (2003) 537
- [41] L. Madler, W. J. Stark, S. E. Pratsinis, *Journal of Applied Physics*, 92 (2002) 6537
- [42] R. Ayouchi, F. Martin, D. Leinen, J. R. Ramos-Barrado, *Journal of Crystal Growth*, 247 (2003) 497
- [43] K.-K. Kim, N. Koguchi, Y.-W. Ok, T.-Y. Seong, S.-J. Park, *Applied Physics Letters*, 84 (2004) 3810
- [44] D. W. Ma, Z. Z. Ye, H. M. Lu, J. Y. Huang, B. H. Zhao, L. P. Zhu, H. J. Zhang, P. M. He, *Thin Solid Films* 461 (2004) 250
- [45] J. Hambrock, S. Rabe, K. Merz, A. Birkner, A. Wohlfart, R. A. Fischer, M. Driess, *Journal of Materials Chemistry*, 13 (2003) 1731
- [46] C. G. Kim, K. Sung, T.-M. Chung, D. Y. Jung, Y. Kim, *Chemical Communications*, (2003) 2068
- [47] D. S. Boyle, K. Govender, P. O'Brien, *Chemical Communications*, (2002) 80
- [48] X. D. Gao, X. M. Li, W. D. Yu, *Materials Research Bulletin*, 40 (2005) 1104
- [49] A. M. Chaparro, C. Maffiotte, M. T. Gutierrez, J. Herrero, *Thin Solid Films*, 431 (2003) 373
- [50] F. Tang, Y. Sakka, T. Uchikoshi, *Materials Research Bulletin*, 38 (2003) 207
- [51] H. Li, R. Wang, C. Guo, H. Zhang, *Materials Science and Engineering B* 103 (2003) 285
- [52] M. Berber, V. Bulto, R. Klib, H. Hahn, *Scripta Materialia*, 53 (2005) 547
- [53] R. E. Marotti, D. N. Guerra, C. Bello, G. Machado, E. A. Dalchiele, *Solar Energy Materials & Solar Cells* 82 (2004) 85
- [54] Z. R. Tain, J. A. Voigt, J. Lui, B. McKenzie, M. J. McDermott, M. A. Rodriguez, H. Konishi, H. Xu, *Nature Materials* 2 (2003) 821
- [55] X. Feng, L. Feng, M. Jin, J. Zhai, L. Jiang, D. Zhu, *Journal of the American Chemical Society*, 126 (2004) 62
- [56] J. Liang, J. Liu, Q. Xie, S. Bai, W. Yu, Y. Qian, *Journal of Physical Chemistry B*, 109 (2005) 9463
- [57] F. Zhou, X. Zhao, H. Zheng, T. Shen, C. Tang, *Chemistry Letters*, 34 (2005) 1114



- [58] Z. Wang, X.-F. Qian, J. Yin, Z.-K. Zhu, *Journal of Solid State Chemistry*, 177 (2004) 2144
- [59] C. Wang, E. Shen, E. Wang, L. Gao, Z. Kang, C. Tian, Y. Lan, C. Zhang, *Materials Letters* 59 (2005) 2867
- [60] X. Ma, H. Zhang, Y. Ji, J. Xu, D. Yang, *Materials Letters* 59 (2005) 3393
- [61] N. Uekawa, R. Yamashita, Y. J. Wu, K. Kakegawa, *Physical Chemistry Chemical Physics* 6 (2004) 442
- [62] J. Zhang, L. Sun, J. Yin, H. Su, C. Liao, C. Yan, *Chemistry of Materials* 14 (2002) 4172
- [63] N. Uekawa, M. Kitamura, S. Ishii, T. Kojima, K. Kakegawa, *Journal of the Ceramic Society of Japan*, 113 (2005) 439
- [64] J. Zhang, L. Sun, C. Liao, C. Yan, *Chemical Communications* (2002) 262
- [65] L. DiLeo, D. Romano, L. Schaeffer, B. Gersten, C. Foster, M. C. Gelabert, *Journal of Crystal Growth*, 271 (2004) 65
- [66] L. Vayssieres, K. Keis, A. Hagfeldt, S.-E. Lindquist, *Chemistry of Materials*, 13 (2001) 4395
- [67] Y. Wang, M. Li, *Materials Letters* 60 (2006) 266
- [68] M. L. Kahn, M. Monge, V. Colliere, F. Senocq, A. Maisonnat, B. Chaudret, *Advanced Functional Materials*, 15 (2005) 458
- [69] Y. He, *Materials Chemistry and Physics* 92 (2005) 609
- [70] J. Y. Liang, G. Lin, X.-H. Bin, L. Jing, L. X. Dong, W. Z. Hua, W. Z. Yu, J. Weber, *Journal of Crystal Growth*, 252 (2003) 266
- [71] J.-F. Hocheplied, A. P. A. de Oliveira, V. Guyot-Ferreol, J.-F. Tranchant, *Journal of Crystal Growth*, 283 (2005) 156
- [72] S. Sakohara, S. Honda, Y. Yanai, M. A. Anderson, *Journal of Chemical Engineering of Japan*, 34 (2001) 15
- [73] W.-W. Wang, Y.-J. Zhu, *Chemistry Letters*, 33 (2004) 988
- [74] L. Spanhel, M. A. Anderson, *Journal of the American Chemical Society*, 113 (1991) 2826
- [75] R. D. Yang, S. Tripathy, Y. Li, H.-J. Sue, *Chemical Physics Letters*, 411 (2005) 150
- [76] P. Li, Y. Wei, H. Liu, X. Wang, *Chemical Communication*, (2004) 2856
- [77] A. Wood, M. Giersig, M. Hilgendorff, A. Vilas-Campos, L. M. Liz-Marzan, P. Mulvaney, *Australian Journal of Chemistry*, 56 (2003) 1051
- [78] K. Borgohain, S. Mahamuni, *Semiconductor Science and Technology*, 13 (1998) 1154
- [79] S. Mahamuni, B. S. Bendre, V. J. Leppert, C. A. Smith, D. Cooke, S. H. Risbud, H. W. H. Lee, *Nanostructured Materials*, 7 (1996) 659
- [80] Z. Y. Xiao, Y. C. Lu, L. Dong, C. L. Shao, J. Y. Zhang, Y. M. Lu, D. Z. Zhen, X. W. Fan, *Journal of Colloid and Interface Science* 282 (2005) 403
- [81] D. W. Bahnemann, C. Kormann, M. R. Hoffmann, *The Journal of Physical Chemistry* 91 (1987) 3789
- [82] E. A. Meulenkaamp, *Journal of Physical Chemistry B*, 102 (1998) 5566
- [83] L. Armelao, M. Fabrizio, S. Gialanella, F. Zordan, *Thin Solid Films*, 394 (2001) 90
- [84] A. P. A. Oliveira, J. F. Hocheplied, F. Grillon, M.-H. Berger, *Chemistry of Materials*, 15 (2003) 3202
- [85] J. Joo, S. G. Kwon, J. H. Yu, T. Hyeon, *Advanced Materials* 17 (2005) 1873



- [86] C. Cannas, M. Casu, A. Lai, A. Musinu, G. Piccaluga, *Journal of Materials Chemistry*, 9 (1999) 1765
- [87] S. I. Yoo, B.-H. Sohn, W.-C. Zin, S.-J. An, G.-C. Yi, *Chemical Communication* (2004) 2850
- [88] H.-M. Xiong, D.-P. Liu, Y.-Y. Xia, J.-S. Chen, *Chemistry of Materials* 17 (2005) 3062
- [89] J. Tang, Y. Wang, H. Liu, Y. Xia, B. Scheider, *Journal of Applied Polymer Science*, 90 (2003) 1053
- [90] S.-C. Liufu, H.-N. Xiao, Y.-P. Li, *Materials Letters*, 59 (2005) 3494
- [91] J.-W. Shim, J.-W. Kim, S.-H. Han, I.-S. Chang, H.-K. Kim, H.-H. Kang, O.-S. Lee, K.-D. Suh, *Colloids and Surfaces A: Physicochemical and Engineering Aspects* 207 (2002) 105
- [92] P. A. Lessing, *Ceramic Bulletin* 68 (1989) 1002
- [93] D. Mondelaers, G. Vanhoyland, H. Van den Rul, J. D'Haen, M. K. van Bael, J. Mullens, L. C. Van Puocke, *Materials Research Bulletin*, 37 (2002) 901
- [94] E. M. Wong, P. G. Hoertz, C. J. Liang, B.-M. Shi, G. J. Meyer, P. C. Searson, *Langmuir* 17 (2001) 8362
- [95] C. F. Baes, R. E. Mesmer, *The Hydrolysis of Cations*, John Wiley & Sons, New York, pp. 287 - 294
- [96] P. Schindler, H. Althaus, W. Feitknecht, *Helv. Chim. Acta* 47 (1964) 982
- [97] W.-W. Wang, Y.-J. Zhu, *Chemistry Letters*, 33 (2004) 988
- [98] M. Haase, H. Weller, A. Henglein, *Journal of Physical Chemistry* 92 (1988) 482
- [99] Z. Hu, D. J. Escamilla Ramirez, B. E. Heredia Cervera, G. Oskam, P. C. Searson, *Journal of Physical Chemistry B* 109 (2005) 11209
- [100] U. Koch, A. Fojtik, H. Weller, A. Henglein, *Chemical Physics Letters* 122 (1985) 507
- [101] N. Uekawa, M. Kitamura, S. Ishii, T. Kojima, K. Kakegawa, *Journal of the Ceramic Society of Japan* 113 (2005) 439
- [102] L. Guo, S. Yang, C. Yang, P. Yu, J. Wang, W. Ge, G. K. L. Wong, *Chemistry of Materials* 12 (2000) 2208
- [103] H. Tang, M. Yan, X. Ma, H. Zhang, M. Wang, D. Yang, *Sensors and Actuators B*, 113 (2006) 324
- [104] J. N. Wang, C. L. Yang, S. H. Wang, L. Guo, S. H. Yang, I. K. Sou, W. K. Ge, *International Journal of Modern Physics B*, 16 (2002) 4363
- [105] K. Borgohain, S. Mahamuni, *Semiconductor Science and Technology*, 13 (1998) 1154
- [106] C.-H. Hung, W.-T. Whang, *Journal of Materials Chemistry*, 15 (2005) 267
- [107] H.-M. Xiong, D.-P. Liu, Y.-Y. Xia, J.-S. Chen, *Chemistry of Materials*, 17 (2005) 3062
- [108] S. Ram, T. K. Kundu, *Journal of Nanoscience and Nanotechnology*, 4 (2004) 1076
- [109] H. A. Ali, A. A. Iliadis, *Thin Solid Films*, 471 (2005) 154
- [110] S. I. Yoo, B.-H. Sohn, W.-C. Zin, S.-J. An, G.-C. Yi, *Chemical Communications* (2004) 2850
- [111] Y. E. Kirsh, *Water Soluble Poly-N-Amides: Synthesis and Physicochemical Properties*, John Wiley & Sons, Chicester, p80
- [112] A. van Dijken, E. A. Meulenlamp, D. Vanmeakelbergh, A. Meijerink, *Journal of Physical Chemistry B* 104 (2000) 1715



- [113] G. Rodriguez-Gattorno, P. Santiago-Jacinto, L. Rendon-Vazquez, J. Nemeth, I. Dekany, D. Diaz, *Journal of Physical Chemistry B*, 107 (2003) 12597
- [114] S.-H. Choi, E.-G. Kim, J. Park, K. An, N. Lee, S. C. Kim, T. Hyeon, *Journal of Physical Chemistry B*, 109 (2005) 14792
- [115] P. D. Cozzoli, M. L. Curri, A. Agostiano, G. Leo, M. Lomascolo, *Journal of Physical Chemistry B* 107 (2003) 4756
- [116] J. Park, K. An, Y. Hwang, J.-G. Park, H.-J. Noh, J.-Y. Kim, J.-H. Park, N.-M. Hwang, T. Hyeon, *Nature Materials*, 3 (2004) 891
- [117] P. M. Pechini, US Patent #3330697, 1967
- [118] A. Sinha, B. P. Sharma, *Materials Research Bulletin*, 32 (1997) 1571
- [119] M. Cerqueira, R. S. Nasar, E. Longo, E. R. Leite, J. A. Varela, *Materials Letters* 22 (1995) 181
- [120] D. W. Lee, J. H. Won, K. B. Shim, *Materials Letters* 57 (2003) 3346
- [121] M. Kakihana, *Journal of Sol-Gel Science and Technology*, 6 (1996) 7
- [122] L. Banyai, S. W. Koch, *Semiconductor Quantum Dots*, World Scientific Series on Atomic, Molecular and Optical Physics, Vol. 2, World Scientific Co. Ltd., Singapore, pp5
- [123] L. Brus, *IEEE Journal of Quantum Electronics* 22 (1986) 1909
- [124] R. Viswanatha, S. Sapra, B. Satpati, P. V. Satyam, B. N. Dev, D. D. Sarma, *Journal of Materials Chemistry*, 14 (2004) 661
- [125] J. Tauc, R. Grigorovici, A. Vancu, *Physica Status Solidi*, 15 (1966) 627
- [126] N. S. Pesika, K. J. Stebe, P. C. Searson, *Advanced Materials* 15 (2003) 1290
- [127] D. M. Bagnall, Y. F. Chen, M. Y. Shen, Z. Zhu, T. Goto, T. Yao, *Journal of Crystal Growth*, 184-185 (1998) 605
- [128] M. H. Huang, S. Mao, H. Feick, H. Yan, Y. Wu, H. Kind, E. Weber, R. Russo, P. Yang, *Science* 292 (2001) 1897
- [129] H. Fu, A. Zunger, *Physical Review B*, 56 (1997) 1496
- [130] M. Shim, P. Guyot-Sionnest, *Journal of the American Chemical Society*, 123 (2001) 11651
- [131] S. Mahamuni, K. Borgohain, B. S. Bendre, V. J. Leppert, S. H. Risbud, *Journal of Applied Physics*, 85 (1999) 2861
- [132] C. R. Gorla, N. W. Emanetoglu, S. Liang, W. E. Mayo, Y. Lu, M. Wraback, H. Shen, *Journal of Applied Physics*, 85 (1999) 2595
- [133] K. Vanheusden, W. L. Warren, C. H. Seager, D. R. Tallant, J. A. Voigt, B. E. Gnade, *Journal of Applied Physics* 79 (1996) 7983
- [134] S. Sakohara, M. Ishida, M. A. Anderson, *Journal of Physical Chemistry B*, 102 (1998) 10169
- [135] Y. W. Heo, D. P. Norton, S. J. Pearton, *Journal of Applied Physics*, 98 (2005) 073502
- [136] W. Que, Y. Zhou, Y. L. Lam, Y. C. Chan, C. H. Kam, B. Liu, L. M. Gan, C. H. Chew, G. Q. Xu, S. J. Chua, S. J. Xu, F. V. C. Mendis, *Applied Physics Letters*, 73 (1998) 2727
- [137] T. Koda, S. Shionoya, M. Ichikawa, S. Minomura, *J. Phys. Chem. Solids*, 27 (1966) 1577
- [138] T. Andelman, Y. Gong, M. Polking, M. Yin, I. Kuskovsky G. Neumark, S. O'Brien, *Journal of Physical Chemistry B*, 109 (2005) 14314
- [139] N. S. Norberg, D. R. Gamelin, *Journal of Physical Chemistry B*, 109 (2005) 20810

- [140] C. Kittel, Introduction to Solid State Physics, 7<sup>th</sup> Ed., 1996, John Wiley & Sons, New York, pp.29-52
- [141] R. Jenkins, R. L. Snyder, Introduction to X-Ray Powder Diffractometry, 1996, John Wiley & Sons, New York, pp. 89-90
- [142] C. Liu, F. Yun, H. Morkoc, Journal of Materials Science: Materials in Electronics 16 (2005) 555
- [143] D. A. Schwartz, K. R. Kittilsveld, D. R. Gamelin, Applied Physics Letters, 85 (2004) 1395
- [144] S. Maensiri, J. Sreesongmaung, C. Thomas, J. Klinkaewnarong, Journal of Magnetism and Magnetic Materials, 301 (2006) 422
- [145] K. G. Kanade, B. B. Kale, R. C. Aiyer, B. K. Das, Materials Research Bulletin, 41 (2006) 590
- [146] Y.-F. Zhou, Y.-J. Zhao, D.-F. Sun, J.-B. Weng, R. Cao, M-C. Hong, Polyhedron, 22 (2003) 1231
- [147] B. D. Cullity, S. R. Stock, Elements of X-Ray Diffraction, 3<sup>rd</sup> Ed., Prentice Hall, New Jersey, 2001, pp.167-171
- [148] N. S. Pesika, Z. Hu, K. J. Stebe, P. C. Searson, Journal of Physical Chemistry 106 (2002) 6985
- [149] CRC Handbook of Chemistry and Physics, 84<sup>th</sup> Ed., 2003. CRC Press LLC, pp.8-48
- [150] Powder Diffraction File 00-025-1029, ICDD, 2006
- [151] Powder Diffraction File 00-037-0718, ICDD, 2006
- [152] Powder Diffraction File 20-1817, ICDD, 2006
- [153] E. Kucur, J. Riegler, G. Urban, T. Nann, Journal of Chemical Physics, 121 (2004) 1074
- [154] Powder Diffraction File 38-1923, ICDD, 2006
- [155] Powder Diffraction File 00-001-0089, ICDD, 2006
- [156] Powder Diffraction File 05-0079, ICDD, 2006
- [157] Y. Chen, M. Kim, G. Lian, M. B. Johnson, X. Peng, Journal of the American Chemical Society, 127 (2005) 13332
- [158] S. C. Erwin, L. Zu, M. I. Haftel, A. L. Efros, T. A. Kennedy, D. J. Norris, Nature, 436 (2005) 91



## 10 APPENDIX

### 10.1 Powders prepared through the use of oxalic acid.

Temperature evolution of powders

#### 10.1.1

**Table A 1 XRD peaks resolvable for precursor particles calcined to 300°C**

Slow addition, 2θ value	Intensity, %	Rapid addition, 2θ value	Intensity, %	Assignment
		15.217	5.2	Unidentified Peak
18.854	100.0	18.854	100.0	C <sub>2</sub> O <sub>4</sub> Zn.2H <sub>2</sub> O (-202)
22.745	27.0	22.737	22.8	C <sub>2</sub> O <sub>4</sub> Zn.2H <sub>2</sub> O (002)
		24.097	33.1	C <sub>2</sub> H <sub>2</sub> O <sub>4</sub> (011)
25.058	8.3	25.152	14.6	C <sub>2</sub> O <sub>4</sub> Zn.2H <sub>2</sub> O (-112)
30.294	36.1	30.258	31.1	C <sub>2</sub> O <sub>4</sub> Zn.2H <sub>2</sub> O (-402)
31.687	5.6	31.907	10.2	ZnO (100)
33.875	6.6	33.473	13.9	C <sub>2</sub> O <sub>4</sub> Zn.2H <sub>2</sub> O (-113)
		34.151	10.9	C <sub>2</sub> H <sub>2</sub> O <sub>4</sub> (021)
35.263	7.0	35.250	11.3	C <sub>2</sub> O <sub>4</sub> Zn.2H <sub>2</sub> O (021)
		36.348	8.8	ZnO (101)
37.647	4.4	37.949	13.5	Slide Background
40.632	5.3	40.636	9.0	C <sub>2</sub> O <sub>4</sub> Zn.2H <sub>2</sub> O (022)
43.622	5.6	43.524	8.8	C <sub>2</sub> O <sub>4</sub> Zn.2H <sub>2</sub> O (-223)
		45.687	7.4	C <sub>2</sub> O <sub>4</sub> Zn (121)
46.378	5.0	46.423	8.5	
47.517	8.4	47.598	12.5	ZnO (102)
48.507	6.1	48.475	9.9	C <sub>2</sub> O <sub>4</sub> Zn.2H <sub>2</sub> O (023)
		49.205	7.7	C <sub>2</sub> O <sub>4</sub> Zn (220)
51.746	4.1	51.600	7.7	C <sub>2</sub> O <sub>4</sub> Zn.2H <sub>2</sub> O (130)
		52.508	5.7	C <sub>2</sub> O <sub>4</sub> Zn (002)
53.622	2.8	53.348	5.8	
		54.287	5.9	C <sub>2</sub> O <sub>4</sub> Zn.2H <sub>2</sub> O (131)
		56.608	6.4	C <sub>2</sub> O <sub>4</sub> Zn (301)
58.246	4.0	58.162	7.1	Unidentified Peak
62.820	3.8	62.968	6.7	C <sub>2</sub> O <sub>4</sub> Zn.2H <sub>2</sub> O (-804)
63.349	3.5	63.296	6.1	C <sub>2</sub> O <sub>4</sub> Zn.2H <sub>2</sub> O (-621)

**Table A2 Resolvable XRD peaks for precursor powders calcined to 375°C**

Slow Addition, 2θ value	Intensity, %	Rapid Addition, 2θ value	Intensity, %	Assignment
11.965	11.2	12.424	5.3	Unidentified peak
13.064	18.7			Unidentified peak
18.037	19.1			C <sub>2</sub> O <sub>4</sub> Zn.2H <sub>2</sub> O (-

				202)
31.911	83.5	31.936	73.7	ZnO (100)
34.537	67.1	34.555	60.0	ZnO (002)
36.396	100.0	36.392	100.0	ZnO (101)
47.706	23.8	47.698	20.6	ZnO (102)
49.418	14.7			Unidentified peak
56.755	34.4	56.763	39.0	ZnO (110)
57.831	14.8			Unidentified peak
59.740	15.2			Unidentified peak
63.049	26.0	62.995	26.0	ZnO (103)
		66.547	10.3	ZnO (200)
68.103	24.8	68.090	26.8	ZnO (112)
69.301	17.7	69.237	15.6	ZnO (201)
72.670	11.9	72.586	7.0	ZnO (004)
73.090	11.0	76.906	6.8	ZnO (202)
		77.325	6.5	Unidentified peak

**Table A3 Resolvable XRD peaks for precursor powders calcined to 400°C**

Slow Addition, 2 $\theta$ values	Intensity, %	Rapid Addition, 2 $\theta$ values	Intensity, %	Assignment
15.359	4.9			Unidentified peak
17.087	5.9			Unidentified peak
17.718	6.6			Unidentified peak
25.232	10.9			Unidentified peak
31.904	71.4	31.903	68.2	ZnO (100)
34.543	56.8	34.526	56.3	ZnO (002)
36.390	100.0	36.378	100.0	ZnO (101)
38.680	6.2			Unidentified peak
47.706	17.9	47.691	16.8	ZnO (102)
52.768	5.0			Unidentified peak
56.766	33.9	56.747	33.7	ZnO (110)
62.240	7.7			Unidentified peak
62.988	23.3	62.970	22.5	ZnO (103)
66.609	8.4	66.556	6.9	ZnO (200)
68.081	23.2	68.081	22.4	ZnO (112)
69.250	13.7	69.229	11.9	ZnO (201)
72.601	5.6	72.578	3.8	ZnO (004)
		76.971	4.2	Unidentified peak
77.247	5.5	77.253	4.2	ZnO (202)

**Table A4 Resolvable XRD peaks for precursor powders calcined to 425°C**

Slow Addition, 2 $\theta$ values	Intensity, %	Rapid Addition, 2 $\theta$ values	Intensity, %	Assignment
27.836	6.5			Unidentified peak
31.898	73.5	32.011	70.1	ZnO (100)
34.533	57.8	34.647	56.7	ZnO (002)



36.381	100.0	36.493	100.0	ZnO (101)
39.505	4.2			Unidentified peak
47.690	16.5	47.784	16.6	ZnO (102)
		54.662	3.3	Unidentified peak
56.744	28.0	56.849	28.5	ZnO (110)
62.987	19.8	63.094	20.7	ZnO (103)
65.538	3.9			Unidentified peak
66.567	6.4	66.647	6.3	ZnO (200)
68.085	17.5	68.181	19.8	ZnO (112)
69.223	10.3	69.340	10.6	ZnO (201)
72.652	4.1	72.695	4.1	ZnO (004)
		73.000	3.4	Unidentified peak
77.312	4.1	77.194	4.2	ZnO (202)

**Table A5 Resolvable XRD peaks for precursor powders calcined to 450°C**

Slow Addition, 2 $\theta$ values	Intensity, %	Rapid Addition, 2 $\theta$ values	Intensity, %	Assignment
		10.464	1.9	Unidentified peak
		19.171	3.5	Unidentified peak
		20.578	3.9	Unidentified peak
		23.701	4.9	Unidentified peak
28.732	6.1			Unidentified peak
29.549	6.2			Unidentified peak
31.880	74.5	31.946	71.0	ZnO (100)
34.519	53.6	34.587	57.5	ZnO (002)
36.364	100.0	36.432	100.0	ZnO (101)
		39.361	3.0	Unidentified peak
		42.046	3.2	Unidentified peak
47.664	16.2	47.732	15.9	ZnO (102)
		52.969	2.8	Unidentified peak
		54.196	2.9	Unidentified peak
		55.181	2.9	Unidentified peak
56.740	29.1	56.791	27.2	ZnO (110)
62.981	19.4	63.038	20.2	ZnO (103)
66.527	6.2	66.585	5.7	ZnO (200)
68.067	18.7	68.121	17.9	ZnO (112)
69.190	9.9	69.286	9.3	ZnO (201)
72.685	4.1	72.686	3.4	ZnO (004)
77.098	4.0	77.116	3.7	ZnO (202)

**Table A6 Resolvable peaks for precursor powders calcined to 500°C**

Slow Addition, 2 $\theta$ values	Intensity, %	Rapid Addition, 2 $\theta$ values	Intensity, %	Assignment
13.363	1.8			Unidentified peak
31.885	73.2	31.889	64.9	ZnO (100)
34.495	43.4	34.557	48.1	ZnO (002)



Slow Addition, 20 values	Intensity, %	Rapid Addition, 20 values	Intensity, %	Assignment
36.333	100.0	36.393	100.0	ZnO (101)
47.646	15.2	47.672	18.4	ZnO (102)
56.708	22.3	56.755	28.0	ZnO (110)
62.961	14.3	62.993	21.5	ZnO (103)
66.474	4.3	66.535	4.2	ZnO (200)
68.038	12.5	68.092	18.0	ZnO (112)
69.175	7.0	69.210	9.1	ZnO (201)
72.665	2.6	72.708	2.4	ZnO (004)
77.026	2.8	77.088	3.0	ZnO (202)

### 10.1.2 TEM Size Distributions

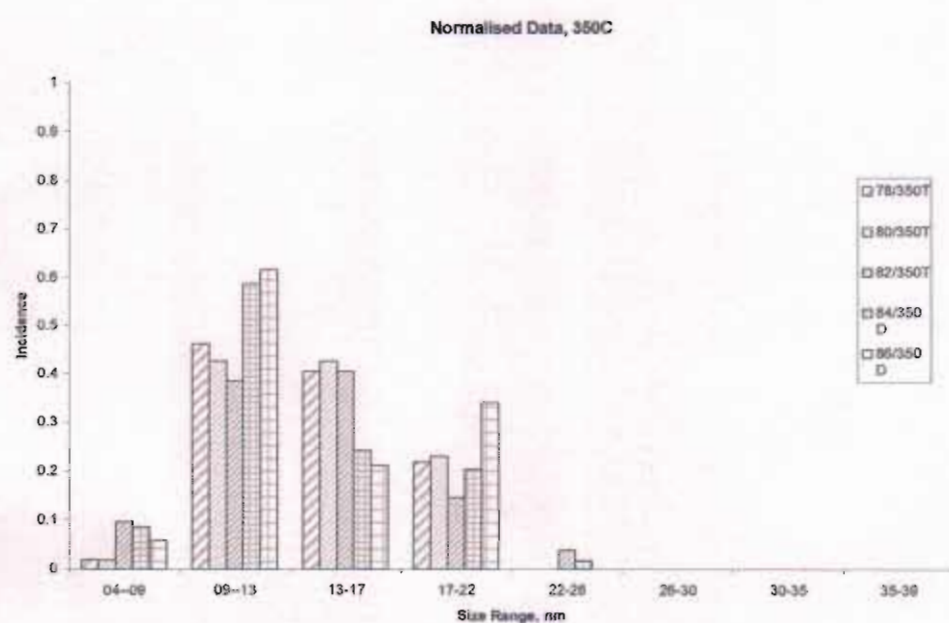


**Figure A 1** TEM Size distributions of particles calcined to 350°C, as a fraction of total

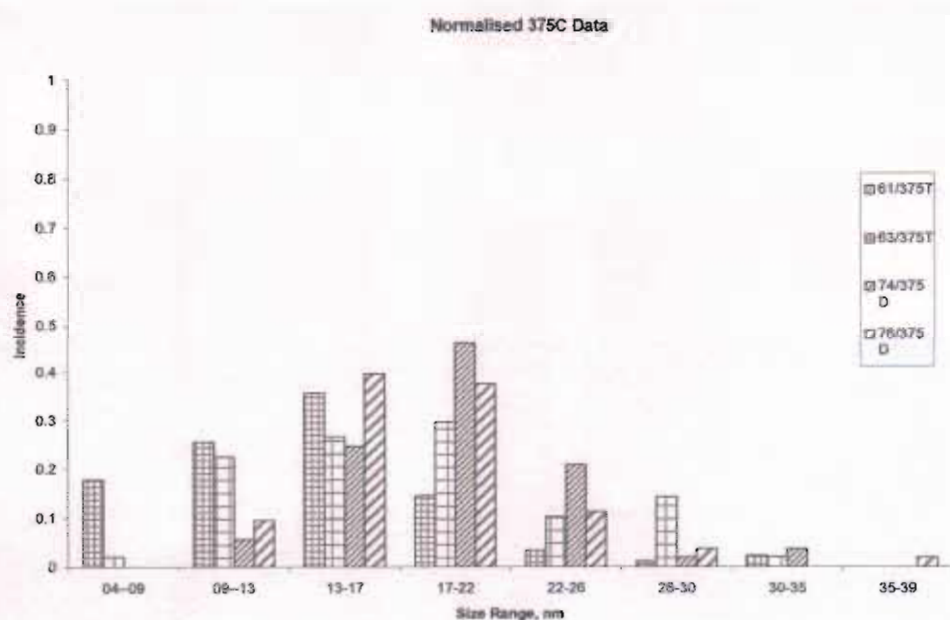


**Figure A 2** TEM size distributions for powders calcined to 375°C, as a fraction of total

### 10.2 Powders prepared through the use of isophthalic acid

Resolvable peaks and their relative intensities for diffraction patterns of powders calcined to 500°C and 800°C.

**Table A7** Resolvable peaks and intensities for XRD patterns for powders calcined to 500°C

1:1 calcined to 500°C	Angle, 2θ°	d value, Angstrom	Intensity, Count	Intensity, %	Assignment
	31.896	2.80348	2412	70	ZnO (100)
	34.551	2.59393	1932	56.1	ZnO (002)
	36.385	2.46724	3445	100	ZnO (101)
	47.695	1.90527	696	20.2	ZnO (102)
	56.745	1.62099	1098	31.9	ZnO (110)
	63.002	1.47421	825	23.9	ZnO (103)
	68.079	1.37611	733	21.3	ZnO (112)
	69.228	1.35606	434	12.6	ZnO (201)
1:2 calcined to 500°C	Angle, 2θ°	d value, Angstrom	Intensity, Count	Intensity, %	
	31.903	2.80288	3173	65.4	ZnO (100)
	34.569	2.5926	2479	51.1	ZnO (002)
	36.397	2.46648	4853	100	ZnO (101)
	47.693	1.90533	1025	21.1	ZnO (102)
	56.744	1.62101	1403	28.9	ZnO (110)
	62.997	1.47433	1126	23.2	ZnO (103)

	68.081	1.37607	928	19.1	ZnO (112)
	69.208	1.35641	554	11.4	ZnO (201)





10.3 Non-hydrolytic synthesis

10.3.1 Variation of oleic acid concentration

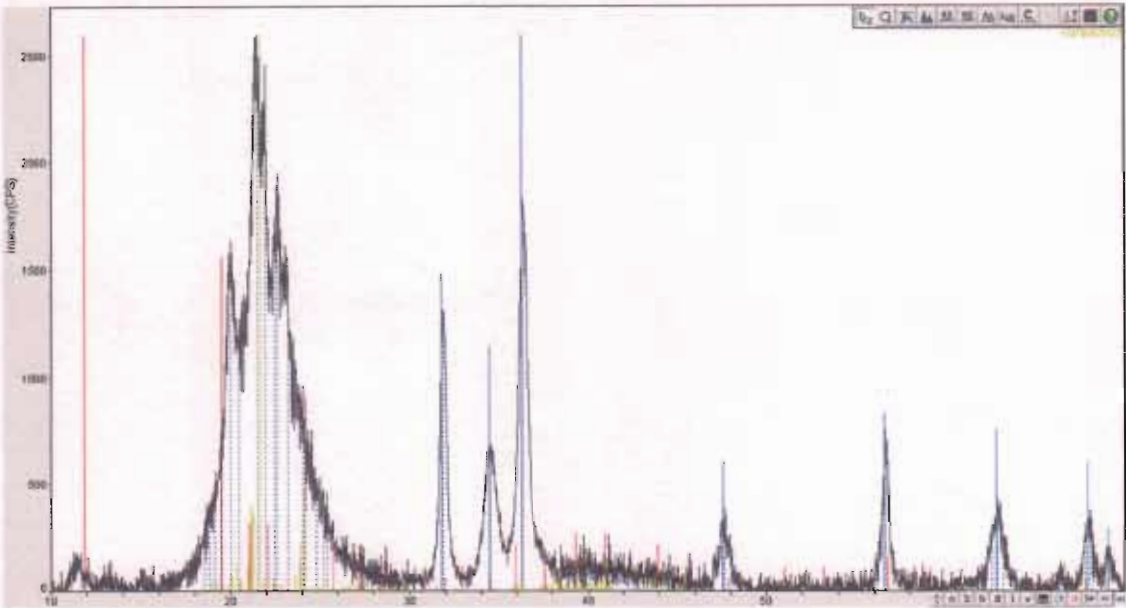


Figure A 3 Identification of peaks for sample synthesized containing 0.38ml oleic acid at 200°C

Table A9 XRD peaks resolved for sample synthesized containing no oleic acid at 200°C

2-Theta	d(A)	Height	I%(h)	Phase ID	( h k l )	2-Theta	Delta
11.563	7.6463	216	14.5	C4H6O4Zn		11.79	0.226
12.117	7.2982	90	6.1	Unidentified peak			
12.575	7.0337	133	9	C36H70O4Zn		12.421	-0.153
12.765	6.9291	72	4.8	Unidentified peak			
14.321	6.1795	66	4.4	Unidentified peak			
14.585	6.0683	99	6.7	Unidentified peak			
16.888	5.2456	96	6.5	Unidentified peak			
17.047	5.1969	102	6.9	Unidentified peak			
17.41	5.0896	87	5.9	Unidentified peak			
19.204	4.6178	263	17.7	C18H36O2	(-3 1 0)	19.116	-0.088
19.404	4.5708	335	22.5	C4H6O4Zn		19.493	0.089
19.927	4.452	87	5.9	C18H36O2	( 2 0 2 )	19.864	-0.063
20.433	4.3429	112	7.5	C18H36O2	( 1 1 1 )	20.485	0.052
21.649	4.1016	140	9.4	C18H36O2	( 3 1 1 )	21.631	-0.018
23.317	3.8118	678	45.6	C18H36O2	( 5 1 1 )	23.573	0.256
23.788	3.7373	193	13	C18H36O2	(-7 1 0)	23.803	0.015



2-Theta	d(A)	Height	I%(h)	Phase ID	(h k l)	2-Theta	Delta
24.476	3.6338	106	7.1	C18H36O2	(1100)	24.571	0.095
24.864	3.578	156	10.5	C18H36O2	(611)	24.78	-0.084
25.686	3.4653	88	5.9	C18H36O2	(702)	25.651	-0.035
27.492	3.2417	85	5.7	C18H36O2	(312)	27.455	-0.037
31.78	2.8134	549	36.9	ZnO	(100)	31.769	-0.01
34.46	2.6004	1486	100	C4H6O4Zn		34.466	0.006
36.26	2.4754	896	60.3	ZnO	(101)	36.252	-0.008
38.383	2.3432	80	5.4	C18H36O2	(1402)	38.387	0.004
38.742	2.3223	57	3.8	C18H36O2	(104)	38.765	0.023
40.469	2.2271	69	4.6	C18H36O2	(1502)	40.452	-0.016
41.182	2.1902	58	3.9	C18H36O2	(504)	41.166	-0.016
42.967	2.1032	65	4.4	Unidentified peak			
43.144	2.095	78	5.2	C18H36O2	(214)	43.384	0.24
45.817	1.9788	68	4.6	C4H6O4Zn		46.034	0.217
47.197	1.9241	146	9.8	Unidentified peak			
47.54	1.911	318	21.4	ZnO	(102)	47.538	-0.002
49.187	1.8508	57	3.8	Unidentified peak			
49.463	1.8412	53	3.6	Unidentified peak			
52.057	1.7553	60	4	C18H36O2	(-1620)	52.036	-0.021
52.153	1.7523	61	4.1	C18H36O2	(-315)	52.164	0.011
52.589	1.7388	60	4	C18H36O2	(-415)	52.389	-0.2
53.219	1.7197	92	6.2	C4H6O4Zn		53.21	-0.009
53.594	1.7086	71	4.8	Unidentified peak			
53.931	1.6987	72	4.8	Unidentified peak			
56.152	1.6367	63	4.2	Unidentified peak			
56.427	1.6293	143	9.6	Unidentified peak			
56.638	1.6238	217	14.6	ZnO	(110)	56.602	-0.037
57.55	1.6002	51	3.4	Unidentified peak			
57.828	1.5931	54	3.6	Unidentified peak			
58.067	1.5872	90	6.1	Unidentified peak			
58.972	1.5649	90	6.1	C4H6O4Zn		59.177	0.205
62.698	1.4806	293	19.7	Unidentified peak			
62.86	1.4772	370	24.9	ZnO	(103)	62.862	0.002
63.296	1.468	194	13.1	Unidentified peak			
66.153	1.4114	67	4.5	C4H6O4Zn		66.227	0.074
66.828	1.3988	57	3.8	Unidentified peak			
67.666	1.3835	62	4.2	Unidentified peak			
67.899	1.3793	156	10.5	C4H6O4Zn		67.859	-0.04
68.194	1.374	100	6.7	ZnO	(112)	67.961	-0.233

**Table A10 XRD peaks resolved for sample synthesized containing 0.25ml OA at 200°C**

2-Theta	d(A)	Height	I%(h)	Phase ID	(h k l)	2-Theta	Delta
---------	------	--------	-------	----------	---------	---------	-------



2-Theta	d(A)	Height	I%(h )	Phase ID	(h k l)	2-Theta	Delta
16.229	5.4573	78	4.9	Unidentified peak			
17.123	5.1743	83	5.2	Unidentified peak			
18.083	4.9015	128	8.1	C18H36O2	( 8 0 0)	17.785	-0.298
18.23	4.8623	85	5.3	C18H36O2	(-2 1 0)	18.446	0.215
19.566	4.5333	115	7.2	C36H70O4Zn		19.58	0.014
20.796	4.2679	89	5.6	C18H36O2	( 2 1 1)	20.934	0.138
21.458	4.1376	148	9.3	C18H36O2	( 3 1 1)	21.631	0.172
21.813	4.0712	103	6.5	C18H36O2	(-4 1 1)	21.841	0.028
22.797	3.8976	130	8.2	C18H36O2	(-5 1 1)	22.771	-0.026
23.13	3.8421	145	9.1	C18H36O2	( 5 0 2)	22.842	-0.288
23.485	3.785	128	8.1	C18H36O2	( 5 1 1)	23.573	0.088
24.348	3.6527	110	6.9	C18H36O2	( 6 0 2)	24.178	-0.17
24.659	3.6072	93	5.9	C18H36O2	( 11 0 0)	24.571	-0.088
25.842	3.4448	111	7	C4H6O4Zn		25.726	-0.115
28.286	3.1525	122	7.7	C18H36O2	(-10 0 2)	28.208	-0.078
28.683	3.1097	101	6.4	C18H36O2	(-10 1 0)	28.737	0.054
29.959	2.9801	77	4.8	C18H36O2	(-11 0 2)	29.909	-0.05
31.8	2.8117	180	11.3	ZnO	( 1 0 0)	31.769	-0.031
34.42	2.6034	1589	100	ZnO	( 0 0 2)	34.421	0.001
36.26	2.4754	359	22.6	ZnO	( 1 0 1)	36.252	-0.008
38.225	2.3526	55	3.5	C18H36O2	(-13 1 2)	38.302	0.077
39.271	2.2922	55	3.5	C4H6O4Zn		39.311	0.04
40.009	2.2517	81	5.1	C18H36O2	(-14 1 2)	40.04	0.031
40.626	2.2189	63	4	C18H36O2	(-8 2 0)	40.643	0.017
41.171	2.1908	55	3.5	C18H36O2	( 5 0 4)	41.166	-0.005
41.427	2.1778	60	3.8	C18H36O2	( 1 2 2)	41.383	-0.044
41.706	2.1639	60	3.8	Unidentified peak			
42.315	2.1342	89	5.6	Unidentified peak			
42.661	2.1176	58	3.7	C4H6O4Zn		42.611	-0.051
47.53	1.9114	122	7.7	ZnO	( 1 0 2)	47.538	0.008
48.951	1.8592	78	4.9	Unidentified peak			
49.192	1.8507	71	4.5	Unidentified peak			
49.51	1.8395	61	3.8	Unidentified peak			
49.881	1.8267	50	3.1	Unidentified peak			
50.551	1.8041	51	3.2	C36H70O4Zn		50.463	-0.088
56.56	1.6258	63	4	ZnO	( 1 1 0)	56.602	0.041
57.155	1.6103	96	6	Unidentified peak			
57.978	1.5894	58	3.7	Unidentified peak			
58.531	1.5757	69	4.3	Unidentified peak			
59.518	1.5519	52	3.3	Unidentified peak			
60.837	1.5214	62	3.9	Unidentified peak			
60.837	1.5214	62	3.9	Unidentified peak			
61.173	1.5138	49	3.1	Unidentified peak			



2-Theta	d(A)	Height	I%(h)	Phase ID	(h k l)	2-Theta	Delta
62.957	1.4751	232	14.6	ZnO	(1 0 3)	62.862	-0.094
64.28	1.4479	49	3.1	Unidentified peak			
66.785	1.3996	58	3.7	Unidentified peak			
67.566	1.3853	55	3.5	C4H6O4Zn		67.859	0.293
67.946	1.3784	78	4.9	ZnO	(1 1 2)	67.961	0.015
67.946	1.3784	78	4.9	Unidentified peak			
68.105	1.3756	66	4.2	Unidentified peak			
68.858	1.3624	55	3.5	Unidentified peak			
69.036	1.3593	73	4.6	ZnO	(2 0 1)	69.098	0.062

**Table A11 XRD peaks resolved for samples synthesized containing 0.5ml oleic acid at 200°C**

2-Theta	d(A)	Height	I%(h)	Phase ID	(h k l)	2-Theta	Delta
12.693	6.9683	69	1.2	Unidentified peak			
12.921	6.846	83	1.5	Unidentified peak			
14.285	6.1949	62	1.1	Unidentified peak			
14.877	5.9499	173	3	Unidentified peak			
19.438	4.5629	256	4.5	C18H36O2	(1 0 2)	19.296	-0.141
19.54	4.5392	248	4.3	C4H6O4Zn		19.493	-0.047
21.801	4.0733	3135	54.8	C18H36O2	(-4 1 1)	21.841	0.04
22.524	3.9442	185	3.2	C18H36O2	(4 1 1)	22.49	-0.034
23.02	3.8603	1265	22.1	C18H36O2	(5 0 2)	22.842	-0.178
24.569	3.6204	126	2.2	C18H36O2	(1 1 0 0)	24.571	0.002
25.099	3.5451	252	4.4	C18H36O2	(-7 1 1)	25.157	0.059
25.285	3.5194	185	3.2	C18H36O2	(-8 1 0)	25.339	0.054
30.139	2.9627	99	1.7	C18H36O2	(6 1 2)	30.241	0.101
31.879	2.8049	2848	49.8	C4H6O4Zn		31.936	0.057
34.5	2.5975	4084	71.4	C4H6O4Zn		34.466	-0.034
36.34	2.4701	5719	100	C18H36O2	(-1 2 0)	36.342	0.002
39.399	2.2851	72	1.3	C4H6O4Zn		39.311	-0.088
39.777	2.2643	86	1.5	C18H36O2	(8 1 3)	39.782	0.005
43.193	2.0928	104	1.8	C18H36O2	(2 1 4)	43.384	0.191
44.097	2.0519	67	1.2	C18H36O2	(6 2 2)	44.05	-0.047
44.362	2.0403	72	1.3	C18H36O2	(-11 2 0)	44.277	-0.084
45.247	2.0024	76	1.3	C18H36O2	(-8 1 4)	45.281	0.034
47.641	1.9072	1606	28.1	ZnO	(1 0 2)	47.538	-0.103
50.687	1.7995	74	1.3	C4H6O4Zn		50.976	0.289
51.577	1.7706	83	1.5	Unidentified peak			
52.049	1.7556	61	1.1	C18H36O2	(-16 2 0)	52.036	-0.013
52.271	1.7487	109	1.9	C18H36O2	(16 1 3)	52.26	-0.011
52.788	1.7327	53	0.9	Unidentified peak			

2-Theta	d(A)	Height	I%(h)	Phase ID	( h k l )	2-Theta	Delta
53.577	1.7091	62	1.1	Unidentified peak			
54.013	1.6963	71	1.2	Unidentified peak			
56.759	1.6206	1747	30.5	C4H6O4Zn		56.781	0.023
63.019	1.4738	2034	35.6	ZnO	( 1 0 3 )	62.862	-0.156
66.462	1.4056	202	3.5	ZnO	( 2 0 0 )	66.378	-0.084
66.638	1.4023	168	2.9	Unidentified peak			
68.02	1.3771	1263	22.1	ZnO	( 1 1 2 )	67.961	-0.059
69.141	1.3575	596	10.4	ZnO	( 2 0 1 )	69.098	-0.043

### 10.3.2 UV/vis absorption spectra

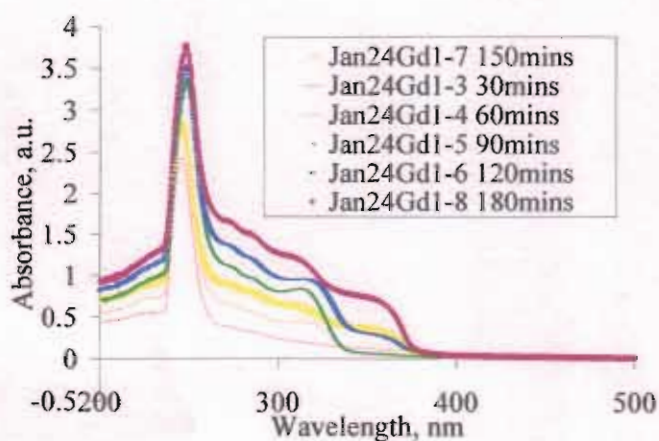


**Figure A 4 Time evolution of samples synthesized at 175°C in a [Zn<sup>2+</sup>]:[OA] ratio of 1:3**



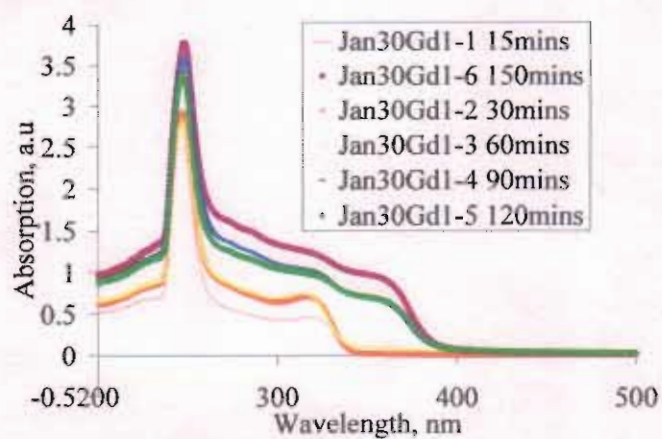


**Figure A 5** Time evolution of samples synthesized at 175°C in a  $[Zn^{2+}]:[OA]$  ratio of 2:5

#### 10.4 Polymer-assisted synthesis

##### 10.4.1 UV/vis spectra

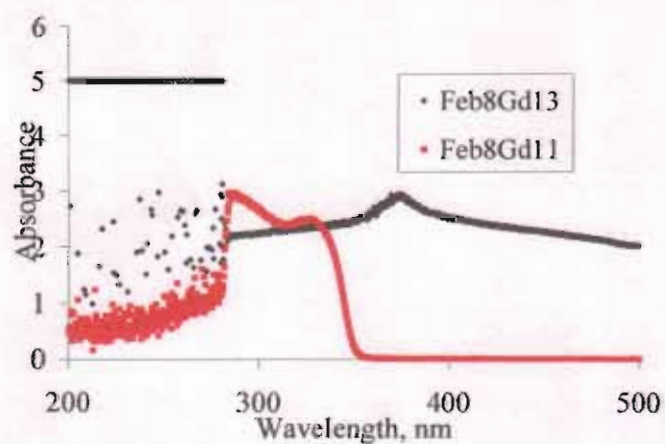


**Figure A 6** Effect of water on particle size

## **Presentations and publications**

*“A novel synthetic route for the production of nanoparticulate zinc oxide using an isophthalate precursor”*, Communication, in preparation.

*“Zinc oxide nanoparticles for next generation computing applications”*, Oral presentation to Mr Michael Ahern, T.D., Minister for Trade and Commerce at the Department of Enterprise, Trade and Employment, FÁS Science Challenge Closing Ceremony, April 26<sup>th</sup>, 2006, Houston, Texas, USA.

*“Zinc oxide nanoparticles for next generation magnetic applications”*, Oral presentation at BioLink USA-Ireland mini-symposium, April 13<sup>th</sup>, 2006, Baylor College of Medicine, Houston, Texas, USA.

*“Effect of variation of processing parameters on the formation of zinc oxide nanoparticles synthesized through sol-gel route”* Poster presentation, Microscopical Society of Ireland 29<sup>th</sup> annual symposium, 7<sup>th</sup>-9<sup>th</sup> September, 2005, FOCAS Institute, DIT Kevin St. and MC7: Functional Materials for the 21<sup>st</sup> Century, 5<sup>th</sup>-8<sup>th</sup> July, 2005, Edinburgh, UK.